Petroleum potential of the Upper Palaeozoic basement of the Songliao Basin, northeast China

Thesis submitted for the degree of Master of Science
Diplomarbeit zur Erlangung des akademischen Grades des Diplomingenieurs

Cosima Theloy
2008

Supervisor:
Ao. Univ. Prof. Dr. mont. Reinhard F. Sachsenhofer
Department of Applied Geosciences and Geophysics
Chair in Petroleum Geology
University of Leoben, Austria

I declare herewith that this thesis is entirely my own work and that I have only consulted references quoted herein.

Leoben, November 2008

Cosima Theloy

Acknowledgements

This master thesis was initiated and supervised by Professor Reinhard F. Sachsenhofer (Institute of Petroleum Geology, University of Leoben), whom I greatly thank for numerous discussions and supportive advices.

Special thanks appertain to Professor Yongjiang Liu (Department of Earth Sciences, Jilin University) for his hospitality and his excellent guiding during the field trip to China. He provided data and information material and always helped me out, when I had questions.

Many thanks to Professor Gerd Rantitsch, who showed me the operation mode of the Leco analyzer and the Rock Eval pyrolysis.

Furthermore I would like to thank Professor Thomas C. Meisel and Dr. Falk (Insititute of General and Analytical Chemistry), who supported me with the XRF analysis.

I am very grateful to Doris Reischenbacher, who explained many technical details of the sample preparation to me and for having motivating chats during the coffee breaks.

I want to thank Na Liu, who always did her best to find information in Chinese papers and translated it into English.

I would like to express my gratitude to Sabine Feuchter, who guided and helped me to polish the sections for vitrinite reflectance measurement.

Last but not least I owe greatest thanks to my family (Monika and Thilo Theloy), who supported and encouraged me over years and always believed in me and my goals.

ABSTRACT

The intracratonic non-marine Songliao Basin is one of the most prolific onshore petroleum provinces in China and comprises more than 80 oil and gas fields. The giant Daqing oil field contributes to 25 % to the total oil production of China. Upper Cretaceous lacustrine shales (Qingshankou Fm., Nenjiang Fm.) are the main source rocks of the Songliao Basin. The fact that most known oil and gas fields within the Mesozoic/Cenozoic basin fill have reached a mature stage of production leads to exploration of deeper levels of the basin as well as its Palaeozoic basement. For the evaluation of the generation potential of basement rocks, 83 samples were taken from surface outcrops in the surroundings of the basin. The collected Devonian to Triassic samples consist of dark grey to black shales of both marine and terrestrial origin.

During Palaeozoic and Mesozoic times the geodynamic regime in northeast China was dominated by successive amalgamation of cratonic units, forming the southeastern part of the Central Asian Orogenic Belt. Significant crustal growth took place through wide spread granitic intrusions, formation of magmatic arcs, and accretion and obduction of ophiolithic sequences. A research group of the Jilin University proposed that northeast China was part of the Jiameng block, a stable micro-continent since late Palaeozoic times. Hence, during the final stages of the formation of the Central Asian Orogenic Belt the sedimentary cover sequences, which represent the basement of the Songliao Basin were not severely deformed or metamorphosed, unlike the traditional opinion. In the late Jurassic crustal thinning, related to a retreating subduction zone at the Pacific margin, induced rifting of the Songliao Basin and was accompanied by magmatic activity. The shallow-lying Moho-discontinuity beneath the Songliao Basin is situated at a depth of ~30 km and causes an elevated thermal regime.

In the present study vitrinite reflectance was measured as a maturity parameter for the Palaeozoic and Triassic rocks. A Leco analyzer was used to determine the total organic carbon (TOC) contents and Rock Eval pyrolysis was performed to evaluate the hydrocarbon generation potential of the samples. Information about the chemical composition of the samples provides the data of the X-ray fluorescence analysis.

The results of the Leco analysis indicate that most samples show fair to good total organic carbon (TOC) contents, ranging from 0.5 to 1.5 %. Only five samples yielded excellent TOC

contents (2 - 5 %). Both marine and terrestrial samples are characterized by low sulphur (S) contents. Most marine rock samples revealed elevated TOC/S ratios, portending high input of allochtonous non-metabolizable organic matter of vascular plants into marine environments. Due to high thermal maturity, no hydrocarbons were released or generated from the samples during Rock Eval pyrolysis.

Vitrinite reflectance values between 2.2 and 5.7 % Rmax (2.0 and 5.3 % Ro) indicate that all samples are overmature, corroborated by the observation of mineralized veins and foliation in outcrops. The anomalous high vitrinite data in Middle and Upper Permian rocks in the adjacent outcrops 10 and 12 (≥ 5 % Rmax) in the southwestern part of the study area might be related to an increase in temperature resulting from nearby granitic intrusions. Most probably maturation of outcrop samples occurred before Jurassic/Cretaceous formation of the Songliao Basin. However, an additional thermal overprint of Palaeozoic rocks might have occurred at the base of the depocenters of the Songliao Basin. Thus, despite of the high maturity, some gas in the Songliao Basin may have derived from Palaeozoic and Triassic rocks.

The data of X-ray fluorescence analysis (Pro-Trace and UniQuant) indicate a silciclastic-dominated hinterland with minor (ultra-)basic rocks. The enrichment factors of element concentrations show minor variations in relation to average values of shales.

Muttergesteinspotential paläozoischer Sedimente im Basement des Songliao Beckens, NE China

KURZFASSUNG

Das nicht-marine, intrakratonische Songliao Becken im Nordosten Chinas gehört zu den ertragreichsten Erdöl und Erdgas Provinzen am chinesischen Festland und umfasst mehr als 80 Lagerstätten. Alleine die Rohölproduktion des Daqing Feldes macht ein Viertel der chinesischen Gesamtölproduktion aus. Die oberkretazischen lakustrinen Schwarzschiefer der Qingshangkou and der Nenjiang Formation bilden die Hauptmuttergesteine des Songliao Beckens. Jedoch, sind fast alle bekannten Erdöl- und Erdgasfelder am Ende der Produktionsphase angelangt, weswegen die tieferen Stockwerke des Beckens sowie der Beckenuntergrund zum Explorationsziel geworden sind. Für die Evaluierung des Muttergesteinspotentials des Beckenuntergrundes wurden 83 Proben aus Aufschlüssen in der

Umgebung des Songliao Beckens entnommen. Die dunkelgrauen bis schwarzen, feinkörnigen Gesteinsproben haben ein devonisches bis triassiches Alter und sind von sowohl mariner als auch terrestrischer Herkunft.

Während des Paläozoikums und des Mesozoikums war das geodynamische Regime in Nordost China geprägt von sukzessiven Kollisionsprozessen kleinere Krustenfragmente, die den südöstlichen Teil des Zentralasiatischen Orogens bilden. Durch weit verbreitete granitische Intrusionen, Entstehung magmatischer Bögen sowie Akkretion und Obduktion von ophiolithischen Sequenzen kam es zu bedeutender Neubildung kontinentaler Kruste. Ein Forschungsteam der Jilin Universität betrachtet Nordost China als Teil des Jiameng Blocks, ein stabiler Mikrokontinent seit dem späten Paläozoikum. Demnach wurden, entgegen der traditionellen Meinung, die auflagernden Sedimente, die den Beckenuntergrund des Songliao Beckens bilden, weder regionaler Metamorphose noch starker Deformation bei der Gebirgsbildung ausgesetzt. Im späten Jura bewirkte eine Ausdünnung der Lithosphäre, aufgrund einer zurückschreitenden Subduktionszone des Pazifischen Ozeans, das Einsacken des entstehenden Songliao Beckens, begleitet von magmatischer Aktivität. Das erhöhte thermische Regime im Songliao Becken wird mit der seicht liegenden Moho-Diskontinuität in Zusammenhang gebracht, die sich in einer Tiefe von zirka 30 km befindet.

Im Rahmen dieser Studie wurde die Vitrinitreflexion als Reifeindikator der paläozoischen und triassischen Gesteinsproben herangezogen. Mittels Leco Messungen wurde der organische Kohlenstoffgehalt (TOC) bestimmt und mit der Rock Eval Pyrolyse wurde das Muttergesteinspotential der Proben untersucht. Aufschluss über die chemische Zusammensetzung der Gesteinsproben gab die Röntgenfluoreszenzanalyse.

Die Ergebnisse der Leco Messungen, zeigen, dass die meisten Proben moderate bis gute Gehalte an organischem Kohlenstoff (TOC) aufweisen (0.5 - 1.5 %). Nur fünf Proben (Unterkarbon, Oberperm) besitzen exzellente TOC Gehalte zwischen 2 und 5 %. Kennzeichnend sind die geringen Schwefelgehalte (S) sowohl der terrestrischen als auch marinen Proben. Letztere zeigten demnach erhöhte TOC/S Verhältnisse, was auf einen signifikanten Eintrag von terrestrischem, organischem Materials in marine Ablagerungsbereiche zurückzuführen ist.
Wegen der fortgeschrittenen Reife der Proben, wurden während der Rock Eval Pyrolyse keine Kohlenwasserstoffe freigesetzt oder gebildet.

Die gemessenen Vitrinitreflexionswerte schwanken zwischen 2.2 und 5.7 % Rmax (2.0 und 5.3 % Ro) und zeigen, dass die Gesteine überreif sind. Mineralisierte Gänge und Schieferung in den untersuchten Aufschlüssen bestätigen diese Aussage. Die außerordentlich hohen Vitrinitreflexionswerte (≥ 5 % Rmax) mittel- und oberpermischer Sedimente in den benachbarten Aufschlüsse 10 und 12 im Südwesten des Untersuchungsgebiets, könnten durch granitische Intrusionen bedingt sein.

Wahrscheinlich erfolgte die Reifung der Oberflächenproben vor der jurassisch/kretazischen Absenkung des Songliao Beckens. Proben im Untergrund von Grabenstrukturen innerhalb des Songliao Beckens könnten jedoch eine Nachinkohlung erfahren haben. Dabei könnten geringe Mengen an Gas gebildet worden sein.

Die Auswertung der Röntgenfluoreszenz Analysedaten (Pro-Trace, UniQuant) ergab, dass das Liefergebiet silziklatstisch dominiert war mit zum Teil (ultra-)basischem Einfluss. Die Anreicherungsfaktoren zeigen, dass die Elementkonzentrationen nur geringfügig von den Durchschnittswerten eines Tonschiefers abweichen.

CONTENTS

1. INTRODUCTION

Roughly 85 % of China's oil production is derived from onshore oil provinces (Energy Information Administration, 2006). In figure 1, major petroliferous basins as the Ordos, Sichuan, Bohaiwan, Tarim, Junggar and the Songliao basins are illustrated, including their conventional hydrocarbon resources (USGS, 2000). Oil production in China has peaked and since 1993 the domestic demand exceeds the supply of national resources, whereas gas production still accommodates the need. This implies both that China has become dependent on imports and intensive exploration and re-evaluation of known petroleum provinces is carried out.

The Songliao Basin is one of the most prolific petroleum provinces in China. It is a non-marine, intracratonic rift basin and is characterized by horst and graben structures, which were initiated in Late Jurassic. The extensional stress regime, which led to the formation of the basin, is attributed to a retreating subduction zone at the Pacific margin. The NNE trending Songliao Basin covers an oval-shaped area of about 260.000 km^2 and is bounded by the Great Xing'an Range to the west, the Zhangguangcai Hills to the east and the Lesser Xing'an Range to the northeast (Zhou, 1998) (figure 2). The basin stretches over parts of three provinces, the Jilin Province, the Heilongjiang Province and the eastern segment of Inner Mongolia Province. The basin fill reaches a thickness of 7.5 km in the central depression and comprises volcanic rocks at the bottom and fluvial, alluvial and lactustrine sediments in stratigraphic younger formations. Organic-rich shales of the Upper Cretaceous lacustrine Qnigshankou and Nenjiang formations are the main source rocks in the Songliao Basin (Zhou, 1998; Ryder et al., 2003).

Two distinct petroleum systems were identified by Ryder et al. (2003) within the Songliao Basin. The Qingshankou – Putahua/Shaertu petroleum system accounts for 99 % of the discovered hydrocarbons to date, but the Jurassic coal – Denlouku/Nongan petroleum system is still underexplored and further major gas findings are expected.

More than 80 fields were found to date in the Songliao Basin (Ryder et al., 2003). The giant Daqing oil field, discovered in 1959, produces more than 900,000 barrels of oil per day, which accounts for one quarter of China's total oil production (Energy Information Administration, 2006). However, as most other major fields also the Daqing field is at a mature phase of production. Because of the depletion of shallow reservoirs, deeper levels of the basin as well as its Palaeozoic basement have become targets of exploration.

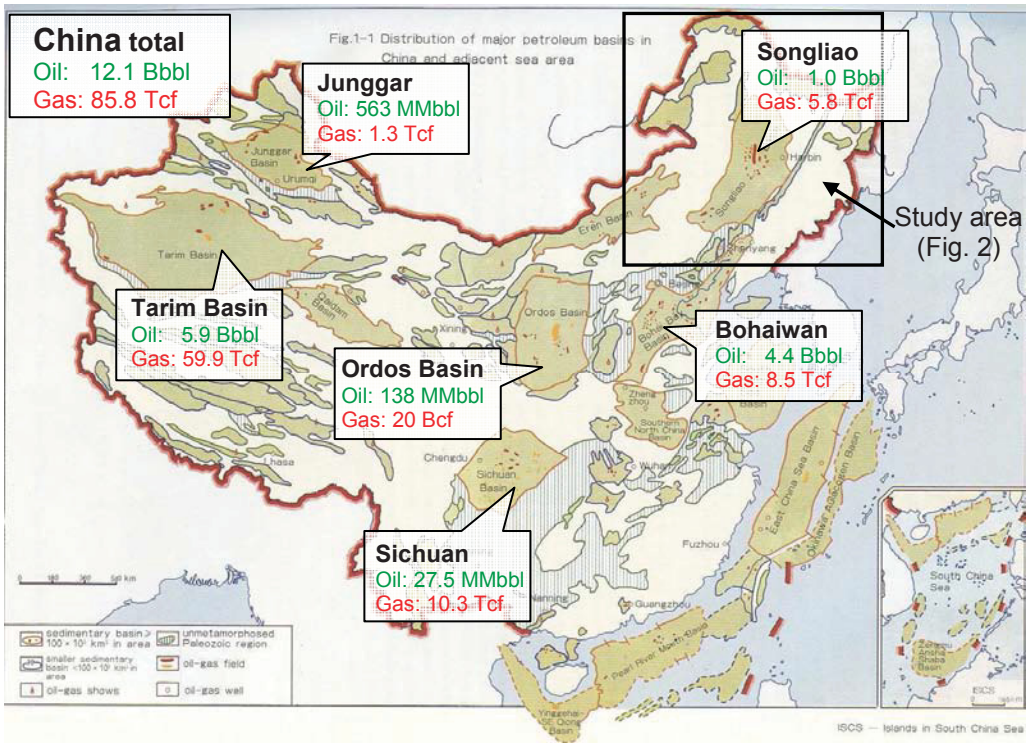

Figure 1: *Distribution of petroliferous basins in China (map after Zhai et al., 2000). Estimates of conventional hydrocarbon resources are taken from USGS (2000).*

The main aim of the present study is to determine the oil and gas generation potential of the late Palaeozoic basement of the Songliao Basin. It has been performed within the frame of a cooperation between Montanuniversität Leoben (Austria) and Jilin University (China). Most researchers during the 1990s concluded that the Upper Palaeozoic sediments were metamorphosed during the Hercynian orogeny (e.g.: Şengör and Natal'in, 1996). However, recent studies conducted by a research group of the Department of Earth Sciences at the Jilin University (Yongjiang Liu, Wei Jin, Cheng-wen Wang, Zhi-Hong Ma, Xing-Zhou Zhang, Jian-bo Zhou, Quan-bo Wen, Guoqing Han, Xiaoguo Chi, Ning Li) suggest that the Paleozoic basement formed a stable block at least since late Palaeozoic times, the Jiameng Block, and that metamorphism was restricted to local contact and minor dynamic metamorphism. Thus it is speculated that hydrocarbons generated in the Paleozoic basement might contribute to hydrocarbons found in the overlying Mesozoic-Cenozoic deposits of the Songliao Basin.

For the present study 83 samples of dark shales have been taken from the surroundings of the Songliao Basin, where Palaeozoic strata are exposed on the surface (stars in figure 2 mark approximate outcrop locations). The age of investigated formations ranges from the early

Devonian to early Triassic. The sediments are mainly of marine and terrestrial origin but also volcanic rocks have been recorded. Rock Eval pyrolysis, vitrinite reflectance measurement and total organic carbon content determination were used to evaluate the quality and maturity of the potential source rocks. Moreover, X-ray fluorescence analysis data provide information on the chemical composition of the shales.

Figure 2: *Location map of the Songliao Basin surrounded by the Great and Lesser Xing'an Range and the Zhangguangcai Hills (modified after Liu et al., 2008, unpubl.). Dashed red line: province boundaries; stars: locations of sampling.*

2. GEODYNAMIC EVOLUTION AND TECTONIC UNITS OF NE CHINA

2.1. Overview

During the Palaeozoic the geodynamic regime in NE China was dominated by successive amalgamation of cratonic units and terranes as well as accretion of magmatic arcs and ophiolites forming the south-eastern part of the Central Asian Orogenic Belt (CAOB; figure 3) (Zonenshain, 1973; Cao, 1989; Shao, 1989; Tang, 1990; Şengör and Natal'in, 1996; Xu and Chen, 1997; De Jong et al., 2006; Lin et al., 2008; Wang et al., 2008). Immense volumes of mafic and granitic magmas were emplaced during this process, implying a substantial growth of continental crust (Jahn et al., 2000; Wu et al., 2002). The CAOB extends from Kazakhstan to probably even the Hida belt in Japan (Arakawa et al., 2000; Jahn et al., 2000) (figure 3: location 11) and was formed as a result of successive accretion of terranes, island arcs and subduction-accretion complexes to the Angaran nucleus (Siberia craton) throughout the Palaeozoic (Suess, 1901a, Zonenshain, 1973; Zonenshain et al., 1990; Mossakovsky et al., 1994; Badarch et al., 2002; Xiao et al., 2003, 2004a). With the closure of the Palaeo-Asian Ocean the Tarim and North China (or Sino-Korean) cratons collided with the Siberian plate, thus terminating the formation of the Central Asian Orogenic Belt. It is assumed that the oceanic basin was closed by a two-way subduction beneath the northern active margin of North China and Tarim micro-continents and the southern margin of Siberia (Wang and Liu, 1986; Xiao et al., 2003), leading to the formation of the Solonker suture zone.

This major lineament can be traced all along the Central Asian Orogenic Belt from Kyrgyzstan in the west to the northern tip of North Korea and even further to the Sea of Japan in the east (De Jong et al., 2006). The Solonker suture separates two orogens, the Altaids referring to the northern orogen and the Manchurides to the southern orogen of the Central Asian Orogenic Belt (Şengör et al., 1993; Şengör and Natal'in, 1996, Windley et al., 2007). The recognition of this suture is an intricate task, because of the similarity in structural features and stratigraphic records of the rock assemblages on both sides (Şengör and Natal'in, 1996). The suture is amidst of two accretion complexes of unequal polarity, the Erdaojing subduction-accretion complex to the north and the Ondor Sum subduction-accretion complex to the south (figure 4). The closure of the Palaeo-Asian Ocean, hence suturing, occurred progressively later from west to east (Dobretsov, 2003; Xiao et al. 2004b, Cope et al., 2005). Timing and location of suturing were often disputed, however it is now widely accepted that

the Solonker suture was formed during the late Permian (De Jong et al., 2006). In the course of the final stages of collision, older sutures of the composite terranes and micro-continents were reactivated as strike slip shear zones (Laurent-Charvet et al., 2003). In proximity to the Solonker suture A-type granites were emplaced as result of post-collisional slab break-off and delamination of the lithosphere (Wu et al., 2002).

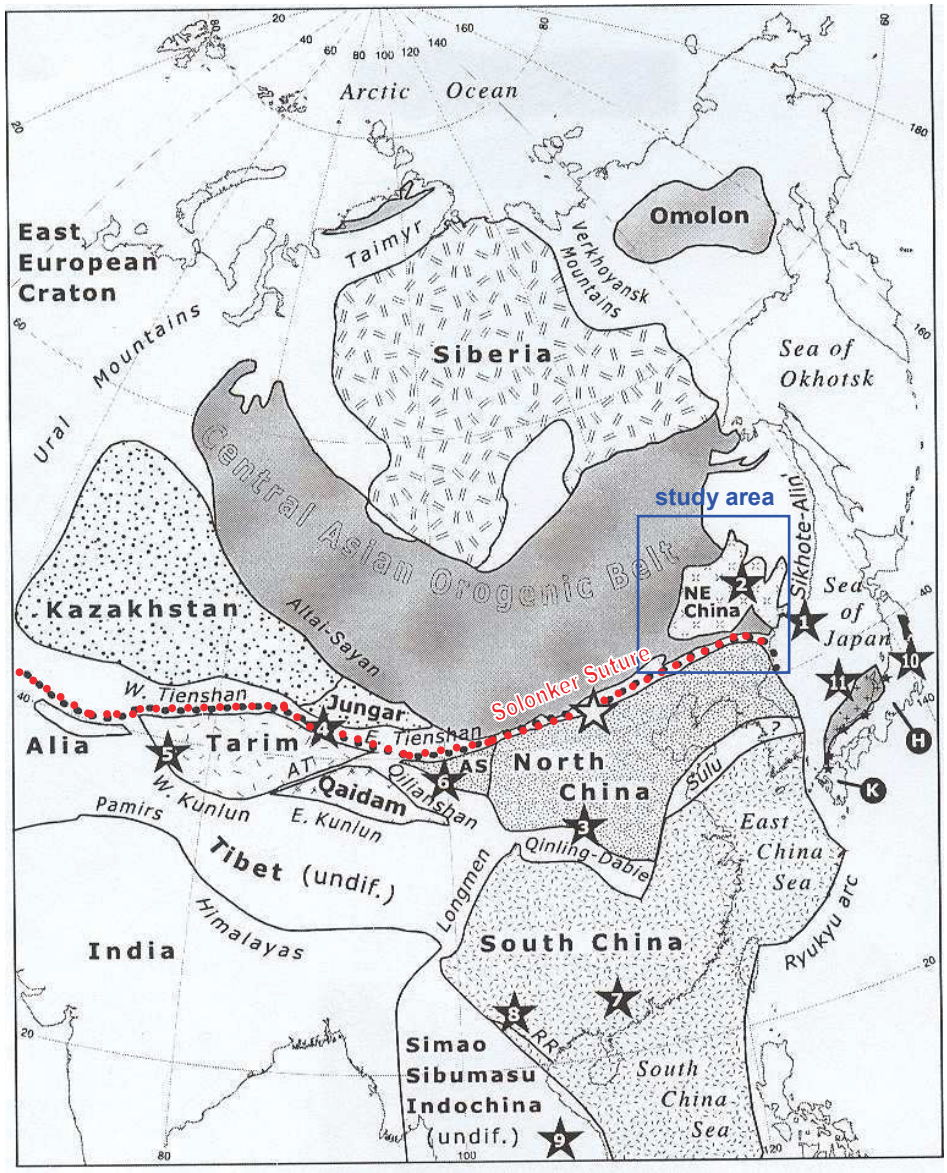

Figure 3: *Tectonic map of Asia showing the distribution of terranes and micro-continents, the Central Asian Orogenic Belt and the Solonker suture (red dotted line; from De Jong et al., 2006; modified after Badarch et al., 2002 and Xiao et al., 2004b). Locations described in the text: white star: Ondor Sum complex; 1: Sergeevka ophiolite of the Khanka superterrane; 2: Songliao-Zhangguangcai and Jiamusi blocks; 10: South Kitakami terrane; 11: Hida belt. Azimuthal equal-area projection.*

Triassic molasse sediments covered the cooled and exhumed plutons signalling the uplift of the orogen. By early Jurassic terrestrial sediments were deposited across the Solonker suture according to Wang and Liu (1986) and data of the Inner Mongolian Bureau of Geology and Mineral Resources (IMBGMR, 1991). The retreating subduction zone of the Pacific applied an extensional stress regime on northeast China, and as consequence rifting of the intracratonic Songliao Basin was initiated in late Jurassic.

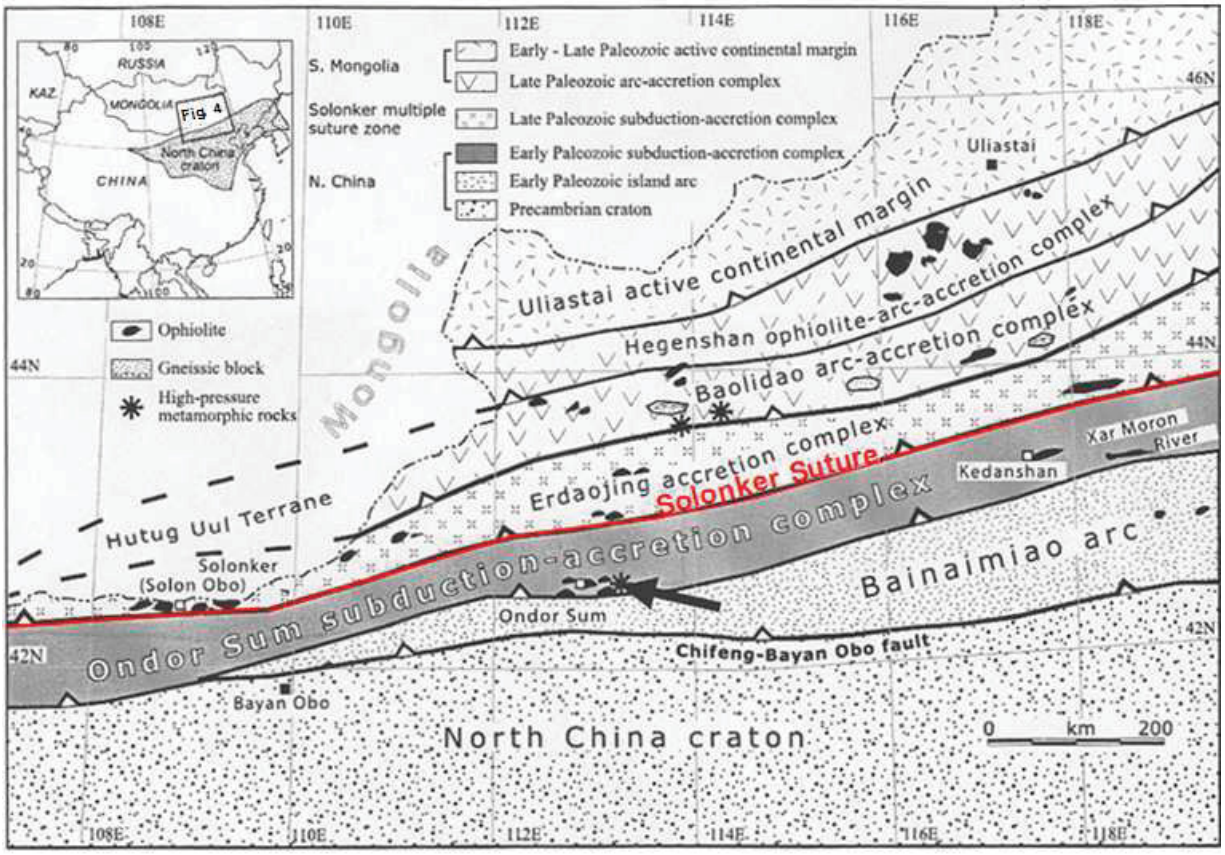

Figure 4: *Tectonic map of central Inner Mongolia. Mesozoic and Cenozoic strata have been removed to uncover the tectonic sequences along the Solonker suture zone (De Jong et al., 2006; modified after Xiao et al., 2003). Although this setting is to the west of the actual study area, it was integrated because it provides the best exposure of the suture zones which continue into NE China.*

With regard to the geodynamic evolution De Jong et al. (2006) advocate a two-staged scenario.

First, during early Palaeozoic times micro-continents like North China, South China, Tarim, maybe even Kazakh terranes, Qiadam, Alashan, Kunlun, South Kitakami, Khanka and probably Indochina (locations in figure 3) were situated in the peripheries of the northeastern Cimmerian margin of Gondwana. The micro-continents were fringed by subduction-accretion

complexes, island arcs or contained calc-alcaline volcanic margins. During this period the Ondor Sum complex was formed. In some cases, crustal fragments collided with each other like for example the Qiadam and Qilian blocks.
Second, North China and Tarim blocks drifted northwards during the middle Palaeozoic implying the closure of the Palaeo-Asian Ocean and eventually they collided with the southern margin of the Central Asian Orogenic Belt and Siberia in the late Permian.

2.2. Early Palaeozoic evolution

There is some controversy about the geodynamic evolution of northeast Asia, especially for the middle to late Palaeozoic times. In order to provide a better understanding of the tectonic history of northeast China and the regional geologic processes, which had an influence on the Upper Palaeozoic basement strata of the Songlaio Basin, also the early Palaeozoic evolution is discussed in some detail.

In a peri-Gondwana orogenic system close to the northeastern Cimmerian margin micro-continental fragments, which nowadays form the mainland of Asia, built up a vast archipelago (De Jong et al., 2006). Palaeogeographical reconstructions by Li and Powell (2001) support a proximal position of the North and South China cratons to the Australia - New Zealand - Antarctica continental margin of the supercontinent. It is not clear whether the micro-continents were located close to or in the Palaeo-Pacific (or Palaeo-Asian) oceanic basin. At the eastern active margin of Gondwana occurred oblique, westward directed subduction of the Palaeo-Pacific lithosphere, which induced a lateral displacement of North and South China and other micro-continents along the subduction zone until they arrived near the Cimmerian re-entrant by the early Ordovician (Li and Powell, 2001; Veevers, 2004; Cawood, 2005). Orogenic activity inferred by a number of subduction zones, which surrounded the micro-continents, and as a consequence, accretion of island arcs and formation of calc-alcaline volcanic arcs at the continental margins dominated the situation.

Formation of Ondor Sum complex and Bainaimaio arc

In this way also the Ondor Sum subduction-accretion complex and the associated Bainaimiao magmatic arc were formed at the northern margin of the North China craton (figure 4).

$^{40}Ar/^{39}Ar$ dating of phengite reveals an age of about 450 Ma for dynamic recrystallization of quarzitic mylonite from the blueschist facies and ductile deformation in the higher part of the Ondor Sum subduction-accretion complex (De Jong et al., 2006). Figure 5 illustrates an oceanward directed subduction zone leading to the formation of the Ulan island arc, which belongs to the Ondor Sum complex. During Ordovician to Silurian times the polarity of the subduction zone had flipped, and thus the northern margin of the North China craton became an active margin. The southward directed subduction of the Paleo-Asian Ocean beneath the

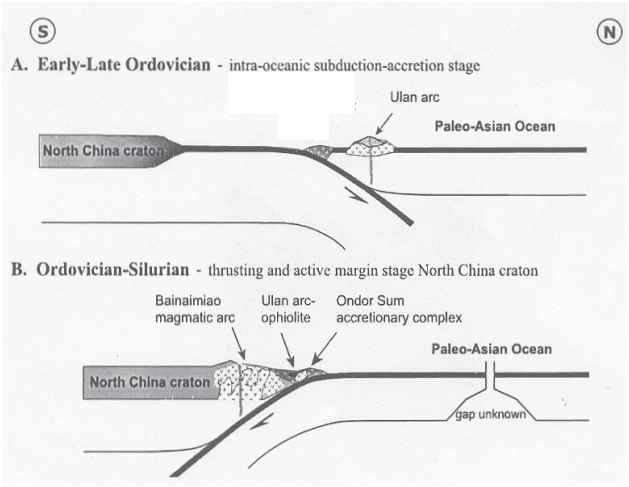

Figure 5: *Tectonic evolution of the northern margin of the North China craton in Inner Mongolia. Development of the Ondor Sum subduction-accretion complex and the volcanic Bainaimiao arc (De Jong et al., 2006; modified after Xiao et al., 2003).*

North China craton resulted in the formation of the volcanic Bainaimiao arc. The petrologic composition of the latter is made up of mainly calc-alcaline tholeiitic basalts, minor felsic lavas, tuffs, gabbros, granodorites and granites (Hu et al., 1990). U-Pb age dating of Zirconium grains yielded an age of 466 Ma, whereas 430 Ma derived from K- Ar dating of muscovites, represent the cooling age of the Bainaimiao arc (Zhang and Tang, 1989). A high initial strontium isotope ratio ($^{87}Sr/^{86}Sr_i = 0.7146$) of granites (Shao, 1989) and a εNd value of 2.4 ± 1.7 of granodiorites (Nie and Bjørlykke, 1999) led Xiao et al. (2003) to the assumption that the magma was sourced of both mantle and melted crustal rocks, hence magma mixing took place. The deposition of Upper Silurian shallow marine carbonates and clastic sediments on top of the exhumed granites and Bainiamiao-type magmatic rocks heralds the extinction of the arc. Until Carboniferous times no other island arcs were accreted to the northern margin of the North China craton (Xiao et al., 2003).

Terranes and micro-continents south of the Solonker suture

Şengör et al. (1993) favour a scenario where all Precambrian crustal fragments in the Central Asian Orogenic Belt originated from Laurentia, which was part of the former supercontinent Rhodinia. In latest Neoproterozoic to early Cambrian times these crustal blocks were separated in form of a single arc, the Kipchak arc, and were accreted subsequently to Siberia's southern margin. Buslov et al. (2001) point out the heterogeneity of the micro-continents and consider them as composite blocks built up of Laurentian- and Gondwana-derived terranes. Other authors like Mossakovsky et al. (1994) and De Jong et al. (2006) rather hold the opinion of a predominant Gondwana origin. Li and Powell (2001) suggest that some of the micro-continents (e.g.: South China, Tarim, Indochina and Kazakh terranes) broke off the Australian portion of Gondwana, and others like North China might have been of Siberian derivation before their peri-Gondwana history. Based on palaeomagnetic data, fossil records and similarities in pre-Ashgill stratigraphies between North China craton and North Australia, Metcalfe (1996, 1998, 2002) and Li and Powell (2001) postulate a position close to the Cimmerian margin of Gondwana at least during Cambrian to Ordovician times, probably even until the Silurian or latest early Devonian. The Tarim block got detached from the supercontinent by the early Cambrian, forming an independent micro-continent like North and South China, whereas close trilobite affinities of these three blocks confirm a location close to Australia (Meert et al., 2001; Li and Powell, 2001; Metcalfe 2002; Choi et al., 2003). Also other terranes and micro-continents such as Indochina, Kunlun, Alashan and Qiadam reveal indications for a conjunct early evolution in proximity to Tarim, North and South China due to stratigraphic, floral and faunal similarities in early Palaeozoic times.

Many blocks of present-day Asia are characterized by the occurrence of early Palaeozoic ultra-high pressure metamorphic rocks, reflecting the tectonically active setting along the Cimmerian margin. The clockwise rotation of Gondwana during the Ordovician to early Devonian might have intensified the tectonic activity in micro-continents situated within the vast marginal orogenic system (Li and Powell, 2001) (figure 6). High-pressure assemblages of belts rimming the micro-continents were overprinted by retrograde metamorphism, which was induced by exhumation and cooling of subducted rocks.

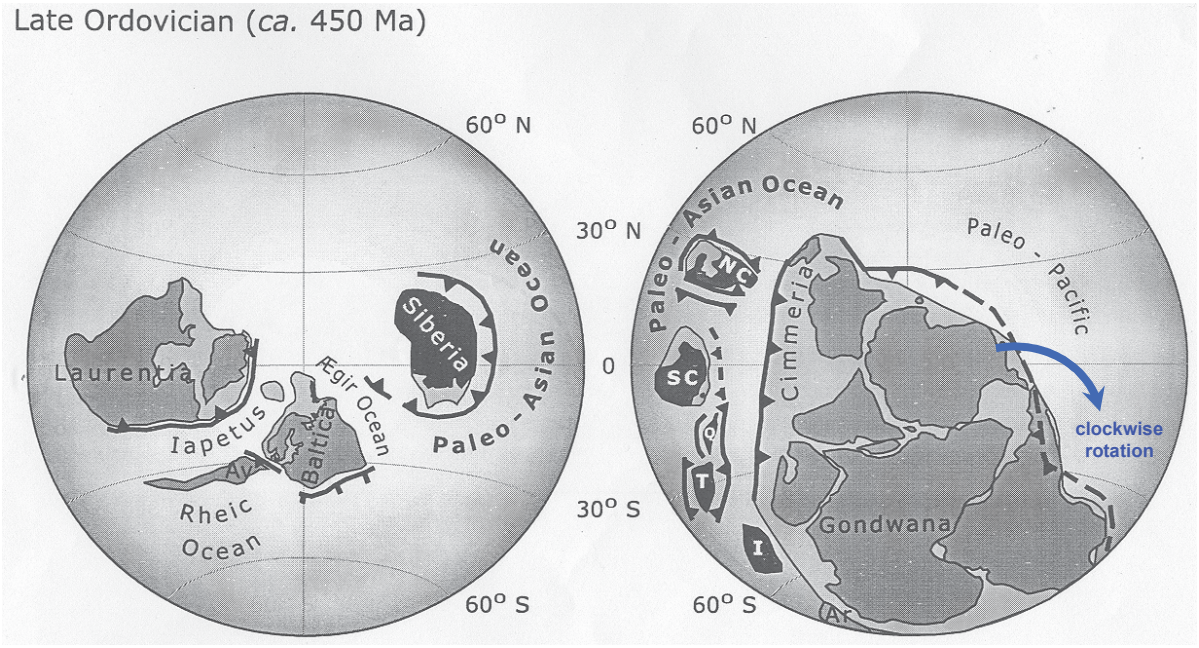

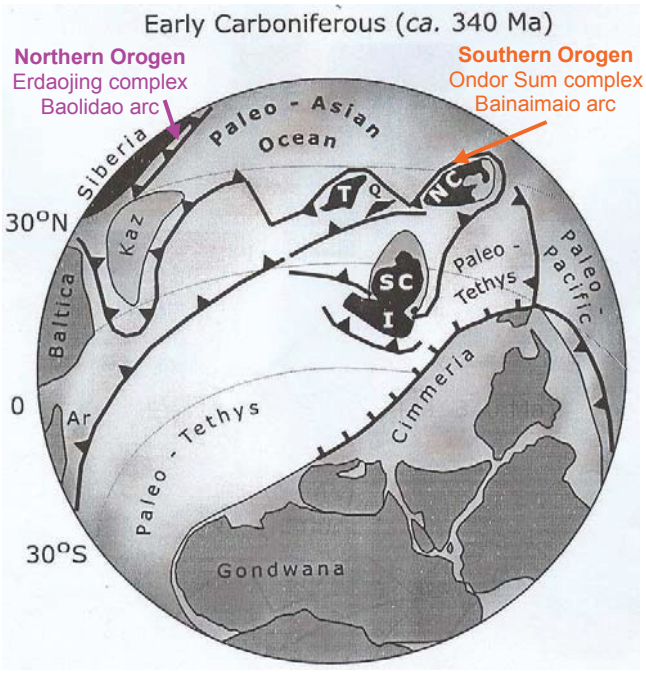

Figure 6: *Palaeogeographic and geodynamic reconstruction for the late Ordovician and early Carboniferous modified after Li and Powell (2001); subduction zones mainly after Pickering and Smith (1995), Li and Powell (2001), Fortey and Cocks (2003), Torsvik and Cocks (2004). Ar = Armorica; Av = Avalonia; I = Indochina; Kaz = Kazakhstan; NC = North China; Q = Qaidam-Qilian; SC = South China; T = Tarim. Locations of the subduction-accretion complexes north and south of the Solonker suture are indicated, though the Erdaojing-Baolidao arc complex was formed during the Permian.*

Terranes and micro-continents north of the Solonker suture

In contrast to micro-continents to the south of the Solonker suture, which have a peri-Gondwana origin, the provenance of some terranes and crustal fragments located north of the lineament remains more enigmatic (De Jong et al., 2006).

In front of the late Neoproterozoic active southern margin of Siberia a complex island arc system developed, which contained a collage of cratonic and metamorphic fragments and relics obducted oceanic lithosphere. Subsequent accretion of younger island arcs, oceanic

islands and formation of subduction-accretion complexes occurred during Cambrian to early Ordovician times (Badrach et al., 2002; Windley et al., 2002; Dobretsov et al., 2003; Khain et al., 2003; Xiao et al., 2004a). Some terranes of possible Gondwana derivation like Tuva-Mongolia, Central Mongolia and Kochetav were annexed to this island arc at about 550 to 490 Ma (million years) before present under formation of (ultra) high pressure rock assemblages (Buslov et al., 2001; Dobretsov, 2003; Dobretsov et al., 2003; Kheraskova et al., 2003). Eventually, in the early Ordovician the whole arc system collided with the southern margin of the Siberian craton (Buslov et al., 2001; Kheraskova et al., 2003).

The Khanka superterrane (figure 3: location 1) is a large composite block that covers the area of the Russian Far East and parts of northeast China. It comprises four units of early to middle Palaeozoic age, representing a suite from continental margin to an island arc and subduction-accretion complexes (Khanchuk et al., 1996; Kojima et al., 2000; Nokleberg et al., 2001). Many radiometric ages of metamorphic rocks of amphibolite- to granulite-facies were within a range from 535 to 450 Ma (Badarch et al., 2002; Dobretsov et al., 2003; Khain et al., 2003). Metagabbros of the Sergeevka ophiolite yielded an age of 470 to 430 Ma for hornblendes. Cambrian microfossil affinities of the Voznesenka terrane, the southern part of Khanka, with Australia allude that it was part of the continental margin of Gondwana. The first sediments that covered the entire Khanka terrane are of middle to late Devonian age, hence Nokleberg et al. (2004) concluded that amalgamation of the crustal fragments took place during the early Palaeozoic in a peri-Gondwana setting, before the whole Khanka block was separated from Gondwana in the Devonian. Unlike Zonenshain et al. (1990) and Wu et al. (2000), who assume that Khanka collided with the North China craton in the early Triassic, Şengör and Natal'in (1996) suggest that Khanka was a part of the northern margin of the North China micro-continent since early Palaeozoic times.

The Jiamusi block (figure 3: location 2) in northeastern China contains metamorphic complexes that reveal an age of ca. 500 Ma. Wilde et al. (2000) conjecture that metamorphism took place while the Jiamusi terrane was situated in the periphery of the Cimmerian margin. However, this remains speculative, because of lacking palaeomagnetic data or palaeontological evidences to corroborate this assumption. It cannot be excluded that Cambro-Ordovician high-grade metamorphic rock assemblages of the Jiamusi block and other terranes north of the Solonker suture were formed during accretion and collision with Siberia's southern margin.

Crustal fragments of the Japanese islands such as the South Kitakami (figure 3: location 10), Hida Gaien (figure 3: location 11), Palaeo-Ryoke and Kurosegawa terranes are of Gondwana

provenance. South Kitakami has been considered to have formed a single entity with the Khanka superterrane (Şengör and Natal'in, 1996; Kojima et al, 2000; Tazawa 2002). Worth highlighting is the almost complete sedimentary succession of the South Kitakami terrane, mirroring the Palaeozoic evolution (Tazawa, 2002; Ishiwatari and Tsujimori, 2003; Yoshida and Machiyama, 2004). Based on abundant biostratigraphic markers, South Kitakami is supposed to have been part of Gondwana until the Devonian and subsequently rifted and drifted northwards (Ehiro, 2000).

2.3 Middle to late Palaeozoic evolution

With the opening of the Palaeo-Tethyan Ocean in middle Devonian time North and South China as well as Tarim were separated from the Cimmerian margin. This is supported by the absence of floral and faunal similarities with the east Gondwana margin from that point of time onwards (Metcalfe, 1998, 2002) and by palaeomagnetic reconstructions (Li and Powell, 2001) (figure 6). Another indicator for the rifting stage can be found in southernmost South China, a transition from Upper Devonian tholeiitic volcanic rocks to Lower Carboniferous alkali basalts, which Guo et al. (2004) interpreted as the result of lithospheric thinning. The independent micro-continents started their northwards drift in mid-Carboniferous and active margins were developed along the northern margins of Tarim and North China cratons during the Pennsylvanian (Xiao et al., 2003, 2004b). According to Dobretsov (2003), Kazakhstan collided with the southwestern margin of Siberia in the middle Carboniferous. Subduction and subsequent closure of the Palaeo-Asian Ocean resulted in collision of the Tarim block with Kazakhstan in middle Permian times (Şengör and Natal'in, 1996). As mentioned in preceding sections, the Solonker suture was formed progressively later from west to east, implying a scissor-like closure of the Palaeo-Asian Ocean.

Formation of the Erdaojing complex and the Baolidao arc

Badarch et al. (2002) argue that in contrast to other Mongolian terranes, the Tsagaan Uul terrane (southernmost Mongolia) and its eastern pendant the Hutag Uul terrane (figure 4) show no fossils in Silurian to Devonian strata with affinity to the Siberian palaeobio-geographic province. Thus, this would imply that these terranes were accreted to the southern edge of the Altaids in post-Devonian time, unlike Tuva-Mongolia and Central Mongolia.

According to Xiao et al. (2003), the Hutag Uul terrane is the equivalent to the Baolidao arc and the associated Erdaojing subduction-accretion complex, which are considered to be of Permo-Carboniferous age. The formation of the Baolidao arc is a consequence of the north-directed subduction of the Palaeo-Asian Ocean. Permian ophiolites, cherts and turbidites characterize the Erdaojing complex (Shang, 2004).
Lin et al. (2008) suggest a correlation between the Erdaojing subduction-accretion complex in Inner Mongolia and the late Permian - early Triassic Jilin subduction-accretion complex in northeast China. With respect to structural and chronological constraints the accretion complexes seem to be comparable, therefore Lin et al. (2008) interpret the Jilin suture as the northeastern continuation of the Solonker suture as far as Yanji, which is located close to the Sea of Japan at the Chinese - North Korean border.

After the collision of the North China craton with the active margin of Siberia and the formation of the Solonker suture in the late Permian, the Central Asian Orogenic Belt was completed (Xiao et al., 2003). Pickering and Smith (1995) recognize some parallels of the tectonic evolution of the CAOB with the Variscan belt in Europe and the Appalachians in North America, since there also much older crustal fragments (e.g.: Avalonia and Armorica) of Gondwana derivation were accreted.

2.4 Tectonic evolution and structural setting of northeast China

New tectonic model of the Department of Earth Sciences, Jilin University

A research group of the Department of Earth Sciences of the Jilin University (Yongjiang Liu, Wei Jin, Cheng-wen Wang, Zhi-Hong Ma, Xing-Zhou Zhang, Jian-bo Zhou, Quan-bo Wen Guoqing Han, Xiaoguo Chi, Ning Li) developed a new tectonic model for northeast China, according to which a stable block, the Jiameng block, should have existed since at least the late Palaeozoic. They argue that because of this, the Upper Palaeozoic sedimentary cover and passive continental margin deposits, which constitute the basement of the Songliao Basin, are well preserved and were not heavily deformed. This contradicts the common opinion of a metamorphosed Palaeozoic basement related to the orogenic processes during the formation of the Central Asian Orogenic Belt.

Based on the new concept, potential source rocks of the Upper Palaeozoic could be still within the thermal stage of metagenesis. This was the starting point of the present study involving the evaluation of maturity and hydrocarbon generation potential of Palaeozoic source rocks.

The summary of the new concept of the Jiameng block and tectonic evolution of northeast China is mainly based on personal communication with Professor Yongjiang Liu, because published papers about this topic are in Chinese and not yet translated into English.

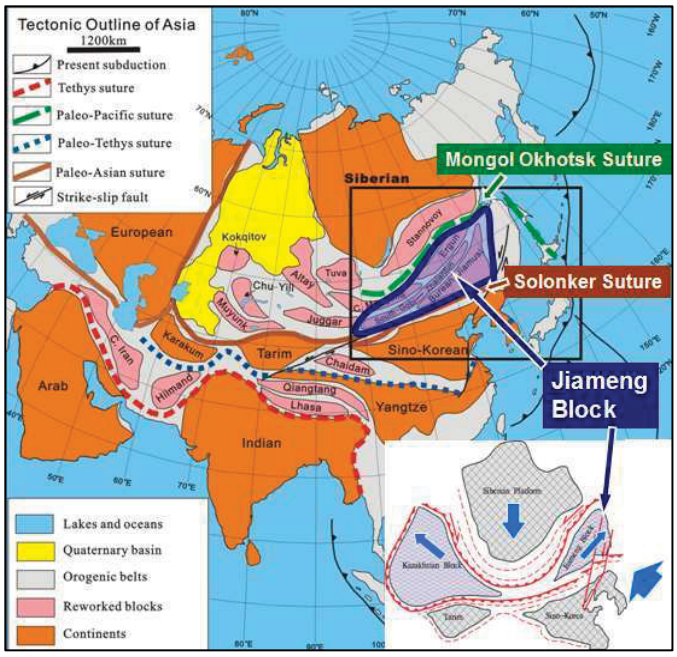

Figure 7: *Illustration of position and size of the Jiameng block within the tectonic framework of Asia; bounded by the Solonker suture to the south and the Mongol-Okhotsk suture to the north. Liu et al., 2007 unpubl., modified after Li (2006). Inset in the lower right corner displays the prevailing stress regime during early Mesozoic times, causing lateral escape of the Jiameng block to the NE (Liu et al., 2007 unpubl.).*

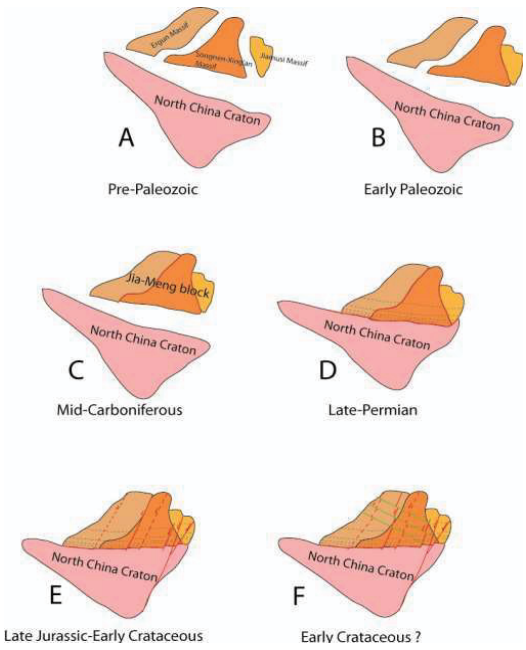

Figure 8: *Simplified sketch of the tectonic evolution of the Jiameng block, modified after Liu et al. (2008 unpubl.). Distances between the blocks are not to scale.*

The term ‘Jiameng’ consists of ‘jia’ referring to the Jiamusi block and ‘meng’ meaning Mongolia. It covers the area of northeast China, the southernmost part of Russia and stretches

into South Mongolia (figure 7). Northeast China is composed of three blocks, the Jiamusi block in the east, the Songliao (or Songnen) - Xing'an block in the center and the Erguna block to the northwest (Liu et al., 2008).

Figure 8 displays the major stages of the tectonic evolution of the Jiameng block:

A) In the Precambrian the Songliao and the Xing'an block formed a single terrane. Liu et al. (2008) doubt about a correlation of the ENE trending Hegenshan suture with the NNE trending Nenjiang fault is admissible, because of lacking geological evidences such as ophiolites. Only in the immediate area of Hegenshan in Inner Mongolia ophiolites were found. Besides Lin et al. (2008) consider the Hegenshan suture of Devonian to Carboniferous age. Poor outcrop conditions make it difficult to determine whether the Nenjiang lineament is a younger fault or an old suture between the Songliao and Xing'an blocks, which became reactivated as a strike slip fault in late Mesozoic times. Liu et al. (2008) suggest based on similar Neodynium model ages (Wu et al., 2000) of the Songliao and Xing'an blocks, that they have been originally one single block, implying that the Nenjiang fault is not a suture.

B) The Songliao-Xing'an block collided along the Mudanjiang suture with the Jiamusi block during the early Palaeozoic. Based on whole rock $^{40}Ar/^{39}Ar$ plateau ages of blueschists and syntectonic granites of the Heilongjiang complex, which belongs to the Jiamusi terrane, Jia et al. (2004) propose an age of about 450 to 410 Ma for suturing. Also Cao et al. (1992) advocate that the closure of the oceanic basin, which separated the Jiamusi and Songliao-Xing'an blocks, was terminated in the Silurian.

C) With the accretion of the Erguna Massif in mid-Carboniferous times, the amalgamation of the Jiameng block was completed. Because of overlying Mesozoic sediments, the recognition and tracing of the Derbugan suture is not an easy task. However, remnants of a magmatic arc, which could be associated with the subduction of an ocean beneath the Xing'an block reveal an early Carboniferous age. Wang et al. (2008) argue that because of a high percentage (up to 75 %) of endemic cold water type brachiopods, the Jiameng block occupied an isolated position until at least the middle Permian, representing an own palaeo-biogeographic province. Palaeogeographic reconstructions by Gordienko and references therein (2006) (figure 9a) support this statement as the large composite block was

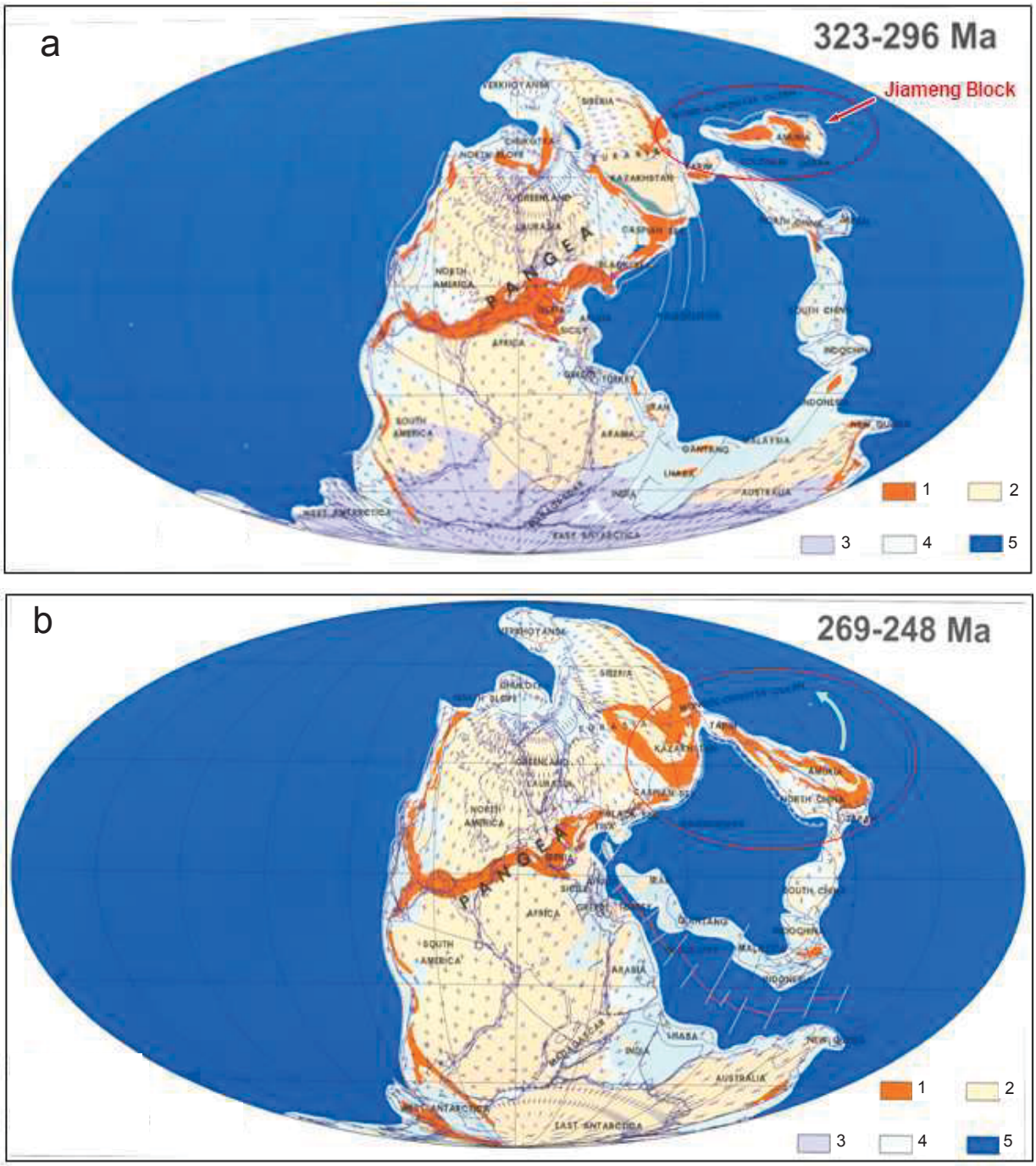

Figure 9: *Palaeogeographic reconstructions show the Jiameng block as isolated micro-continent in the late Carboniferous (a) and after the closure of the Paleo-Asian Ocean (or Solonker Ocean) and subsequent collision with North China craton in the late Permian (b). A counter-clockwise rotation of the amalgamated micro-continents led to the subduction of the Mongol-Okhotsk Ocean and accretion to Siberia by late Jurassic (modified after Gordienko and references therein, 2006). 1: orogenic belts; 2: stable continents and cratons; 3: shelf regions; 4: continental margins; 5: oceanic basins.*

surrounded by the Palaeo-Asian Ocean to the south and the Mongol-Okhotsk Ocean to the north. Apparently, the oceanic basins were still deep and wide enough, based on the occurrence Zhesi brachipods in the middle Permian (Wang et al., 2008). Lower Devonian and Permian continental margin cover sequences were observed from Russia in the east to Inner Mongolia in the west.

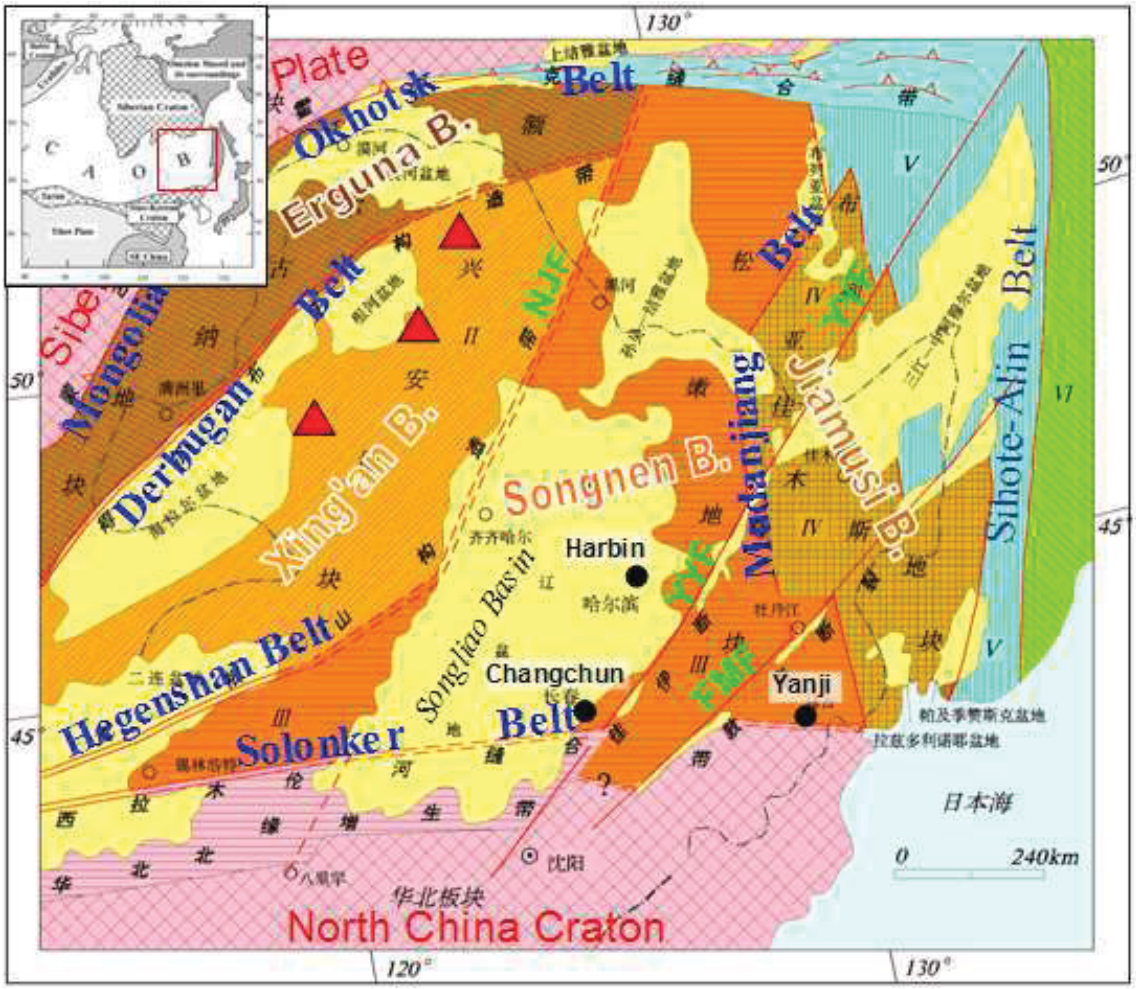

Figure 10: *Tectonic units and structural elements of northeast China. Dark brown: Erguna block; light orange: Xing'an block; dark orange: Songliao block (or Songnen); light brown: Jiamusi block; yellow: Meso-Cenozoic basins; pink: North China craton and Siberian plate; blue: Jurassic accretion complex; green: Cretaceous continental margin; NJF: Nenjiang fault; YYF: Yilan-Yitong fault; FMF: Fushun-Mishan fault; red triangles: remains of a Carboniferous magmatic arc related to the accretion of the Erguna block to Xing'an-Songliao block (modified after Liu et al., 2008; inset map after Wu et al., 2000).*

D) In accordance with the general opinion, the Palaeo-Asian Ocean was subducted in late Permian times and the North China craton collided along the Solonker suture with the Jiameng micro-continent (see also figure 9b). Some crustal shortening, thrusting and gentle folding occurred at the southern margin of the Jiameng block as consequence of the collision, indicated by green lines in figure 8d. The prevailing palaeo-stress regime during the early Mesozoic induced lateral escape of the Jiameng block as a whole due to N-S compression (figure 7, lower right corner). The Upper Palaeozoic strata were not severely deformed during this process. In the following, a counter-clockwise rotation of the amalgamated micro-continents, enhanced by the opening of the Neotethys (figure 9b), led to a constriction narrowing(?) of the Mongol-Okhotsk oceanic basin.

E) Eventually in the late Jurassic the Jiameng-North China micro-continent collided with the active Siberian margin causing the formation of the Mongol-Okhotsk suture. Oblique subduction of the Izanagi oceanic plate (= part of the Pacific plate), inferred a NE to NNE trending sinstral strike slip fault pattern, comprising the Fushun-Mishan, Yilan-Yitong and Nenjiang faults (figure 10). Liu et al. (2008) report an offset of about 160 to 170 km for the Fushun-Mishan fault and approximately 40 km offset at the Nenjiang fault in the area of the southwestern corner of the Songliao Basin. In late Jurassic to early Cretaceous times rifting of the NNE-SSW trending Songliao Basin was initiated in response to an extensional stress regime related to the retrogressive subduction zone of the pacific Izanagi plate.

Alternative models

According to Wu et al. (2000) northeast China occupies the eastern part of the Xingmeng Orogenic Belt, which belongs to the CAOB. ‘Xing’ stands for Xing’an and ‘meng’ means Mongolia. Ye et al. (1994) and Wu et al. (1995) suggest a subdivision of northeast China into three micro-continental blocks: the Xing’an block in the northwest, the Songliao block in the middle and the Jiamusi block in the southeast, separated by the Nenjiang and Mudanjiang faults, respectively.

During the Devonian to early Carboniferous the composite Jiamusi-Songliao block was accreted to the Xing’an-Central Mongolian block along the Nenjiang fault, forming the ultimate Xingmeng block (Ye et al., 1994; Yu et al., 1996). The extent of the Xingmeng block covers the area of southeast Russia, northeast China and central Mongolia. Wu et al. (2000) mention that timing of collision between the North China craton and the composite Xingmeng

block is still subject of discussion. Zhao et al. (1990) suggest based on palaeomagnetic data an age of amalgamation before the late Permian, however Zonenshain et al. (1985, 1990) rather opt for a collision in the late Triassic. Subsequently, the subduction of the Mongol-Okhotsk Ocean led to the accretion of the Xingmeng block to the Siberian plate in late Jurassic times.

In contrast, Lin et al. (2008) regard the Khanka and Jiamusi blocks as a single microcontinent, which collided with the Inner Mongolian Xilinhot block along the Mudanjiang suture in the early Palaeozoic, however, underlining that the relationship between these three blocks remains speculative.

Evolution and structural setting of the Songliao Basin

Zhou (1998) subdivides the evolution of the Songliao Basin into a pre-rift phase, a syn-rift phase, a post-rift phase and a compression phase.

The pre-rift phase during the Triassic to middle Jurassic was characterized by regional uplift and erosion. Crustal extension led to the formation of numerous small-scale horst and graben systems in late Jurassic times. The rifting stage was accompanied by emplacement of granitic plutons and volcanic activity, which is reflected in the early sedimentary fill of the basin. The acme of rifting occurred during the earliest Cretaceous when smaller, separated grabens evolved into a few large grabens, induced by back arc extension due to a retreating subduction zone at the Pacific margin.

Thermal subsidence occurred during the post-rift phase in the early Cretaceous (Nøttvedt et al., 1995), resulting in the formation of the Songliao Basin as a whole. A change from volcanoclastic to predominantly fluvial and lacustrine sediments portend that volcanic activity had abated. The Lower Cretaceous Denlouku Formation covered the underlying filled grabens and even the horsts received sedimentation for the first time. Six drainage systems poured sedimentary freight into the central basin area, indicating an increase of accumulation space, which peaked in a basin-wide lake transgression. By end of the Cretaceous roughly 6500 m of sediments were accumulated in the Qijia-Goulong depression (Yang, 1984; Li, 1995) (figure 11).

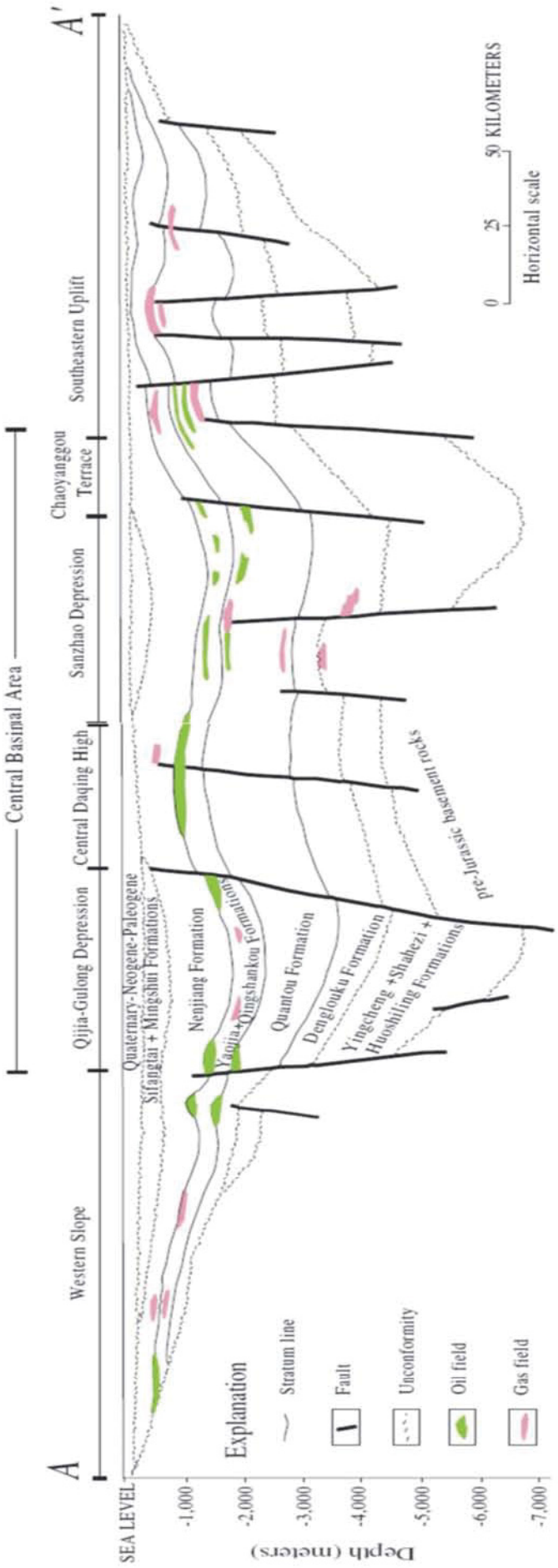

Figure 11: *Cross section through the Songliao Basin including major oil and gas fields (Ryder et al. 2003; modified after Hu and Krylov, 1996). Location of cross section A-A' is indicated in figure 12.*

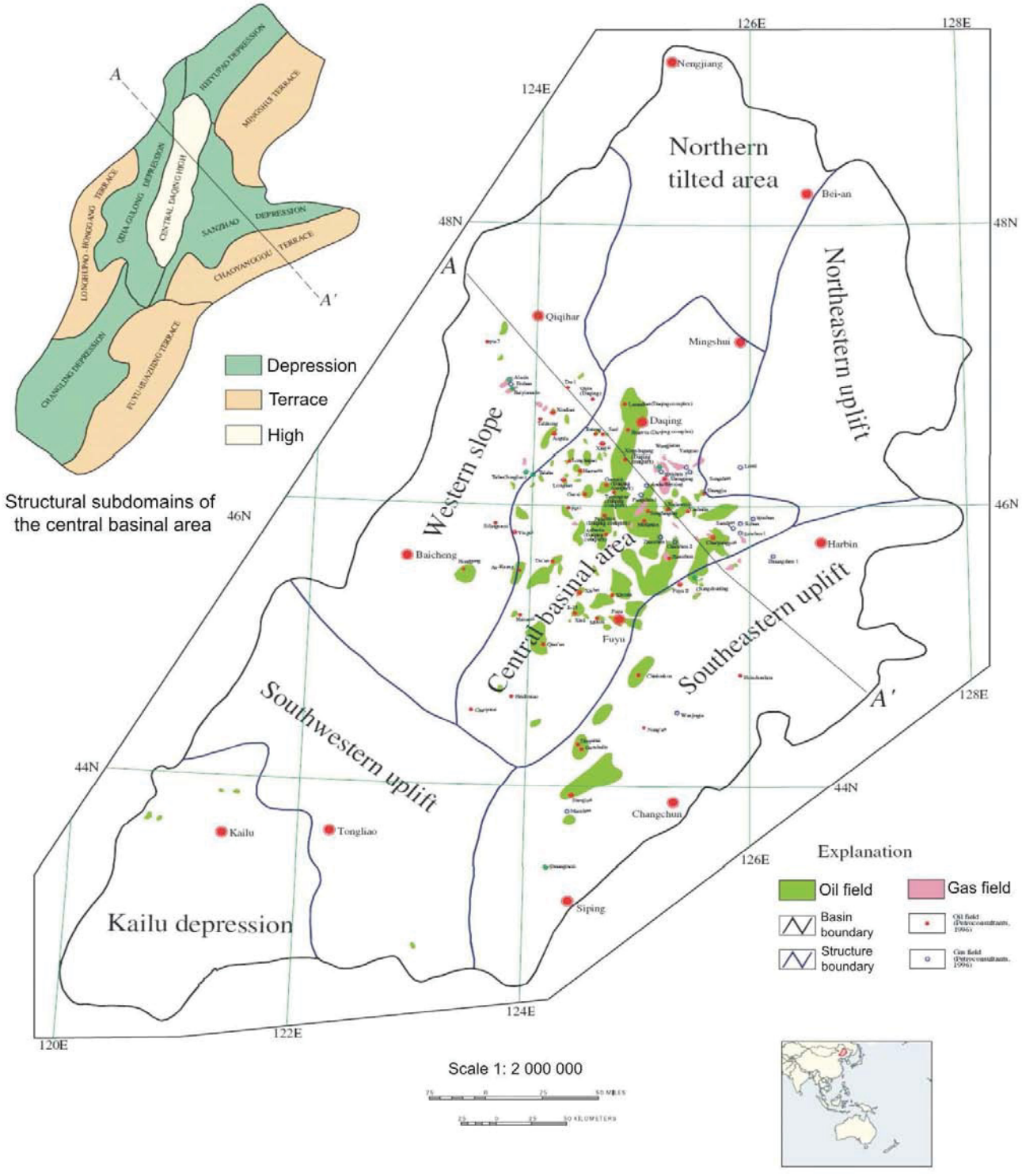

Figure 12: *Structural domains of the Songliao Basin after Ryder et al. (2003). Outlines of oil and gas fields are from Hu and Krylov (1996); points indicating oil and gas fields after Petroconsultants (1996).*

The basin became partly inverted in latest Cretaceous / early Tertiary times, triggered by the onset of spreading of the Sea of Japan (Ma et al., 1989). The compressional regime caused uplift and erosion of the eastern flank of the Songliao Basin, which in turn evoked a westward shift of the depocenter into the central depression and differential subsidence. The present-day structural framework of the Songliao Basin (figure 11 and 12) is the result of maximum compression during the Tertiary, when structural traps like the Daqing and Chaoyanggou anticlines were formed.

Yang J. (1985) and Yang W. (1985) divide the Songliao Basin into seven domains: central basinal area, northern tilted area, northeastern uplift, southeastern upflift, southwestern uplift, Kailu depression and the western slope (figure 12).

3. GEOLOGICAL SETTING

3.1 Geological outline

Apart from a number of Meso-Cenozoic rift basins such as the Songliao and Hailaer Basins, northeast China is occupied by the Great Xing'an Range, the Lesser Xing'an Range and the Zhangguangcai Range, where numerous granitic plutons and minor Palaeozoic strata crop out (figure 13). The granitic intrusions, which represent at least 50 % of the area in mountainous regions according to the regional geological survey (JBGMR, 1988; HBGMR, 1993; IMBGMR, 1990), are traditionally considered to be of late Palaeozoic age and related to the

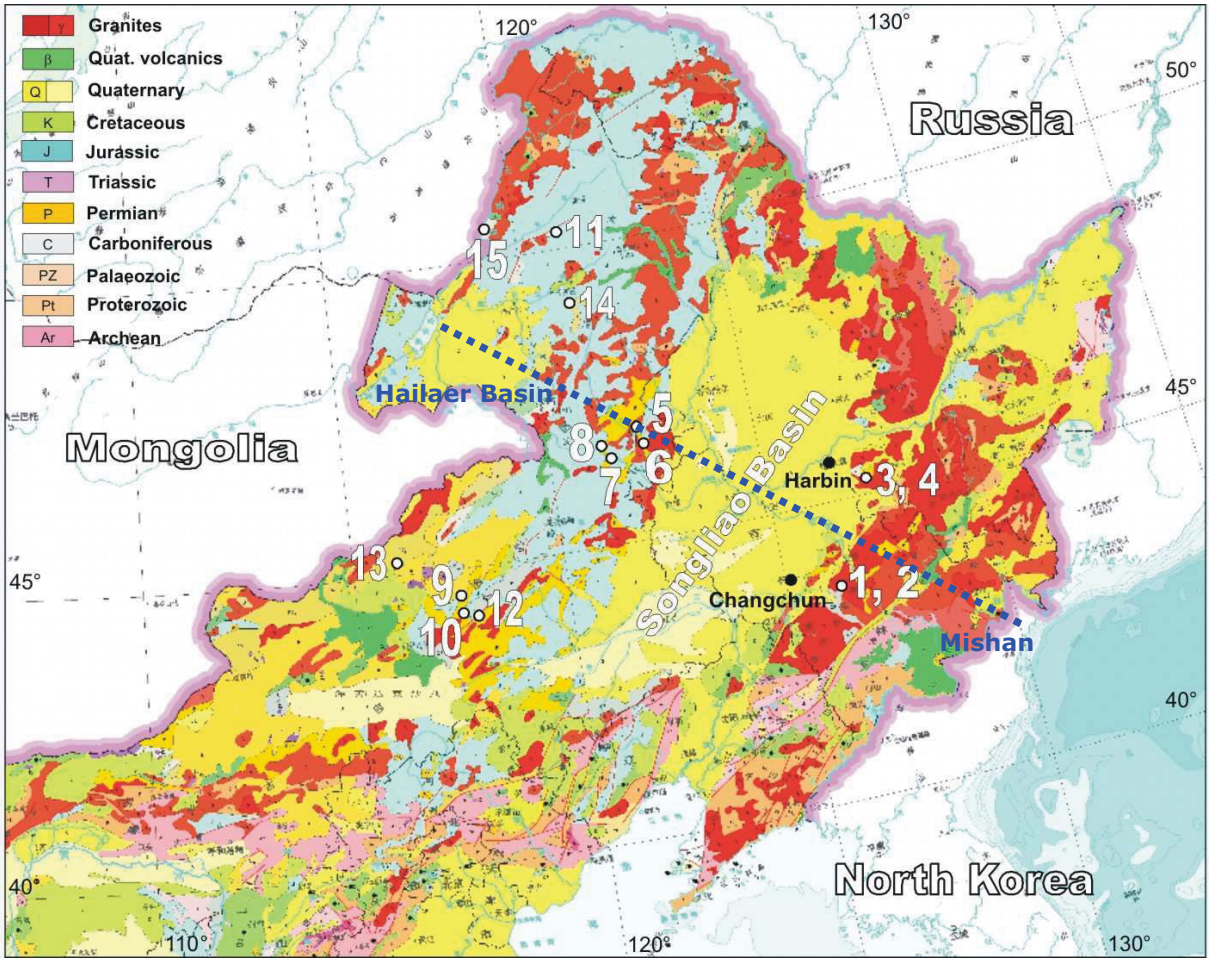

Figure 13: *Geological map of NE China (scale 1: 4000000; Geological Survey of China, 2004). Numbers refer to locations of studied outcrops; dashed blue line indicates cross section of stratigraphic table in figure 14.*

formation of the CAOB. In contrast Wu et al. (2000, 2003) and Jahn et al. (2001) revealed in their detailed studies, that emplacement took place during several periods throughout the Phanerozoic and that 'true' late Palaeozoic granites are rare. Most widespread are granitic intrusions of both early and late Mesozoic ages in the context of post-orogenic extensional collapse and back-arc related crustal thinning, respectively. Highly fractionated I-type and A-type granitoids are characterized by positive εNd (T) values and low $(^{87}Sr/^{86}Sr)_i$ ratios pointing to significant input of mantle derived magmas. Similar isotopic compositions were also observed in adjacent areas to northeast China, evidencing substantial production of juvenile crust, hence growth of continental crust. Wu et al. (2000, 2003) associate A-type granites genetically to underplating processes of mafic magma in an extensional setting. A Moho depth of less than 30 km in area of the Songliao Basin advocates considerable lithospheric extension during late Mesozoic times, which was accompanied by volcanic activity and emplacement of granitic intrusions throughout the basement of the basin.
Implications regarding the thermal influence of intruded plutonic rocks on the maturation of Upper Palaeozoic source rocks will be discussed in chapter 5.3.

3.2 Lithostratigraphy

Stratigraphy of Upper Palaeozoic strata

The sedimentary column from the early Devonian to late Permian is built up of mainly marine and terrestrial sediments as well as volcanic rocks (figure 14). The Lower Devonian sequence is dominated by marine sediments extending over wide areas in a west-east direction. From the middle Devonian until middle Permian an increasing influence of both terrestrial and volcanic deposits was observed. Prof. Y. Liu (Jilin University) favours a passive continental margin setting of deposition, however he points out that this remains questionable because of the occurrence of widely distributed volcanic rocks and volcanoclastic sediments. It cannot be excluded that sedimentation of the Upper Palaeozoic strata took place at an active continental margin while the Palaeo-Asian oceanic lithosphere was subducted beneath the Jiameng block. Based on reflection seismic data, Yu et al. (2003) estimate the combined thickness of Carboniferous and Permian strata with more than 7000 m. In order to accommodate several thousands meters of sediments an extensional setting is necessary, induced by for example a retreating subduction zone at an active continental margin. The transition from marine to

terrestrial deposits and the subsequent lack of stratigraphic record in the Xing'an area from the early Permian onwards, could possibly be correlated with the accretion of the Erguna block, followed by uplift of the orogen.

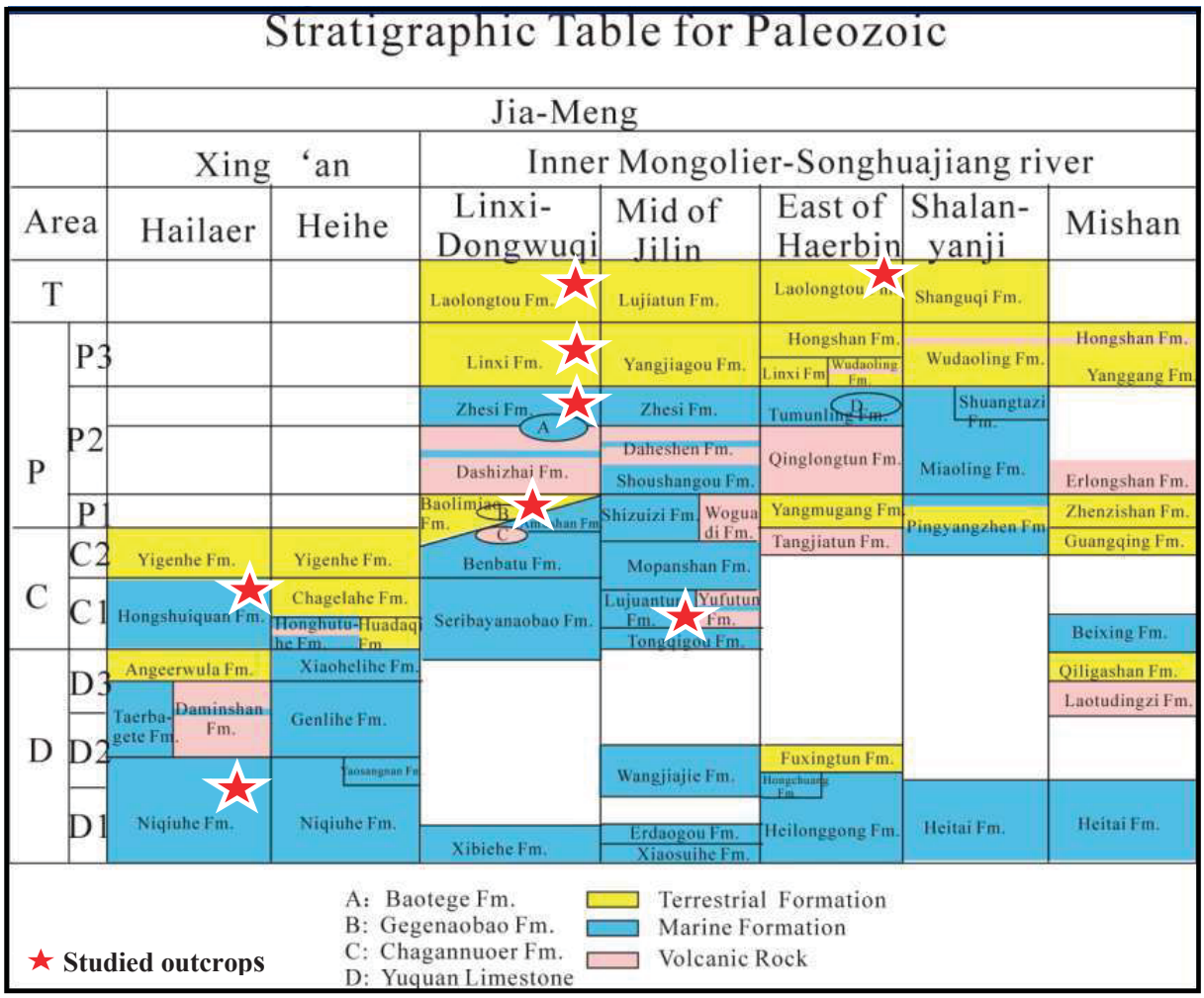

Figure 14: *Stratigraphic table of the Upper Palaeozoic strata (Wang et al., 2008, unpubl.). Location of the cross section from the Hailaer Basin to Mishan is shown in figure 12. Stars indicate formations from which samples were taken for source rock analysis. D: Devonian; C: Carboniferous; P: Permian; T: Triassic.*

The Middle Permian marine Zhesi Formation and its eastern correlatives are characterized by abundant fossils, shown in figure 15. The well-preserved state of early Devonian and middle Permian fossils has been used as an argument that they have not been exposed to high temperatures and pressures characteristic for metamorphosed rocks. The facial distribution of the Middle Permian sediments along the southern margin of the Jiameng block is displayed in figure 16. Later, the sinistral strike slip faults caused displacement of the Permian strata.

Figure 15: *Well preserved fossils of the early Devonian and middle Permian from the southern continental margin of the Jiameng Block, indicating that the Upper Palaozoic strata did not undergo strong metamorphism (Wang et al., 2008, unpubl.).*

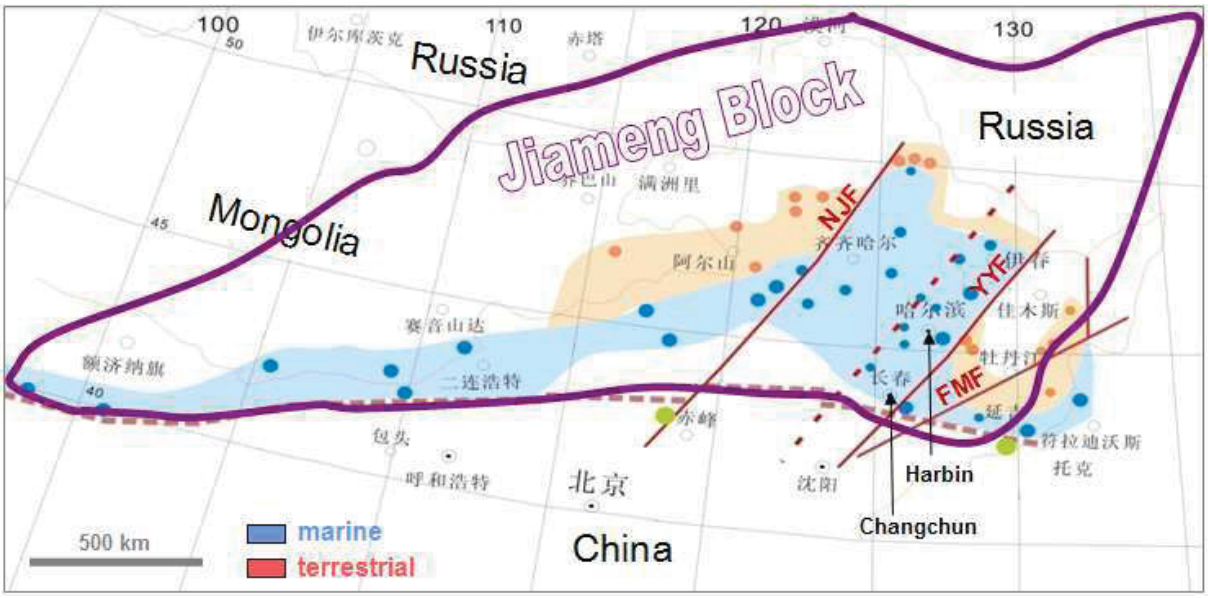

Figure 16: *Distribution of shallow marine and terrestrial facies along the southern margin of the Jiameng Block during middle Permian times (modified after Wang et al., 2008). NJF: Nenjiang fault; YYF: Yilan-Yitong fault; FMF: Fushun-Mishan fault.*

The marine Zhesi Formation is overlain by terrestrial sediments, inferring that the Palaeo-Asian Ocean was closed by the collision of the North China craton with the Jiameng block in the late Permian.

Published papers about the stratigraphy of the Upper Palaeozoic strata are in Chinese and detailed lithological descriptions, information about thicknesses, the depositional environment and facies distribution of the formations are not yet available in international journals. Therefore, brief descriptions of outcrops of the investigated formations are provided in the following section.

Outcrop description

The locations of the 15 outcrops are indicated in figure 13. Eighty three source rock samples were taken from the surroundings of the Songliao Basin in order to evaluate their maturity and hydrocarbon generation potential. The GPS coordinates of the sample locations are shown in appendix I, at which the outcrops are listed in an ascending order of their stratigraphic age.

Outcrop 1 is situated south of Mingcheng in Jilin Province. The samples T1 – T5 were taken from the Lower Carboniferous Lujuantun Formation, which consists of alternating limestone and black shale layers. This formation is overlain by the carbonatic Mopashan Formation. Mineralized veins (figure 17) and incipient foliation were observed in the steeply bedded layers, indicating that the thermal regime had reached an anchi-metamorphic stage.

Figure 17: *Mineralized veins in the black shales of the Lower Carboniferous Lujuantun Formation. Sample location of T3 in outcrop 1.*

Outcrop 2 is located south of Yantongshan in Jilin Province at a road-cut. Here, the Lower Carboniferous Lujuantan Formation is unconformably overlain by the Triassic Laolongtou Formation. Sample T6, a light brown shale, derives from the Triassic formation, whereas the samples T7 to T10 come from underlying Carboniferous black shales. The sample locations within the Lujuantun Formation are separated by a 50 m thick limestone bank. Some folded, thin sandstone layers within the dark, fine-grained sediments could be attributed to slumping events (figure 18).

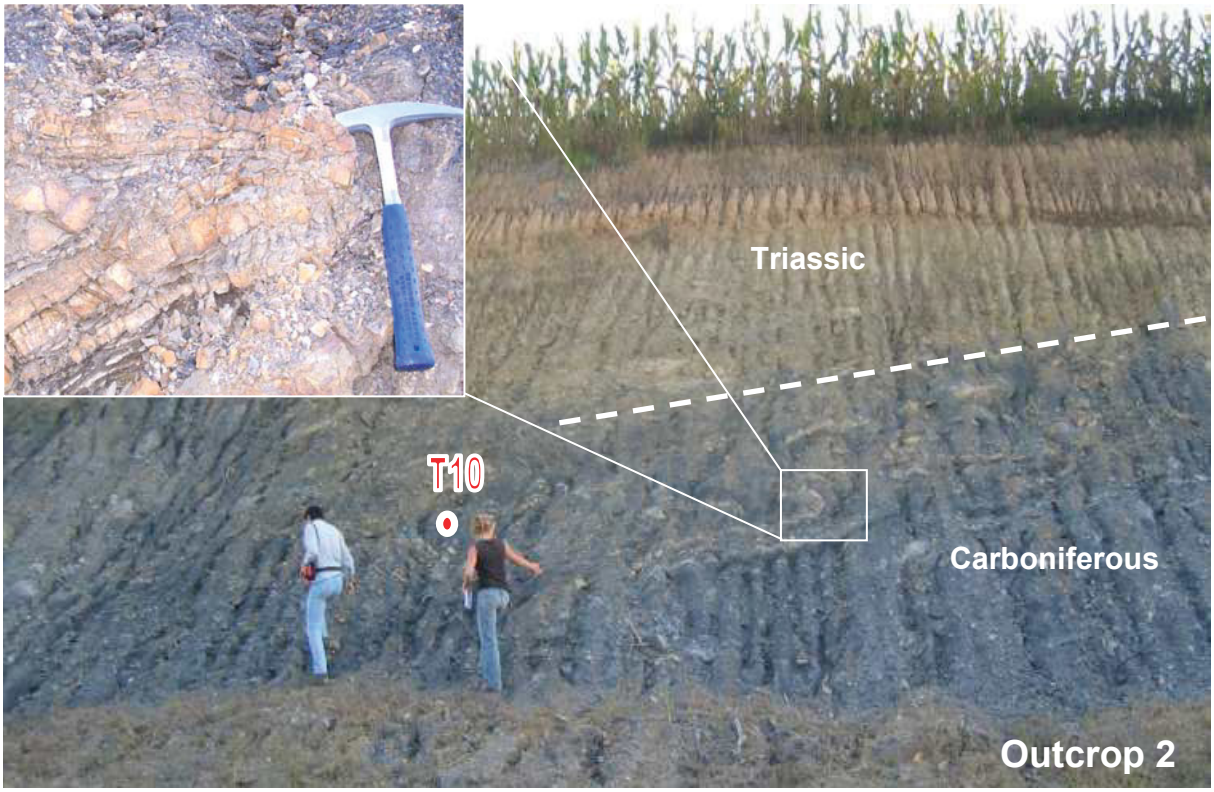

Figure 18: *The Lower Carboniferous Lujuantun Formation in outcrop 2 shows slumping features and is unconformably overlain by the Triassic Laolongtou Formation. Sample location of T10 is indicated.*

Outcrop 3 is in Heilongjiang Province, approximately 40 km southeast of Harbin and south of Yuquan. The marine Middle Permian Zhesi Formation is composed of dark shales, which are intercalated with limestones. The samples T11 – T15 were collected. Sample locations of T11 – T13 are shown in figure 19.

Outcrop 4 is in a quarry close to Yuquan. The investigated stratigraphic thickness of the Middle Permian Zhezi Formation was about 70 m, at which the major part is constituted by black shales. The thicknesses of the limestone layers vary between 90 cm and 5 m. In figure 20 the sample locations of T16 and T17 are indicated. T18 to T22 were taken further up the dirt track.

Figure 19: *In outcrop 3 the Middle Permian Zhesi Formation consists of dark shales and limestones. Sample locations of T11 – T13.*

Figure 20: *Sample locations of T16 and T17 in outcrop 4, a quarry in proximity to Yuquan.*

Outcrop 5, on the western side of the Songliao Basin, is located 55 km southwest of Zhalantun at a road-cut of the Inner Mongolia highway. Sanhecun in the county Huifengchuan is the nearest village. The samples T23 – T30 were taken from thin-bedded flysh-like sediments of the Triassic Laolongtou Formation. The beds of sand and shale reveal a thickness of 5 to 20 cm. Observed features like fining upward gradation and sand, which had subsided into the clay, are characteristic for flysch deposits. Figure 21 shows the sample location of T30.

Figure 21: *Thinly bedded flysh-like sediments of the Triassic Laolongtou Formation in outcrop 5 in Inner Mongolia. Sample location of T30 is indicated.*

Outcrop 6 is on the same Inner Mongolia highway, 41 km to the north of outcrop 5 and 7.5 km south of Xilin. The outcropping strata of the Xilin Formation is of early Permian age and is composed of mainly black shales, interlayered with sandstones, tuffs and a 4 m thick basalt layer (figure 22). The bedding is steep (156/74) like in most other outcrops. Three samples (T31 – T33) were collected at this site.

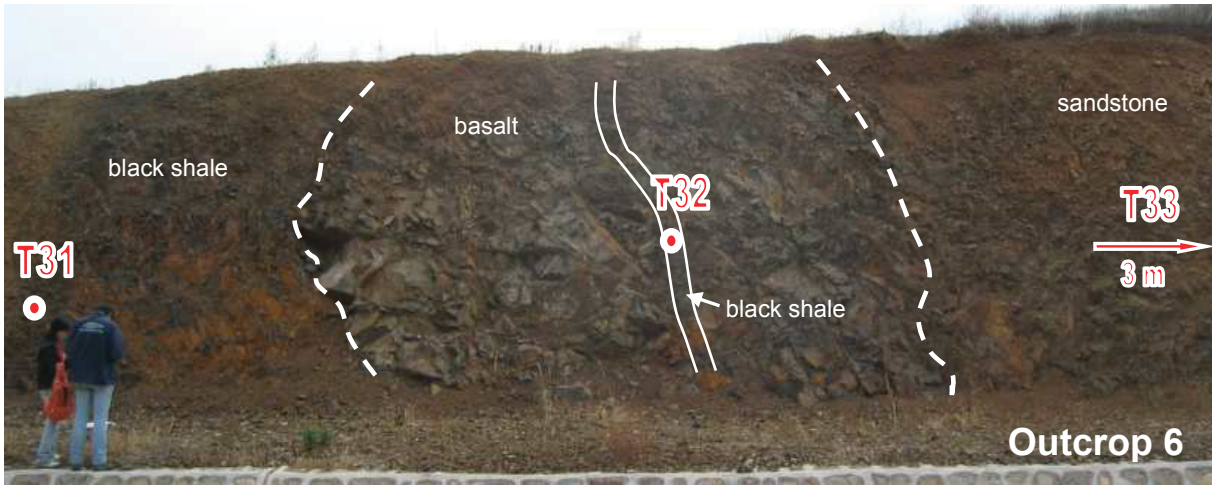

Figure 22: *Basalt layer and sample locations of T31 –T33 of the Lower Permian Xilin Formation.*

Outcrop 7 is a more than 1000 m long NW-SE trending profile, situated 6 km southeast of Suolun. The samples T34 - T47 (beginning at the southeastern end) were taken every 25 to 50 m, where the Middle Permian Zhesi Formation was not covered by vegetation. A transition in lithology from mainly sandstones interbedded with some thin shales layers to almost pure shale deposits after the sample location of T39 was observed. Figure 23 displays a foliated (181/65) shale layer between moderately dipping (170/47) sandstone beds at the sample location of T39. At T42 a roughly 4 m thick folded quartz vein is in discordant contact with the black shale layers (figure 24). The latter were greenish discoloured at the contact, probably as result of chloritization when the quartz vein intruded.

Figure 23: *Foliated shale layer of the Middle Permian Zhesi Formation at the sample location of T39 in outcrop 7, six km southeast of Suolun in Inner Mongolia.*

Figure 24: *Quartz vein next to sample location T42 in outcrop 7.*

Outcrop 8 is located 1.3 km north of Suolun. Along the profile of the Upper Permian Linxi Formation some ripple marks, slight bioturbation, plant remains and a folded coquina horizon (figure 25) were found, pointing to a shallow marine setting. However, in the stratigraphic table (figure 14) the Linxi Formation is indicated as terrestrial. The samples T48 – T56 were taken in this outcrop.

Figure 25: *Coquina horizon in outcrop 8 of the terrestrial Upper Permian Linxi Formation close to Suolun in Inner Mongolia.*

The samples of outcrops 9 to 15 (L1 – L28) were taken by Chinese colleagues and forwarded to Leoben. The GPS coordinates and the investigated formations are indicated in appendix I.

Stratigraphy of the Songliao Basin

The non-marine basin fill of the Songliao Basin is dominated by Cretaceous fluvial and lacustrine sediments with minor volcanoclastic intercalations, making up most of the total thickness of about 6000 to 7500 m (Yang, 1984). Generally, the stratigraphic sequence from Upper Jurassic to Tertiary sediments is subdivided into twelve formations using the stratigraphic time scale of Gradstein et al. (1994).
The following formation descriptions are based on an overview provided by Zhou (1998) about lithofacies and distribution of the formations, whereas thicknesses of the formations, assigned to the deepest graben structure, the Qijia Gulong depression, were taken from Yang (1984). The latter author assumes generally lower values for thicknesses than Zhou (1998), who suggests a total thickness of nearly 10,000 m.
The basin fill of the Songliao Basin is divided into three sections separated by two regional unconformities.

The oldest sediments in the Songliao Basin form the Upper Jurassic Houshiling Formation (J3h) (figure 26) which consists of mainly volcanoclastic and volcanic rocks interbedded with some coal seams. The sediments are restricted to the bottom of the graben structures and overlie unconformably the basement.

The Lower Cretaceous Shahezi (K1sh) and Yinchenzi (K1yc) Formations are characterized by alluvial, fluvial, swamp and lacustrine deposits comprising sandstones, conglomerates, shales and coal seams. Seismic data reveal that fan-delta sandstones grade into the lacustrine mudstones of the basin center facies. Ma et al. (1989) suggest multi-stage volcanic activities based on numerous layers of volcanic debris and pyroclastics.

Separated by a regional unconformity, the Lower Cretaceous Denlouku Formation (K1d) oversteps the deep central depression zone and spreads widely over the horsts and the lower flanks of the basin. The 1900 m thick formation comprises four members according to sedimentary cycles of coarse-grained sandstones and conglomerates at the bottom, fine-grained sandstones in the middle part, which coarsen upwards again towards the top. In the area of the central depression 40 to 80 m of dark grey, lacustrine mudstones were deposited. The uppermost part of the Denlouku Formation is composed of sand-shale interbeds.

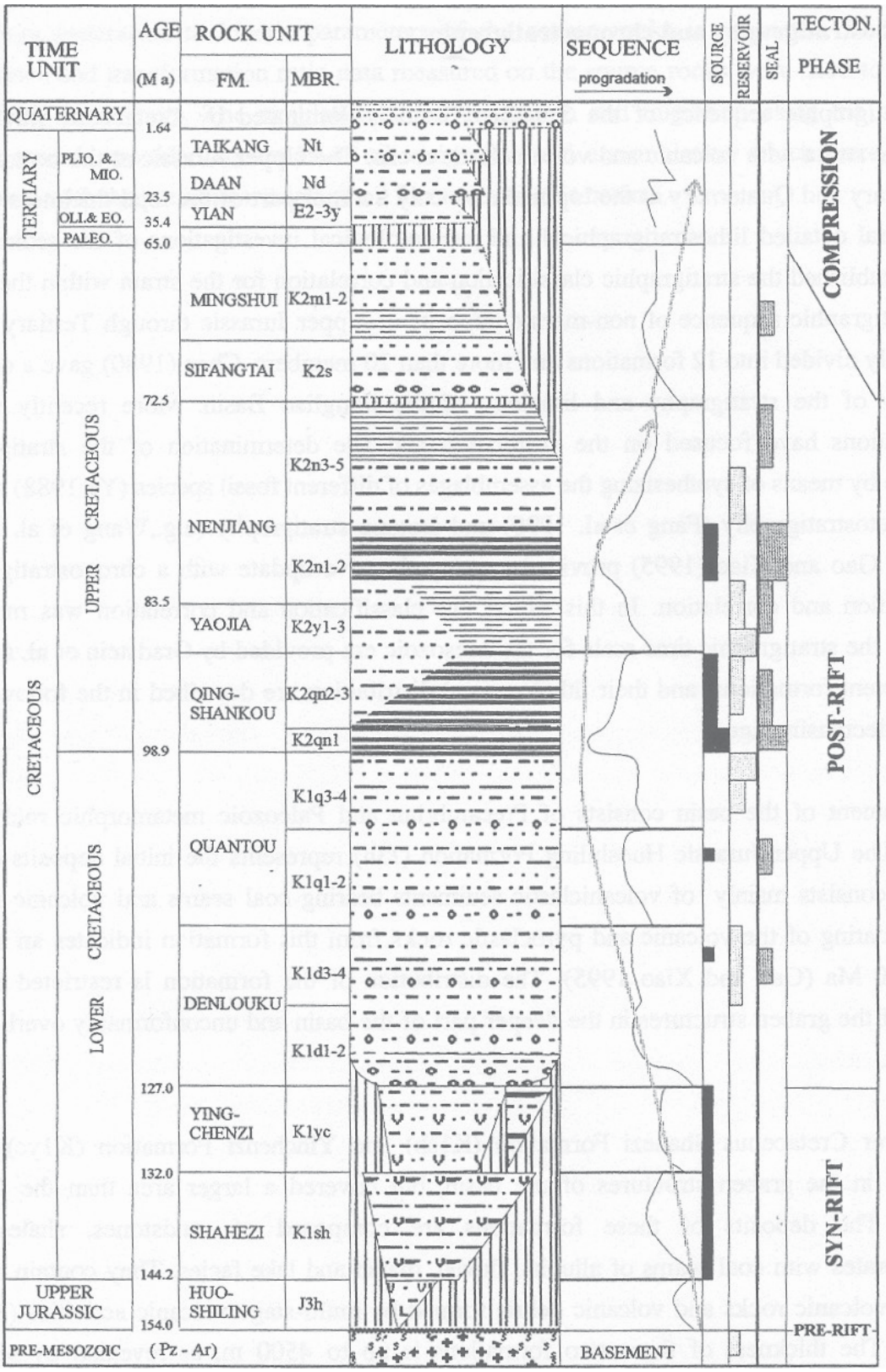

Figure 26: *Stratigraphic chart of the Songliao Basin. Reservoir rocks, source rocks and seals are indicated (Zhou, 1998).*

Similar to the Denlouku Formation also the Aptian Quantou Formation (K1q) contains important reservoir horizons, especially in the eastern part of the basin. Interlayered sandstones and shales were deposited in a fluvial environment and covered the margins of the Songliao Basin. The sequence is subdivided into four members and reaches a thickness of approximately 1600 m in the Qijia Gulong depression.

The main source rock of the Songliao Basin is the widely distributed lacustrine Upper Cretaceous Qingshankou Formation (K2qn), deposited during a large scale lake transgression and subsequent regression. Wang et al. (1994) put the lake transgression into context with a global sea level rise. Figure 27 taken from Li et al. (1995) illustrates the facies distribution of the two members of the Qingshankou Formation.
The lower member (K2qn1) contains lacustrine, organic-rich, black shales, 75 to 120 m thick, forming major oil-prone source rocks. The deeper lacustrine facies covers a vast area (~ 87,000 km²) including the central depression and the southeast uplift zone changing into terrestrial facies along the northern, western and southwestern margins. Zhou (1998) advocates that the inlet for the transgression was situated on the southwestern side of the basin according to the distribution pattern of deeper lacustrine facies.
Within the upper member of the Qingshankou Formation (K2qn2-3) the deep lake facies is confined to the central depression, indicating a fall of water table and, thus, regression of the lake. Interbedded sandstones and shales were deposited in floodplains and deltas of the tributaries. The total thickness of the lacustrine Qingshankou Formation is about 400 m.

The 200 m thick Upper Cretaceous Yiaojia Formation (K2y) comprises fluvial-deltaic sandstones intercalated with shales. The sandstone bodies form the major reservoirs of the Songliao Basin which were charged by the underlying source rocks of the Qingshankou Formation (Xu and Wang, 1981). For example, sands of the Yiaojia Formation represent the reservoir rock in the northern part of the giant Daqing oil field. Wang et al. (1994) propose that six major, prograding fluvial systems shed sedimentary freight from the hinterland into the lake, which occupied the central depression, on the basis of palaeoenvironmental reconstructions.

During a second transgressive period the Upper Cretaceous lacustrine Nenjiang Formation (K2n) was deposited. The formation is more than 1000 m thick and is subdivided into

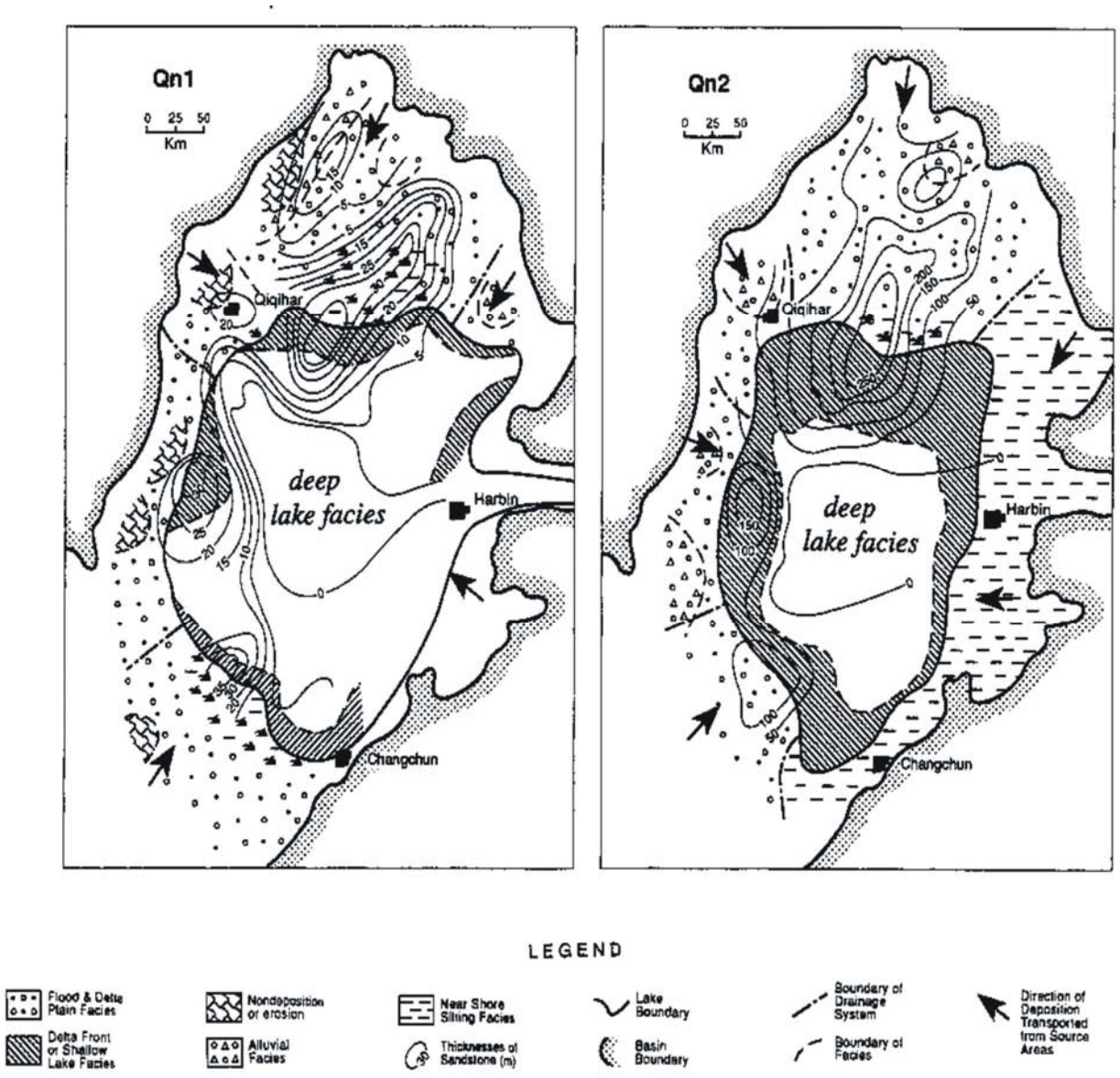

Figure 27: *Facies distribution of the lower (K2qn1) and upper (K2qn2-3) member of the Qingshankou Formation, the main source rock in the Songliao Basin (Zhou, 1998; modified after Li et al., 1995).*

five members. The accumulation of greyish-black, organic rich shales and silty mudstones of the first two members reflect a vast lacustrine palaeoenvironment covering an area of about 100,000 km² (Yang et al., 1984), which developed during the Santonian and Campanian. The lower members of the Nenjiang Formation act as regional seal for the reservoir horizons of the Yiaojia Formation and represent also the second important source rock interval in the Songliao Basin. The upper members consist of muddy siltstones and silty mudstones, at which the top of the formation is truncated, in particular at the southeastern uplift, signalling the second regional unconformity.

The Sifangtai (K2s) and the Mingshui (K2m) Formations are of Maastrichtian age (Ma et al., 1989) and overlie unconformably the Nenjiang Formation. Ryder et al. (2003), referring to the stratigraphic classification of Li (1995), consider the Sifangtai Formation as Cenomanian in age and the Mingshui Formation as Danian in age. Whether or not a regional unconformity exists between the Sifangtai and Mingshui Formation plays an important role for burial history and petroleum generation reconstructions. Assumed that no unconformity is present would result in an aberrantly high geothermal gradient (> 50 °C/km) to account for the significant oil production of the Qingshankou source rocks. Related to the late Cretaceous – Tertiary partial inversion of the Songliao Basin, either the suggested unconformity between the Sifangtai and Mingshui Formations or an unconformity between the Mingshui Formation and the Tertiary Yian Formation could have resulted in uplift and erosion of 500 – 1000 m of Upper Cretaceous sediments.
Wang et al. (1994) mention that deposition of the concerned formations was influenced by westward migration of the main depocenter, due to uplift and erosion of the eastern margin of the Songliao Basin. The Sifangtai Formation is composed of alluvial and fluvial red sandstones and shales, whereas the 400 m thick Mingshui Formation comprises thick sandstones and sandy conglomerates at the base and an increasing number of shale layers in the upper part. The reddish colour of the alluvial plain and alluvial fan deposits is attributed to prolonged subaerial exposure (Ryder et al., 2003).

Zhou (1998) advocates for a gap in the stratigraphic record between 65 and 35.4 Ma as indicated in the stratigraphic chart in figure 26, followed by the deposition the Oligocene Yian Formation, the Miocene Daan Formation and the Pliocene Taikang Formation. Tertiary sediments accumulated to a thickness of 400 m and consist of fluvial plain deposits like mudstones, shales, sandstones and sandy conglomerates, restricted mainly to the northwestern part of the Songliao Basin. Overlying loose gravels and flood plain clays constitute the Quaternary deposits, reaching a thickness of 100 m.

2.3 Petroleum geological aspects of the Songliao Basin

Two separate petroleum systems were identified in the Songliao Basin (Ryder et al., 2003). First, the Upper Cretaceous Qingshankou – Putahua/Shaertu system and second the Jurassic coal – Denlouku/Nongan system. Although 99 % of known petroleum derives from the

Qingshankou – Putahua/Shaertu system, the Jurassic system provides important information about potential basement source rocks. The aerial distribution of the oil and gas fields in the Songliao Basin (figure 11 and 12) shows that the majority of the hydrocarbon accumulations are situated within the central basinal area. The remainder is spread over the western slope, the southeastern uplift and the northeastern uplift. Until 1996, estimated 17.6 BBOE (billion barrels oil equivalent) of ultimately recoverable oil and 0.3 BBOE of associated gas were produced (Ryder et al., 2003). Ulmishek (1993) expects that numerous smaller oil and gas fields will be discovered in the Songliao Basin, though the augmentation in total resources would account for only a small percentage of those discovered to date.

Upper Cretaceous Qingshankou – Putahua/Shaertu petroleum system

Crude oils of the Qingshankou – Putahua/Shaertu petroleum system show relatively consistent API gravity values (30 – 35°), high paraffin content (12 - 30 %), low sulphur content (0.05 – 0.23 %) and gas-oil ratios of GOR = 50 to 300 ft^3 of gas per barrel of oil. However, subtle differences of biomarker distributions induced Li et al. (1987) to speculate about two distinct petroleum systems, the Qingshankou – Putahua system and the Nenjiang – Shaertu system. Ryder et al. (2003) state that the number of conducted biomarker analyses is yet too small and at least 100 additional analyses would be required to discern the Qingshankou – Putahua and the Nenjiang – Shaertu petroleum systems. Even if these systems could be distinguished, the processes of generation, migration, entrapment and preservation are very much alike so that assessment and recovery of the resources would probably not be enhanced.

The lacustrine organic-rich mudstones and shales of the Qingshankou Formation are the main source rocks the petroleum system as well as of the whole Songliao Basin (figure 28), followed by the lower member of the Nenjiang Formation, representing the second most important source rock. The black shales were deposited under deep-water, eutrophic lacustrine conditions and extended over an area of 100,000 km^2 covering the central depression as well as parts of the western slope and the northeastern and southeastern uplift zones. The organic matter in the deeper portions of the lake is dominated by algae and bacteria, whereas some terrestrial input of land plants, which flourished at the lake shores and its surroundings, can be observed in shallow-water marginal areas (Yang et al., 1985).

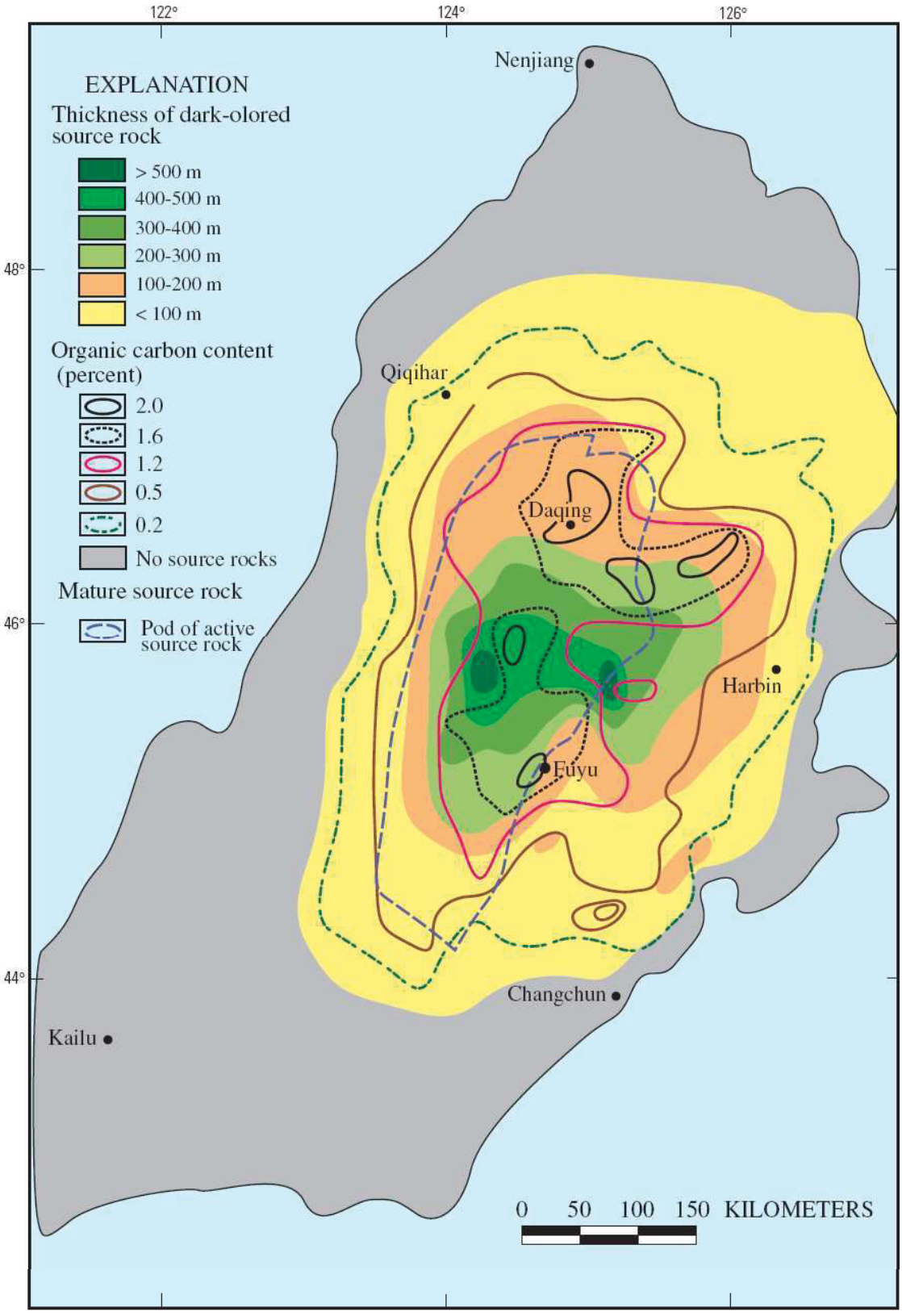

Figure 28: *Distribution of thickness and total organic carbon content of the Qingshankou source rocks. Dashed blue line indicates limit of mature source rocks, which coincides with central basinal area in figure 12 (Ryder et al., 2003).*

A marine influx during maximum stage of transgression, influencing the deposition and composition of the organic matter was proposed by Ye and Wei (1996) and Schwans et al. (1997).

Total organic carbon contents (TOC) range from 1.5 to 8.4 % in the Qingshankou and Nenjiang Formations and average out at 2.5 % in Qn1, the lower member of the Qingshankou Formation, 1.5 % in the upper Qn2 member, and 2.9 % in N_1, the lower member of the Nenjiang Formation (Zhang, 1984; Yang et al., 1985; Li et al., 1987; Li, 1995; Zhou, 1998). The hydrogen index (HI) in the two concerned formations varies from 200 to 900 mgHC/g orgC, reflecting that the organic matter is predominantly of the oil-prone kerogen type I (> 650 HI) and type IIA (450 – 650 HI) (Yang et al., 1985; Zhou, 1998). In the central basinal area and parts of the western slope where burial depths amount to 2500 m, the Qingshankou Formation is fully within the oil window, revealed by vitrinite reflectance values ranging from 0.64 to 1.4 % Ro (Zhou, 1998). In contrast, the less deep buried Nenjiang Formation has only reached a marginal stage of maturity (0.5 – 0.7 % Ro). The lateral variations of both thickness and the total organic carbon content as well as the pod of thermally mature source rocks of the Qingshankou Formation are displayed in figure 28.

A short introduction about source rock parameters such as HI and OI indices, kerogen types, TOC and maturity is given in the chapter ‘analytical approach and methods’.

Most of the oil was generated in the Qijia-Gulong, Shanzhao and Changling depressions (inset in figure 12), migrated updip into the Gaotaizi, Putahua and Shaertu reservoirs and accumulated in the growing central Daqing anticline and the adjacent western slope and southeastern uplift (Yang, 1985) (figure 29). Some of the produced petroleum was expelled downwards into to conformably underlying Fuyu and Yangdachengzi reservoirs of the Quantou Formation. The 250 to 500 m thick Gaotaizi reservoir intertongues with the upper member of the Qingshankou Formation. According to Xu and Wang (1981) and Yang (1985) are the Putahua and the Shaertu reservoirs of the Yiaojia Formation and the basal Nenjiang Formation the most prolific ones, since 12.1 BBOE (Ryder et al., 2003) of the total amount of recovered hydrocarbons were produced from these reservoirs. Vertical migration paths appear to be minimal and simple, because numerous traps have been filled directly by source rocks in immediate proximity (Yang, 1985; Li et al., 1987). Distances of lateral secondary migration are usually within a range of 10 to 50 km (Yang, 1985).

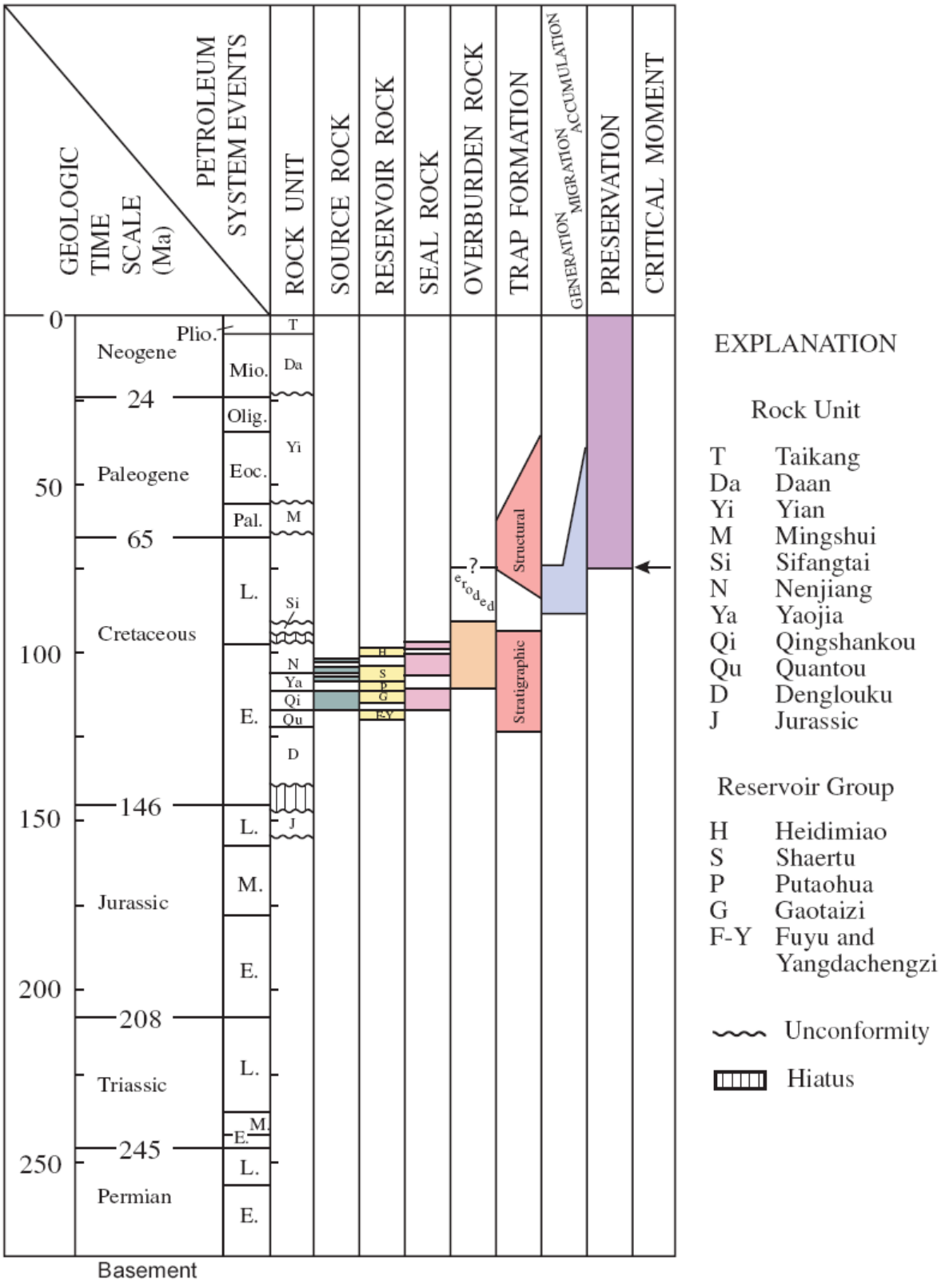

Figure 29: *Events chart of the Upper Cretaceous Qingshankou – Putahua/Shaertu petroleum system (Ryder et al., 2003).*

The predominant source rock for the Yangdachengzi, Fuyu, Gaotaizi and Putahua reservoirs is the Qingshankou Formation, based on oil-source rock correlations using biomarker distributions and $\delta^{13}C$ data. In contrast, the Heidimiao reservoir is entirely charged by the underlying Nenjiang source rocks, because the up to 220 m thick black shales of the lower member of the Nenjiang Formation represent a tight regional seal (Gao and Liu, 1984; Kong, 1984; Li et al., 1987). There is some controversy whether the source rocks of the Qingshankou or the Nenjiang Formation replenished the Shaertu reservoir. Ryder et al. (2003) suggest that both source rocks were important, however because of the thermally higher maturity of Qingshankou source rocks, they consider that the latter had a greater influence.

Jurassic coal – Denlouku/Nongan petroleum system

Only about 1 % of the discovered hydrocarbons derive from the Upper Jurassic coal-bearing strata, but this still amounts to 37 MMBOE (million barrels oil equivalent) (Petroconsultants, 1996). At least 10 fields of the total 81 in the Songliao Basin are affiliated either partly or fully with this petroleum system (Ryder et al., 2003). More discoveries are expected, since exploration focuses on the deeper, undrilled parts of the basin. The U.S. Geological Survey (2000) estimates as a mean value 3.21 TCF (trillion ft^3) of undiscovered conventional gas resources in structural traps of the Jurassic coal – Denlouku/Nongan petroleum system.
To clarify, Ryder et al. (2003) include into the Jurassic coal-bearing strata the Shahezi and Yingcheng Formations, which Hu and Krylov (1996) and Zhou (1998) regard as Lower Cretaceous formations.

Coal seams of the Upper Jurassic Shahezi and Yingcheng Formations are assumed to be the main source rocks of the petroleum system, although a gas-source correlation based on geochemical investigations has not yet been performed. The deeper parts of the Songliao Basin are still underexplored and only a few wells penetrated the Jurassic rocks. The existence of coal beds is rather deduced from commercial outcrops at the flanks of the basin (Yang and Shen, 1986; Wang and Hu, 1993; Cheng et al., 1997; Lu et al., 1997). The occurrence of some oil in the Nongan reservoir in the lowest member of the Quantou Formation portends that oil-prone Jurassic source rocks exist in the basin. Li et al. (1987) rather believe that the liquid hydrocarbons were derived from the Upper Cretaceous Qingshankou Formation by downwards migration or across fault blocks. Another possibility would be that the small amount of oil was generated locally by shaly interlayers either in the Denlouku or the

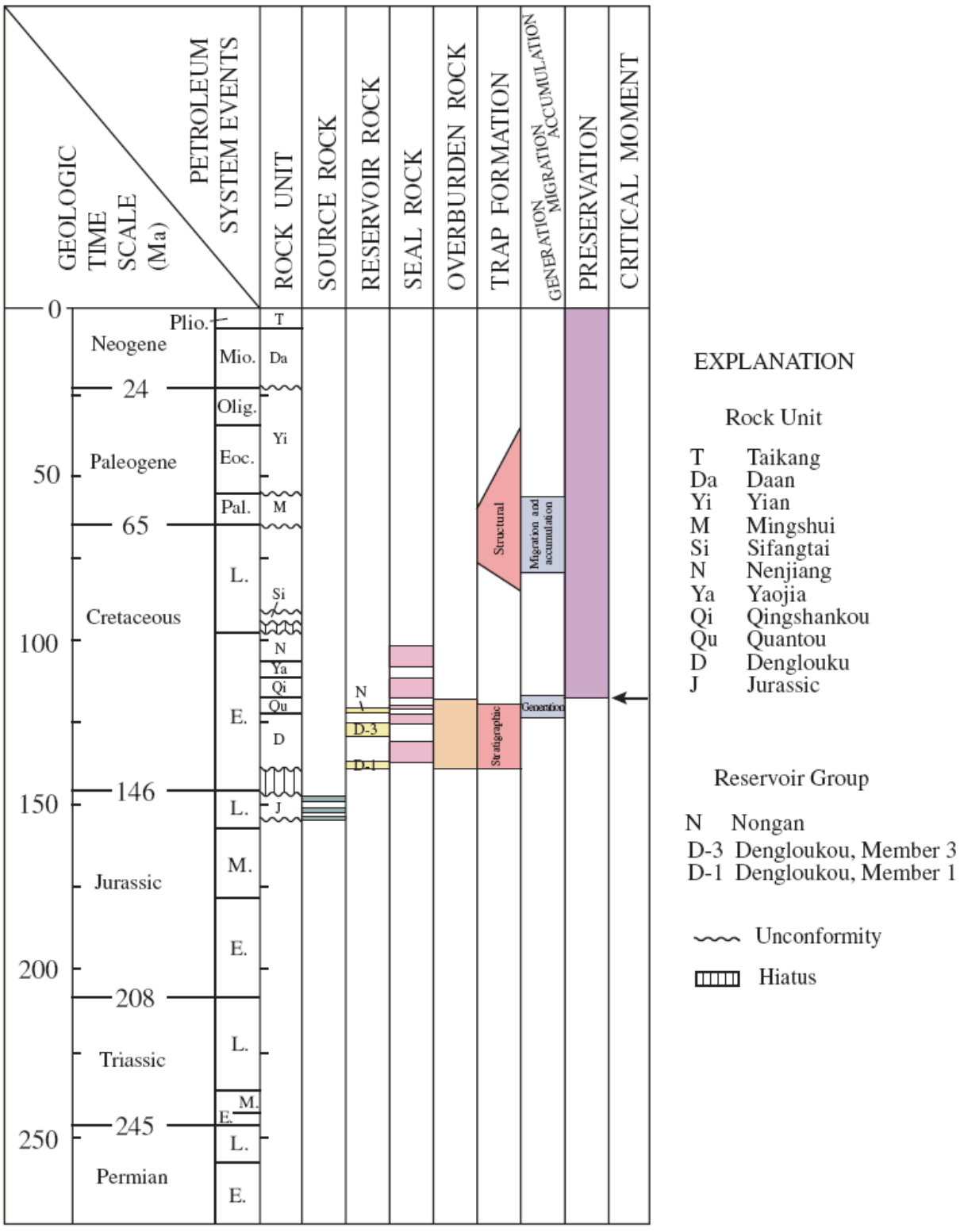

Figure 30: *Events chart of the Jurassic coal – Denlouku/Nongan petroleum system (Ryder et al., 2003).*

Quantou Formation. To date, no petrographic and geochemical data from the Jurassic coal beds are available, though the type of organic matter is considered to be of the gas-prone kerogen type III. By the means of coalification gradients, derived from five wells, vitrinite reflectance values (Ro) are prognosticated to range from 3 to 5 % in the deep graben structures and 1 to 3 % at the flanks of the Songliao Basin (Wu et al., 1991). With regard to basement source rocks this would imply that Permian-Carboniferous black shales are likely to be overmature beneath the deep depressions, but closer to the basin margins they could be still within the maturity window for hydrocarbon generation.

The reservoir intervals of the Jurassic coal – Denlouku/Nongan petroleum system include the first (D1) and the third (D3) member of the 1900 m thick Denlouku Formation as well as the lowest member (N, Nongan) of the Quantou Formation (figure 30). D1 overlies uncomformably the Jurassic coal-bearing strata, whereas the base of D3 and the Nongan reservoir are situated 900 and 1700 m, respectively, above the top of the source rock sequence. The natural gas, which was generated in the early fill of the grabens and half grabens migrated vertically upward, mainly along fault zones and eventually accumulated in the Lower Cretaceous sandstone reservoirs of the Denlouku and Quantou Formations (Yang, 1981; Hu et al., 1998). Very little lateral migration is assumed, because of the contiguousness of known gas fields to the Jurassic coal-bearing grabens. Rapid subsidence inferred that gas generation was initiated as early as early Cretaceous.
The gaseous hydrocarbons were trapped in stratigraphic traps, such as pinch-outs, and palaeostructures. Compressional tectonics during late Cretaceous to early Tertiary times led to a redistribution of the accumulated gas into the numerous anticlinal and inverted fault-block structures (Song, 1997; Hu et al., 1998).
Ryder et al. (2003) reckon that this petroleum system has good potential for undiscovered gas fields, because most of the major anticlines have not yet been drilled into or through the Denlouku Formation. Expected drilling depths for potential gas findings range between 2500 and 4000 m.

In addition to Jurassic source rocks, Ma et al. (2008) argue for Palaeozoic source rocks within the basement of the Songliao Basin. This gas might be trapped either within the Palaeozoic succession or might have migrated upward into the Mesozoic basin fill.

Thermal and burial history of the Songliao Basin

According to Cai (1995) and Pang and Lerche (1997) the present-day heatflow varies between 50 and 70 mW/m² in the Songliao Basin. Adjacent areas reveal a significantly cooler thermal regime than the Songliao Basin, which is related to shallow-lying Moho-discontinuity beneath the basin (Wu and Xie, 1985) (figure 31). Magmatic activity during late Jurassic times is recorded in the sediments of the Huoshiling, Shahezi and Yingchenzi Formations, advocating that the highest temperatures were attained during the syn-rift phase of the basin. This is in agreement with the rift basin evolution model of McKenzie (1978) and Kusznir et al. (1995) in which uprising asthenosphere induces rapid syn-rift subsidence followed by slow exponential post-rift subsidence (figure 32).

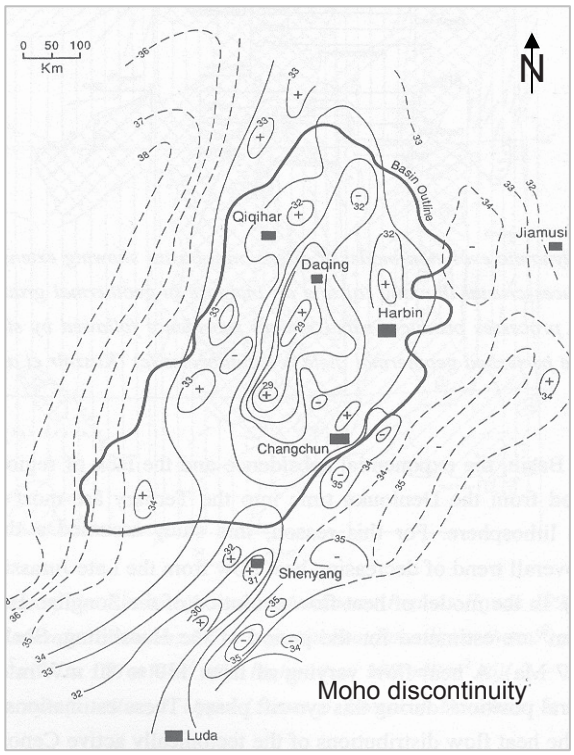

Figure 31: *Regional distribution of the Moho-discontinuity in northeastern China (Li et al., 1995).*

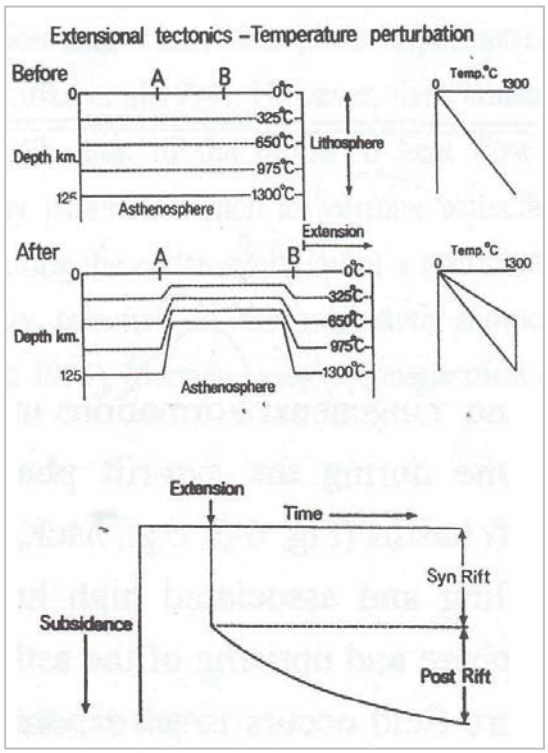

Figure 32: *Effects of crustal thinning on the geothermal gradient and rate of subsidence (Kusznir et al., 1995; modified after McKenzie, 1978).*

The Songliao rift basin bears analogy with the Cenozoic Rhine-Rhône rift system. Based on that, Zhou (1998) estimates that heat flows had ranged from 80 to 110 mW/m² during the syn-

rift stage depending on structural positions (figure 33). Higher heat flows were to expect in graben structures and along zones of active faulting and volcanism, whereas rift shoulders and horst blocks are usually characterized by a lower thermal regime. The palaeo-heat flow evolution for the time from the late Cretaceous to early Tertiary was calibrated by vitrinite reflectance data derived from five wells along the cross section. The values vary between 70 and 80 mW/m².

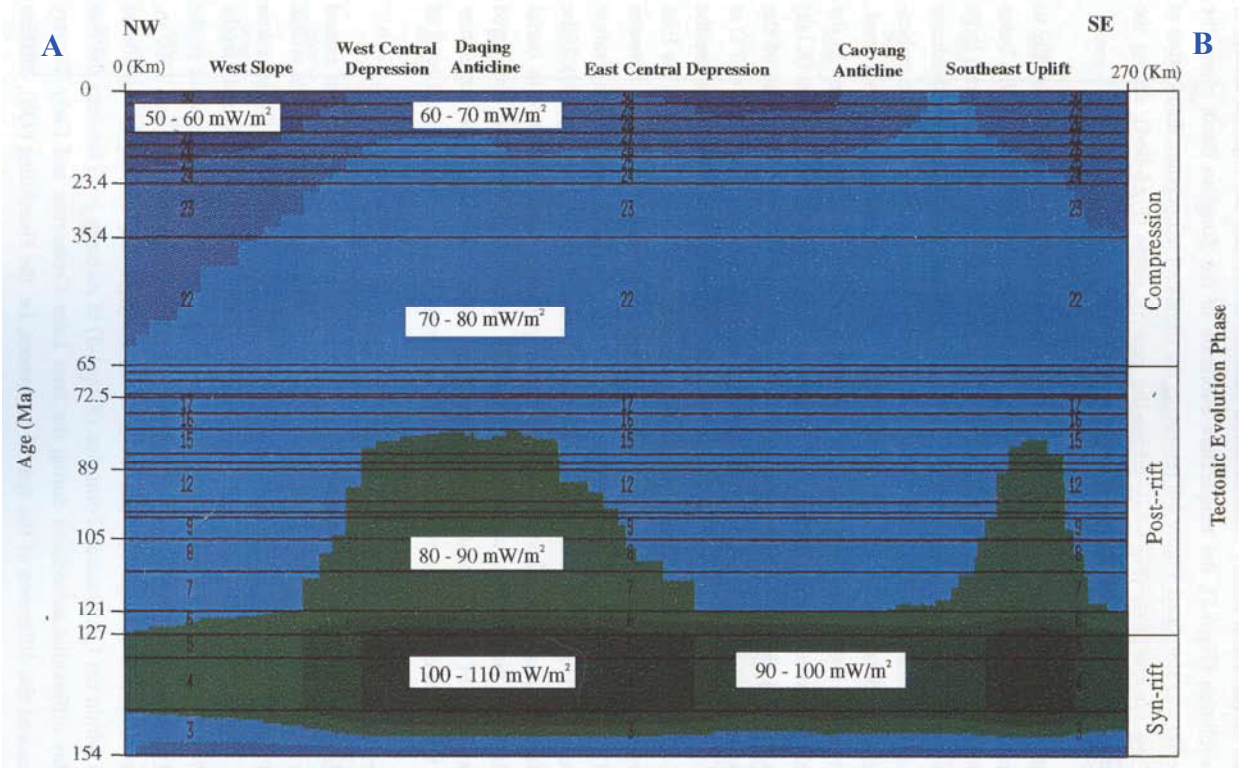

Figure 33: *Modelled heat flow evolution through time along a profile across the Songliao Basin (Zhou, 1998). Location of cross section (A-B) is indicated in the inset map in figure 34.*

Burial and thermal history reconstructions are a valuable tool to determine the timing of hydrocarbon generation and to get a better understanding of the petroleum system. Figure 34 shows a burial history plot for the Qingshankou – Putahua/Shaertu petroleum system of Ryder et al. (2003). To mention is that Ryder et al. (2003) consider the Qingshankou Formation of late Aptian age, referring to the stratigraphic classification of Li (1995). The time of major oil generation (= critical moment) of the petroleum system occurred during the late Campanian, when overburden rocks for the Qingshankou Formation attained a maximum thickness of about 3000 m. These 3000 m of overburden rocks comprise the Yiaojia, Nenjiang and

Sifangtai Formations as well as estimated 1000 m of eroded, unnamed Upper Cretaceous strata.

In simulations, an assumed geothermal gradient of 45 °C/km in combination with the presence of additional 1000 m of overburden rocks would result in the anticipated high rates of oil and gas generation for the period from 85 to 75 Ma (figure 34). If the 1000 m of eroded thicknesses were reduced to 500 m using the same geothermal gradient, only incipient oil generation and no gas generation would be yielded (Ryder et al., 2003). Similar results of burial and thermal history modelling were achieved by Yu et al. (1997). Also the calculated geothermal gradient of 46.6 °C/km by Wang and Xing (1991), deduced from fluid inclusions in the Shanzhao depression, supports this model.

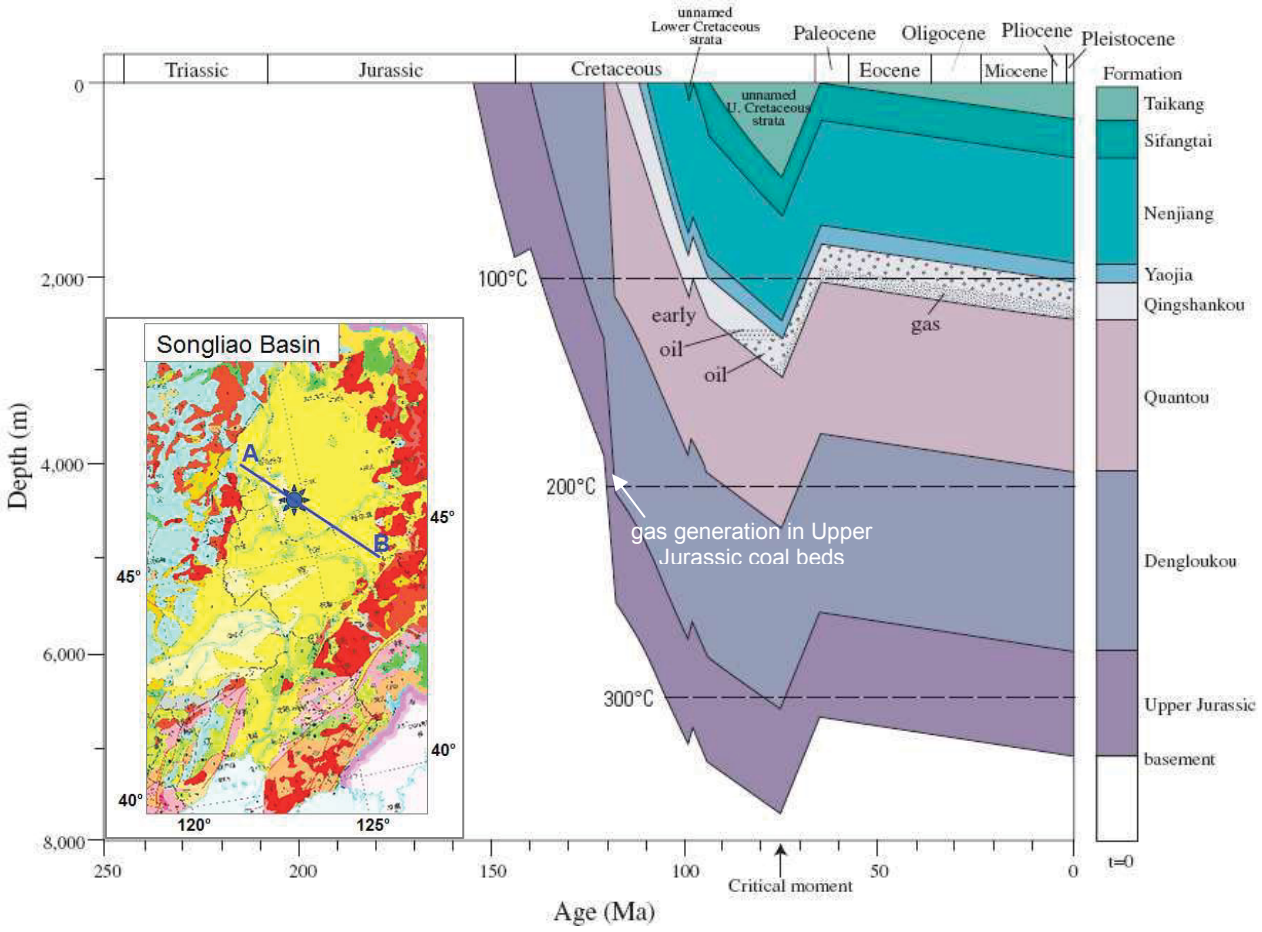

Figure 34: *Burial history plot for the Qingshankou – Putahua/Shaertu petroleum system in the Qijia-Guolong depression (modified after Ryder et al., 2003). The location within the Songliao Basin is indicated by a star in the inset map (modified after the Geological Survey of China, 2004). The profile (A-B) refers to the heat flow model in figure 33.*

However, using different approaches, other authors do not confirm the necessity of additional ~ 1000 m of removed Upper Cretaceous strata.

Li et al. (1987) suggest that the source rocks in the Songliao Basin reached the main oil generation phase at unusually low maturities (< 0.7 % Ro), based on biomarker distributions in the oils. Though, this conjecture is somewhat contradictory to the general opinion that kerogen type I, which is the main kerogen type in the Qingshankou and Nenjiang Formations, reaches peak oil generation at relatively higher levels of maturity. Moreover, Zhou (1998) reports of vitrinite reflectance values of up to 1.4 % (Ro) in the lower member of the Qingshankou Formation.

Hou et al. (1999) rather ascribe the lower maturation levels in the oils to a stage of elevated salinity during the deposition of the Qingshankou Formation. Although sulphur rich kerogen tend to attain oil generation at an earlier stage of maturity, higher salinities are not reflected in the very low sulphur content (0.05 - 0.23 %) of the crude oils.

By using variable palaeo-heat flows through time (figure 33) in combination with different kinetic reaction parameters, Zhou (1998) and Zhou and Littke (1999) created a model which yielded considerable oil generation of the Qingshankou Formation during Palaeocene-Eocene times, without significant removal of overburden rocks. However, the model is not consistent with the huge amounts of oil found in the basin.

Thus, the question about the thickness of overburden rocks eroded during the late Cretaceous compression and uplift phase remains open.

4. ANALYTICAL APPROACH AND METHODS

By the means of source rock parameters such as total organic carbon content and vitrinite reflectance, the quality and maturity of 83 samples of greyish to black shales of the Upper Palaeozoic basement of the Songliao Basin was determined. Information about the type and origin of organic matter can be obtained from RockEval parameters (hydrogen and oxygen index) as well as sulphur content. At first, a brief introduction is given about the process of coalification and the influence of different kerogen types on timing and products of hydrocarbon generation. Description of sample preparation and operating mode of Leco, Rock Eval pyrolysis, vitrinite reflectance measurement and X-ray fluorescence analysis is subject of the following sections in this chapter.

4.1 Coalification process and kerogen types

Kerogen is a complex three-dimensional macromolecule with aromatic cores connected by aliphatic bridge structures and side chains (Killops and Killops, 1997). It develops during burial of organic-rich sediments. Here, the term ‘diagenesis’ is used for the interval of shallow burial where temperatures do not exceed 50°C. Figure 35 displays the evolution of organic matter during diagenesis and catagenesis. Microbial activity enhances fragmentation and degradation of organic matter to humic substances and geopolymers. The different compounds of organic matter like carbohydrates, proteins, lipids and lignin are affected by processes of condensation, loss of hydrophile functional groups (e.g.: -OH, -COOH) and elimination of unstable components, though to a varying degree. Carbohydrates and proteins are split enzymatically into smaller molecules such as peptides, amino acids and saccharides, to be assimilated by bacteria. Remains of bacteria (hopanes), lipids and lignin are more resistant against biodegradational processes and may survive the stage of diagenesis almost unaltered. Even easily degradable matter can be preserved when it was incorporated into the stable kerogen matrix. At the end of diagenesis the kerogen consists of organic matter which is insoluble in organic solvents. In contrast, bitumen remains soluble and is made up of relatively small molecules broken off the kerogen structure.

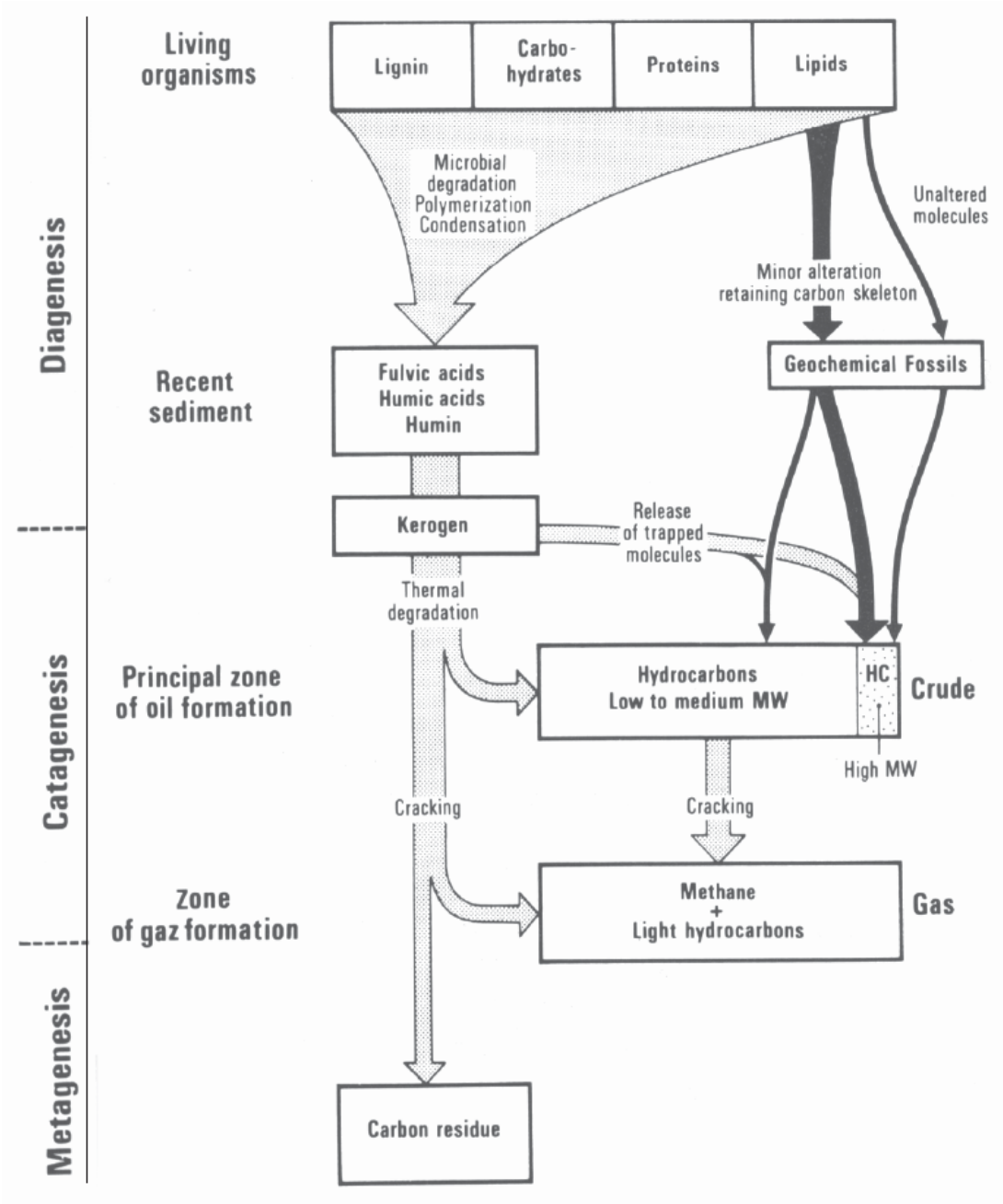

Figure 35: *Evolution of organic matter during diagenesis and catagenesis (Tissot and Welte, 1978).*

With increasing temperature and pressure mircrobial activity comes to a halt and the catagenetic stage begins. During catagenesis the carbon content increases, oxygen content decreases and hydrogen content remains relatively constant until late stage. Based on ongoing elimination of peripheral functional groups and aliphatic cross links the formation of compact aromatic structures is favoured. At temperatures between 100 and 150 °C the main phase of

oil generation occurs (oil window). The produced liquid hydrocarbons have relatively high molecular weights, however, when temperature rises hydrocarbons of decreasing molecular weight are formed. The limiting factor of hydrocarbon generation is the supply of hydrogen. The cyclisation and aromatisation of the residual kerogen leads to a release of hydrogen which is conveyed to split off alkyl chains. With increasing thermal energy the C-C bonds of the produced hydrocarbons become weaker and thermal cracking sets in. At the final stage of catagenesis the percentage of methane rises drastically indicating the transition to the metagenetic stage.

As the composition of kerogen is dependent on the original organic matter and consequently the depositional environment, there are also differences in the abundance of certain binding types (e.g.: C-C, C-S, C-O). Thus, the kerogen type has an influence on the hydrocarbon products and the timing of their generation (Tissot and Welte, 1978):

Kerogen type I

Kerogen type I, also called liptinite type, is relatively rare and shows a very high oil generation potential due to an initially high H/C ratio. Its high content in lipids, especially long aliphatic chains, derive from algal matter and remains of bacteria. The typical depositional environments are oxygen-deficient, quiet lagoons and lakes. Aromatic components and hetero-atoms (N, S, O) are of minor importance. For the destruction of predominant strong C-C bonds, higher thermal energies are required. Hence, the onset of the main oil generation phase takes place at higher levels of maturity in comparison to kerogen types II and III.

Kerogen type II

Kerogen of the type II refers to a marine depositional environment where autochtonous phyto- and zooplankton together with microbial material accumulates. The exinite type is the most common type and has both high H/C and O/C ratios and. It contains often considerable amounts of sulphur. The latter can either be reduced under the formation of pyrite provided that abundant Fe ions are available, which are supplied by clastic sediments, or the sulphur becomes incorporated into the kerogen structure by forming thiophenes, due to a lack of Fe in carbonatic environments. Allochtonous input of higher land plants effect the intermediate character of kerogen type II, which has a good oil and gas generation potential.

Especially sulphur-rich kerogens (type II-S) tend to an early production of hydrocarbons due to weak S-S and C-S bonds.

Kerogen type III

The vitrinite type consists of mainly polyaromatic cores and only minor aliphatic components such as short-chained groups, methyl-groups and some long-chained waxes and cuticles of leaves. This type derives principally from vascular plants, corroborated by recognizable plant remains (e.g.: spores, pollens, resins, woody structural components, cuticles of leaves). Kerogen type III reveals high O/C ratios and low H/C ratios, which is the reason why almost no liquid hydrocarbons are generated. The main product is gas.

Inertinit exhibits no hydrocarbon generation potential and probably originates from higher land plants, which were burned under oxidizing conditions for example in forest fires.

4.2 Total organic carbon and sulphur contents

The total organic carbon content (TOC), measured in weight % of the dry sample, indicates how much organic carbon is present in a rock, hence its quality as source rock. As a rule of thumb, TOC values exceeding 2 % are considered as excellent source rocks, whereas contents between 0.5 and 2 % are of moderate to good quality. From an economical point of view the minimum organic carbon content should not fall below 0.5 %, though this limit is dependent on the type of organic matter. A smaller amount of kerogen type I might produce more hydrocarbons than a relatively lager amount of organic matter of type III (Killops and Killops, 1997).

Two times, 100 mg of finely ground sample powder were treated with alcohol to measure the total carbon content. For measuring the organic carbon content the inorganic carbon content had to be eliminated by adding hydrochloric acid and alcohol another two times per sample. After drying, the samples were burned at 1500 °C in an oxygenated atmosphere with a LECO 300 CS^{TM} analyzer. Carbon reacts to CO_2 and is measured by an infrared detector. The amount of produced CO_2 gives information about the total and organic carbon content, respectively. The difference between total carbon content and organic carbon content is the percentage of inorganic carbon, which is a measure of the abundance of carbonate minerals.

The determination of sulphur content follows the same procedure, using the samples, which were treated with alcohol only. While burning, sulphur reacts to SO_2. The ratio of organic carbon to sulphur is used to distinguish freshwater facies from marine depositional environments. Berner (1984) assumes that TOC/S ratios of 2.8 ± 1.5 are typical for marine conditions, whereas higher ratios indicate freshwater environments. Lower ratios might indicate anoxic conditions. Calibration by C and S standards was conducted after every tenth measurement.

4.3 Rock Eval pyrolysis

Rock Eval pyrolysis is a method to mimic the process of thermal maturation of organic matter in a laboratory (Espitalié et al., 1977). It provides information about the hydrocarbon generation potential and the type of organic matter at lower levels of maturity, according to hydrogen index (HI) and oxygen index (OI). The transformation ratio and T_{max} are used as indicators for the stage of maturity the source rock sample attained. Figure 36 shows the process and the application of the results of Rock Eval pyrolysis.

For this study a Rock Eval 2 plus analyzer from VINCI Technologies was used in combination with Rockplus software. For the analysis, 100 mg of powdered sample were heated up to 300 °C. For three minutes the temperature was held constant, meanwhile free hydrocarbons in the sample turned into gaseous state and were recorded as S_1 peak (mg HC / g sample). Subsequent heating with a rate of 25 °C per minute up to a final temperature of 550 °C, induced generation of hydrocarbons by thermal cracking of non-volatile organic matter. The expelled hydrocarbons were measured by a flame ionization detector (FID), constituting the S_2 peak. The generated CO_2 during heating was trapped and measured by an infrared detector as S_3 peak.
The sum of S_1 and S_2 represents the petroleum generation potential of the source rock sample. The ratio of volatile hydrocarbons present in the sample to those, which were generated by thermal heating, is called transformation ratio or production index ($= S_1 / (S_1 + S_2)$). This ratio is directly proportional to maturity, implying that with increasing maturity the S_1 peak increases at the expense of a decreasing S_2 peak. Another maturity parameter is T_{max}, the temperature when maximum hydrocarbon production occurs during pyrolysis. This indicator is based on the principle that at higher levels of maturity more thermal energy is necessary to

release the remaining hydrocarbons from the kerogen matrix (Killops and Killops, 1997). According to Peters (1986) and Espitalié and Joubert (1987) the S_2 peak and T_{max} can be influenced by the mineral-matrix effect when heavy hydrocarbons are adsorbed and retained by clay minerals.

All samples have been measured twice and after ten samples both a standard and a blank (= empty cup) were measured for calibration.

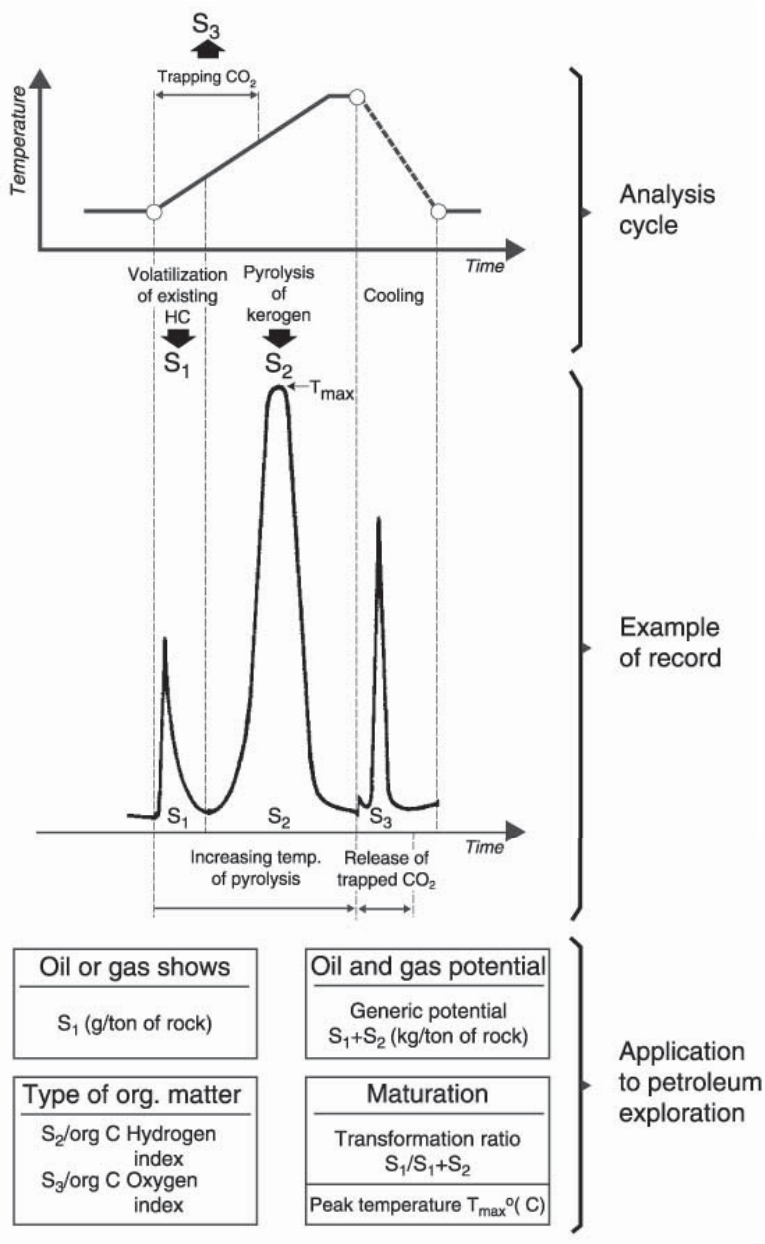

Figure 36: *Process and application of Rock Eval pyrolysis (Tissot and Welte, 1984)*

By the means of the S_2 and S_3 peaks the hydrogen index (HI) and oxygen index (OI) are calculated:

HI = S_2 * 100 / TOC (mg HC / g TOC)……generated hydrocarbons normalized to TOC
OI = S_3 * 100 / TOC (mg HC / g TOC)…… generated CO_2 normalized to TOC

In a Van Krevelen diagram the oxygen index is plotted versus the hydrogen index. Based on the distribution of the data points, the kerogen type and the stage of maturity can be identified. The maturation paths of the three kerogen types follow a convergent trend until in the end overmature, 'dead' kerogen with no hydrocarbon generation potential is left.

4.4 Vitrinite reflectance

This is an optical technique derived from coal petrography to determine the degree of maturity based on the reflectance of vitrinite group macerals (e.g.: Tissot and Welte, 1984; Mukhopadhyay and Dow, 1994). The reflectance increases progressively with thermal maturation, implying that it is an irreversible process and represents the highest thermal impact in the geologic history of the investigated rock sample. According to Killops and Killops (1997) this method is only applicable for kerogen types II and III, because of absence of vitrinite macerals in type I.
Vitrinite reflectance values from 0.65 % to 1.3% (Ro) represent the oil window and at higher levels of maturity a transition to gas generation phase takes place. Ro values exceeding 2 % refer to overmature source rocks and no hydrocarbons are expelled anymore.
Under a microscope vitrinite appears grey-coloured and brightens with increasing maturity, hence its reflectance increases (Stach et al., 1982; Schenk et al., 1989). The ordinary vitrinite reflectance (Ro) is measured under non-polarized light. Typically, inertinite reveals a higher reflectance than vitrinite, though a characteristic feature to distinguish vitrinite clearly from inertinite in (mature and) overmature samples is the bireflectance of the first. The anisotropy becomes apparent while rotating the section under polarized light. When the surface of the section is oriented the way that the maximum axis is aligned with the ray of incident light, the maximum reflectance (Rmax) is obtained. At right angles to Rmax the apparent minimum reflectance (Rmin) is measured (Taylor et al., 1998). With increasing maturity the anisotropy

becomes more evident, influenced by a preferred orientation of lamellae due to increasing burial load (Levine and Davis, 1989b). Lipitinite can be differentiated from other maceral groups because of its fluorescence under UV light. At higher levels of maturity (> 1.3 % Ro) liptinite begins to decompose due to instability with growing temperature.

The two samples with the highest TOC values of each outcrop were selected for vitrinite reflectance measurements. The organic matter in shales is finely dispersed and TOC values of at least 1 % are preferred in order to ensure validity of the results. The samples were cut perpendicular to the bedding plane and subsequently embedded in epoxy resin. The section preparation was conducted in six steps of grinding and polishing using silicon carbide powder (graining: 220, 800, 1200) and alcoholic diamond suspension (3 μm, 1 μm, 0.05 μm). For clay rich samples ethylene glycol instead of water was used during the procedure, to avoid destruction of the section.
Vitrinite reflectance measurements were made by using the incident light microscope DMXR of Leica with a 100x oil immersion objective and a standard of 1.699 % reflectance. Commonly, a 50x magnification is sufficient, but due to small particle size 100x magnification was necessary. The photomultiplier emits monochromatic light at a wave length of 546 nm to measure the reflectance of the vitrinite grains.
The microscope was calibrated at least after every tenth Rmin – Rmax measurement.

4.5 X-ray fluorescence analysis

XRF is a fast, accurate and non-destructive method to determine the chemical composition of samples (Brouwer, 2003). The elemental range goes from Berrylium to Uranium and concentrations in ppm range are measured precisely with very high reproducibility of the results. For elements with higher atomic number the detection limits are usually better than for lighter elements. X-rays are electromagnetic waves with wavelengths in nm scale (0.01 – 10 nm) and energies between 0.125 – 125 keV related to the equation:

$E = h \cdot c / \lambda$ ..... E = energy; h = Planck's constant; c = velocity of light; λ = wavelength.

Pressed powder tablets were irradiated with X-rays, at which one fraction of the radiation was absorbed and produced fluorescent radiation, another fraction passed through the sample and yet another fraction was scattered back (Compton and Rayleigh scatter). The energy of the X-

rays and the composition, density and thickness of the material influence fluorescence and scatter.

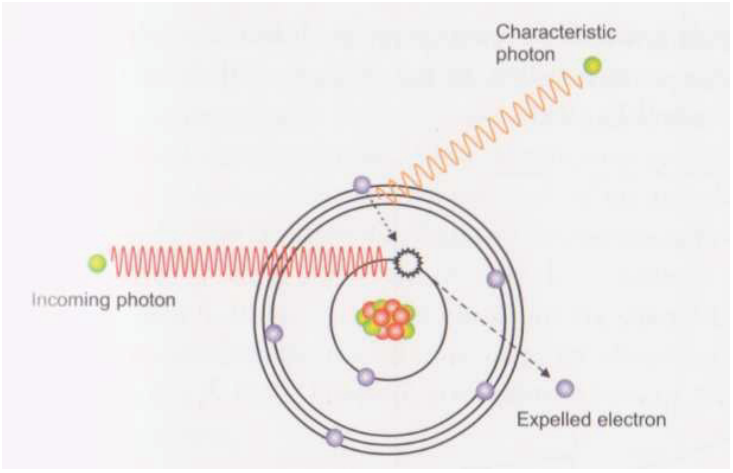

Figure 37: *Generation of characteristic radiation (Brouwer, 2003).*

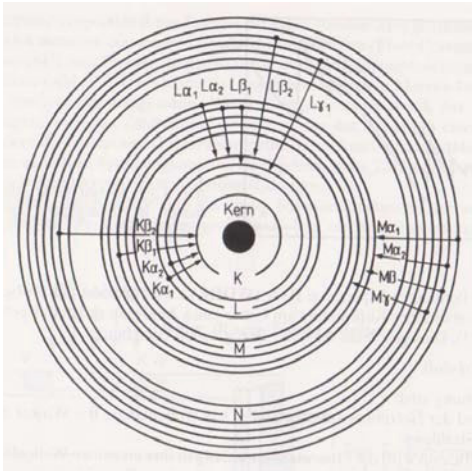

Figure 38: *Energetic electron orbits with lines of fluorescent radiation (Pavićević and Amthauer, 2000).*

When an atom is irradiated with X-rays, the collision of an incoming photon with an electron of the inner shells may lead to expulsion of the electron, provided that the energy of the X-rays is higher than the binding energy of the electron (figure 37). Subsequently, an electron of a higher shell falls into the gap of the expelled electron. By transferring the electron of the higher energetic shell into a lower energetic shell the energy surplus is emitted as characteristic fluorescent radiation (K-, L-, M- lines) (figure 38). Based on specific energy levels of each atom, the different positions where holes are produced and which electrons fill up these holes, the spectrum of lines constitutes a 'fingerprint' for each element (Brouwer, 2003).

XRF spectrometers are commonly separated into two groups according to the detection system: energy dispersive systems (EDXRF) and wavelength dispersive systems (WDXRF) (figure 39). EDXRF spectrometers can detect directly the emitted radiation of the sample, however, lower dispersion (Na to U) and lower detection limits are disadvantages of this system. In this study the wavelength dispersive spectrometer was used. The emitted X-rays from the sample pass the primary collimator and are diffracted (reflected) by an analyzing

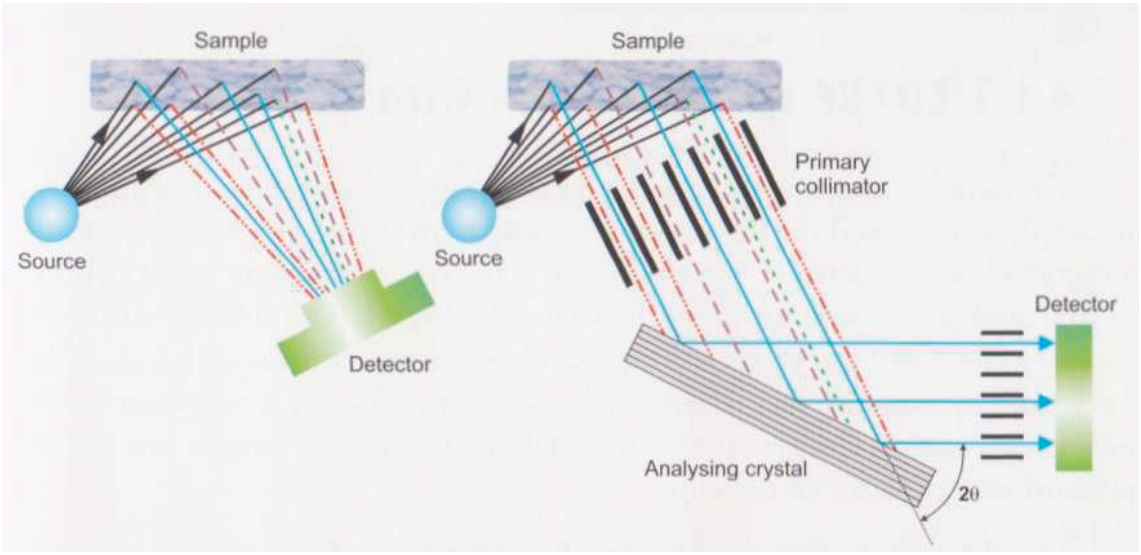

Figure 39: *Schematic sketch of energy dispersive (EDXRF, left) and wavelength dispersive (WDXRF, right) spectrometers (Brouwer, 2003).*

crystal according to Bragg's law:

$n \cdot \lambda = 2 \cdot d \cdot \sin(\theta)$ …… n = order; λ = wavelength; d = interplanar spacing; θ = angle of between beam and crystal plane.

The reflected fluorescent radiation passes a second collimator before reaching the detecting system. A flow counter (long wave) and a scintillation counter (short wave) transform the X-ray quanta in electric impulses. The amplitudes of the electrical signals are proportional to the energy of the incoming X-rays (Pavićević and Amthauer, 2000).

23 samples from outcrops 1, 2, 4, and 8 were selected for X-ray fluorescence analysis. Samples from outcrops 1 and 2 were included because of their outstanding TOC contents, whereas outcrops 4 and 8 provide information on stratigraphic trends in well exposed sections. For sample preparation four grams of finely ground sample (< 63µm) were mixed with one gram of wax powder. The homogenous mixture of sample and wax was pressed to tablets by using hydraulic pressures of 10 tons. The measurements were conducted with a PANalytical Axios and the Pro-Trace software program. Pro-Trace emphasizes on trace element contents, whereas UniQuant® 5 software was used for determination of principal element contents of the samples from outcrops 4 and 8.

5. RESULTS AND INTERPRETATION

5.1 TOC and sulphur contents

The Leco data (total carbon content, total inorganic carbon content (TIC), total organic carbon content (TOC), sulphur content, TOC/S ratios) are summarized in appendix II.

13 out of 82 samples showed very low (< 0.5 %) total organic carbon contents implying a "poor" hydrocarbon potential (nomenclature after Peters, 1986). These samples derived mainly from outcrops 11, 14, and 15 northwest of the Songliao Basin (figure 13), but also the shales in outcrop 9 in the southwest are rather poor in organic matter. The majority of the source rock samples revealed a "fair" TOC between 0.5 and 1 %, at which most of the 38 samples are located in the outcrop cluster (5, 6, 7) to the west of the basin and in the southwest (10, 13), minor in outcrop 3 and 4 east of Harbin. "Good" TOC values, ranging from 1 to 1.5 %, were measured in 21 samples, at which samples of the outcrops 8 and 12 fall almost entirely into this category. The organic carbon contents of 5 samples vary between 1.5 and 2 %. Three of those samples were taken in outcrop 2 and one each in outcrops 7 and 8. The best TOC values ("excellent") of 2 to 5 % are exhibited by three samples of outcrop 1, close to Changchun, and two samples of outcrop 12 to the southwest of the Songliao Basin.

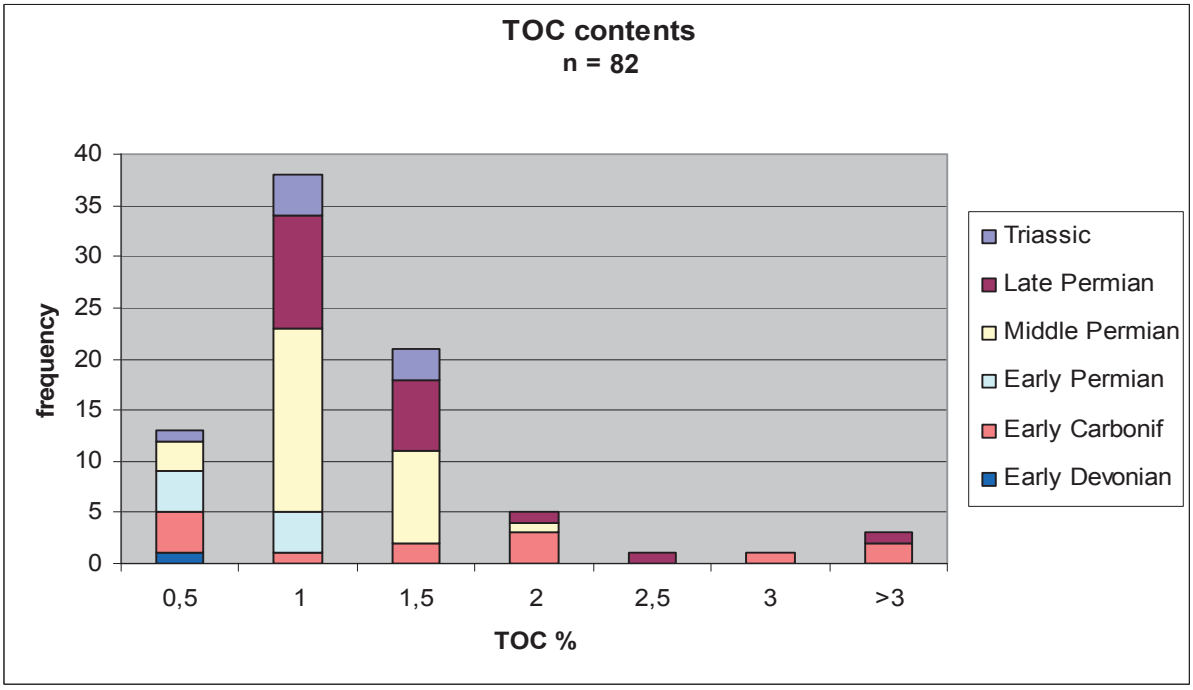

Figure 40: *TOC values of 82 samples with a Lower Devonian to Triassic age.*

The stratigraphic distribution of total organic carbon contents in Lower Devonian to Triassic rocks is displayed in figure 40. Of the Lower Devonian Wunuer Formation only one sample was analyzed, hence the low TOC value cannot be considered as representative. The highest contents were found in samples from the Lower Carboniferous Lujuantun Formation (outcrop 1 and 2), whereas its western pendant, the Hongshuiquan Formation, bears very little organic matter. The Lower Permian Gegen'aobao and Xilin Formations are characterized by poor to fair values. Most samples derive from the Middle Permian Zhesi Formation and reveal on the eastern side of the Songliao Basin slightly higher TOC contents than on its western side. Altogether they fall into the category of fair to good quality. Consistently good TOC data (1 – 1.5 %) can be reported of the samples of the Middle Permian Beidashan Formation (outcrop 12). Two samples of the Upper Permian Linxi Formation showed excellent values, though generally the TOC contents of outcrop 10 are moderate. Further to the north, in outcrop 8, the TOC values mainly range between 1 and 1.5 %. In Triassic samples of the Laolongtou Formation the organic carbon contents can be classified as fair to good.

All investigated formations are either of marine or terrestrial origin according to the stratigraphic table in figure 14. Usually, preservation of organic matter is better in lacustrine environments than in marine depositional settings. Therefore, the average TOC values of marine and terrestrial samples were calculated. The result is practically identical: 1.06 % for marine samples and 0.97 % for terrestrial samples.

Berner (1984) suggests that TOC/S ratios of 2.8 ± 1.5 are typical for marine conditions, whereas higher ratios indicate freshwater environments. Most marine samples are characterized by significantly higher ratios and only 7 out of 45 marine samples fit into that range (appendix II). Maybe this is because of high input of (non-metabolizable) terrestrial organic matter into the marine environment. The average sulphur content of marine samples is approximately 9-times higher than that of terrestrial samples (marine: 0.106 %; terrestrial: 0.012 %), but still rather low for marine deposits.

Two outcrops offer the possibility to study vertical variations in TOC, TIC and S contents in marine (outcrop 4) and terrestrial successions (outcrop 5) (figure 41).

Outcrop 4 – Big quarry close to Yuquan; Middle Permian Zhesi Formation (marine)

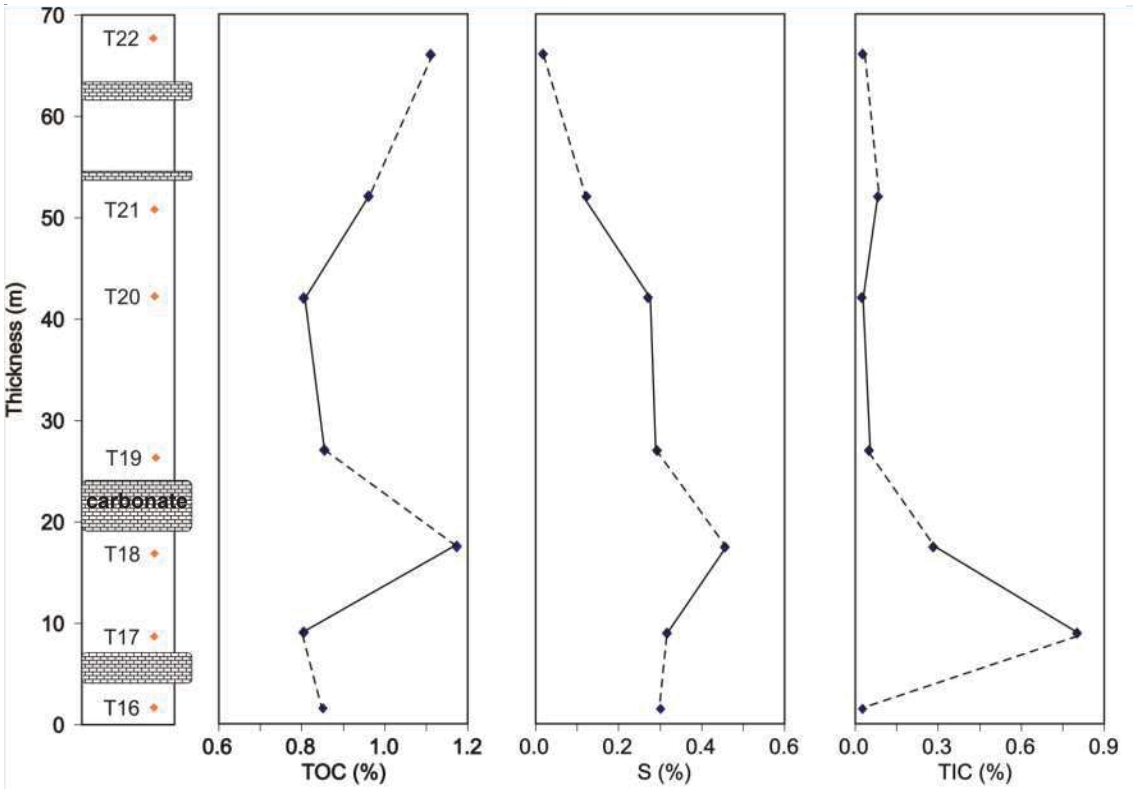

Outcrop 5 – 55 km SW of Zhalantun; Triassic Laolangtou Formation (non-marine)

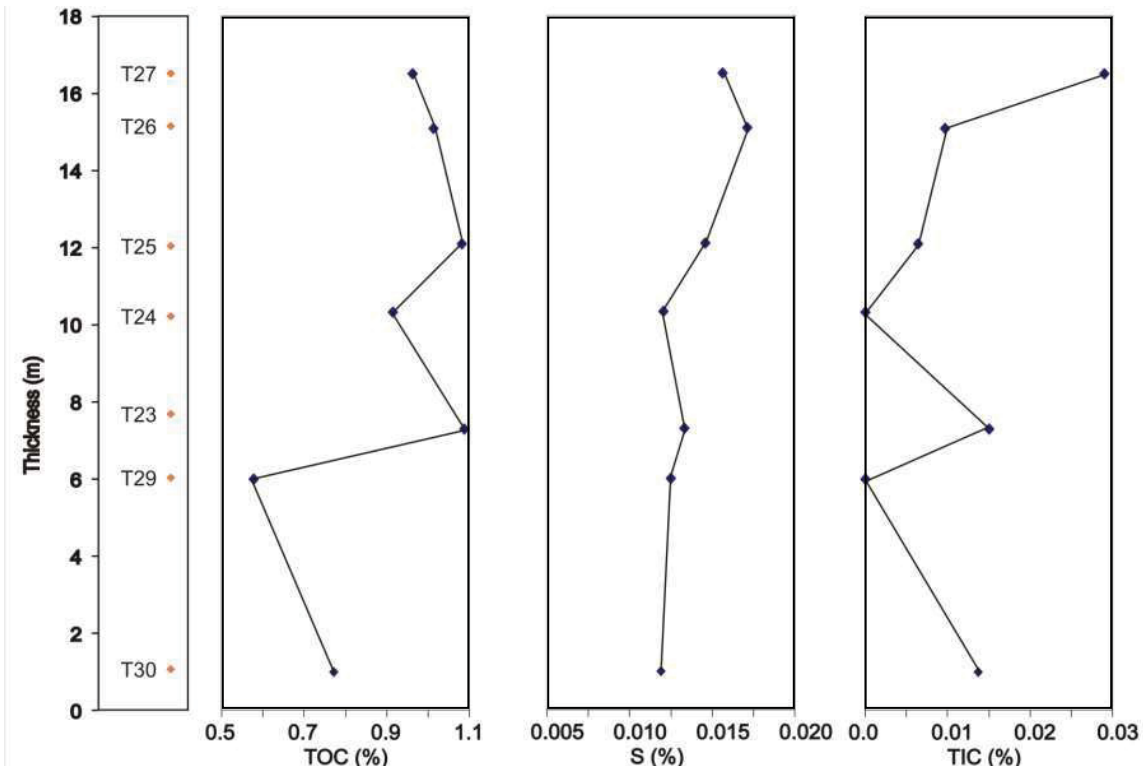

Figure 41: *TOC, S and TIC trends along stratigraphic profiles of outcrops 4 and 5.*

A 70 m long stratigraphic section within the marine Middle Permian Zhesi Formation has been studied in outcrop 4. It is composed of black shale interfingering with carbonate layers.
TOC contents in pelitic rocks average at about 1 % and show little vertical variation. S contents are low and display a general upward decrease. TOC/S ratios from the lower and middle part of the profile (2.5 – 3.0) are typical for rocks deposited in a normal marine environment, whereas the low S contents in the uppermost samples result in TOC/S ratios, which are considered as typical for non-marine environments. Perhaps this trend indicates an increasing freshwater influence.
Most samples are nearly free of carbonate minerals. The only samples with a slightly elevated TIC content (indicating 2 – 7 % calcite) occur between the lower two carbonate layers (T17, T18).

Non-marine rocks of the Triassic Laolongtou Formation, 17 m thick, are exposed at outcrop 5. TOC contents are similar to those in outcrop 4. Slightly higher values (>0.9 %) occur in the upper part than in the lower part (<0.9 %). S and TIC contents are significantly lower in outcrop 5 than in outcrop 4. This is in agreement with the postulated non-marine depositional environment of the Laolongtou Formation.

5.2 Rock Eval pyrolysis

Samples T1 – T42 were selected for Rock Eval pyrolysis. The results are displayed in table 1. Neither the S_1 nor the S_2 peak developed while heating the samples to 550 °C, implying that no hydrocarbons were liberated or generated. Most of the samples show a transformation ratio (PI) of 1. Both results show that all samples are overmature.
The few T_{max} temperatures listed in table 1 are artefacts, which occur when the instrument picks one of the tiny peaks of the background noise as S_2 peak. Moreover, T_{max} values of less than 400 °C are unrealistic, because such low values are restricted to immature lignite samples. At least a S_2 value of 0.2 mg HC / g rock is necessary to obtain reasonable T_{max} temperatures (Peters, 1986).
Because Rock Eval pyrolysis is not useful for the characterization of overmature rocks, this method was not applied to samples T43 to T56 and L1 to L28.

Figure 42 shows the position of the Palaeozoic source rock samples in the Van Krevelen diagram (HI versus OI). At this stage of maturity, where the maturation paths of the different

kerogen types merge together, no conclusion can be drawn upon the depositional environment of the investigated samples. In contrast, source rock samples of the Qingshankou and Nenjiang Formations are clearly of lacustrine origin, hence of kerogen type I (Zhou, 1998). Despite the high maturity, Ma et al. (2008) consider the organic matter in the dark mudstones of the Lower Carboniferous Hongshuiquan Formation as kerogen type I. Kerogen type II should be predominant in the Lower Carboniferous Lujuantun Formation as well as in the Upper Permian Linxi Formation. According to Jiang et al. (2008) Permo-Carboniferous source rocks include type II and III kerogen. It remains unclear on which data (Rock Eval?) these classifications are based on.

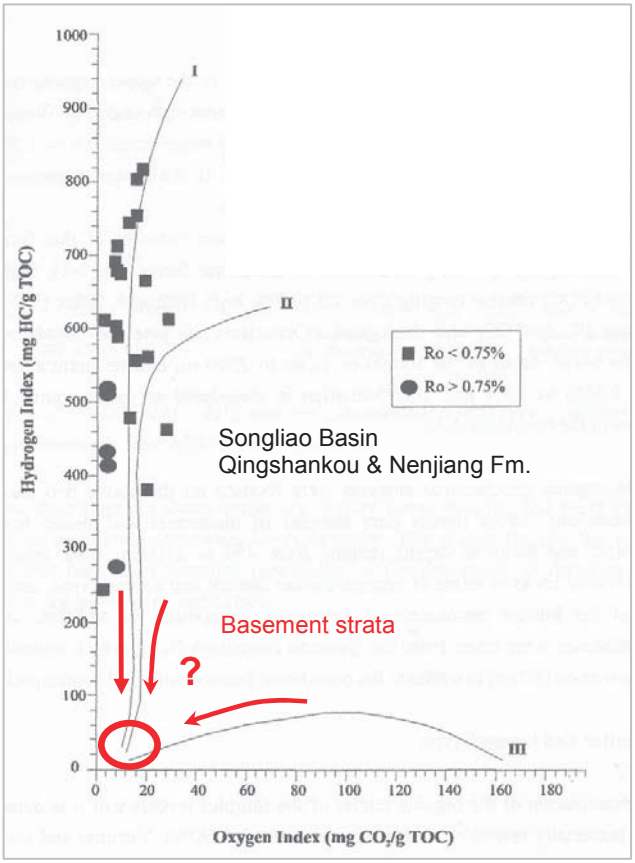

Figure 42: *Source rocks of the Songliao Basin (black dots) and basement strata (red circle) in a Van Krevelen diagram, modified after Zhou (1998).*

Samples	Rock Eval measurements				Indices			
	S1	S2	S3	Tmax	S1+S2	PI	HI	OI
	mg HC/g	mg HC/g	mg CO2/g	°C	mg HC/g	S1/(S1+S2)	S2/TOC	S3/TOC
T1	0,02	0,00	0,08		0,02	1,00	0,0	1,7
T2	0,03	0,00	0,10		0,03	1,00	0,0	6,4
T3	0,03	0,00	0,03		0,03	1,00	0,0	1,0
T4	0,03	0,00	0,16		0,03	1,00	3,6	15,4
T5	0,05	0,01	0,24	309	0,06	0,83	1,7	5,3
T6	0,02	0,00	0,28		0,02	1,00	4,3	27,0
T7	0,07	0,11	1,94	385	0,17	0,38	9,8	99,0
T8	0,10	0,16	1,00	376	0,26	0,38	9,1	36,6
T9	0,39	0,91	1,20	364	1,30	0,30	48,8	54,5
T10	0,03	0,02	0,41	386	0,05	0,60	1,7	13,3
T11	0,02	0,00	0,32		0,02	1,00	1,0	14,4
T12	0,08	0,10	0,51	368	0,18	0,43	9,6	37,3
T13	0,01	0,00	0,27		0,01	1,00	0,8	17,0
T14	0,02	0,00	0,31		0,02	1,00	1,0	13,0
T15	0,02	0,00	0,34		0,02	1,00	0,6	16,3
T16	0,03	0,00	0,02		0,03	1,00	1,2	2,4
T17	0,02	0,00	0,06		0,02	1,00	1,2	5,0
T18	0,01	0,00	0,04		0,01	1,00	0,4	2,1
T19	0,02	0,00	0,01		0,02	1,00	1,2	1,2
T20	0,02	0,00	0,01		0,02	1,00	0,0	1,2
T21	0,02	0,00	0,03		0,02	1,00	0,5	1,0
T22	0,02	0,00	0,16		0,02	1,00	0,9	6,3
T23	0,02	0,00	0,28		0,02	1,00	0,5	13,3
T24	0,02	0,00	0,25		0,02	1,00	0,5	13,1
T25	0,02	0,00	0,30		0,02	1,00	0,5	13,9
T26	0,01	0,00	0,29		0,01	1,00	0,5	14,8
T27	0,01	0,01	0,27	403	0,02	0,50	1,0	26,0
T29	0,02	0,00	0,28		0,02	1,00	0,9	20,8
T30	0,02	0,00	0,21		0,02	1,00	0,6	12,3
T31	0,02	0,00	0,12		0,02	1,00	1,5	7,7
T32	0,03	0,00	0,08		0,03	1,00	3,3	8,8
T33	0,01	0,00	0,13		0,01	1,00	1,0	8,7
T34	0,03	0,00	0,14		0,03	1,00	26,4	52,7
T35	0,01	0,00	0,16		0,01	1,00	10,4	20,7
T36	0,04	0,00	0,28		0,04	1,00	18,3	36,6
T37	0,02	0,00	0,33		0,02	1,00	11,5	22,9
T38	0,01	0,00	0,27		0,01	1,00	18,5	37,0
T39	0,02	0,00	0,16		0,02	1,00	9,6	19,3
T40	0,01	0,00	0,14		0,01	1,00	9,6	19,1
T41	0,01	0,00	0,20		0,01	1,00	12,2	24,5
T42	0,01	0,00	0,12		0,01	1,00	8,0	16,1

Table 1: *Results of the Rock Eval pyrolysis; PI: production index (transformation ratio); HI: hydrogen index (mg HC / g TOC); OI: oxygen index (mg CO_2 / g TOC). Note that T_{max} values are artefacts.*

5.3 Vitrinite reflectance

22 samples were selected for vitrinite reflectance measurement, based on high organic carbon contents and their spatial and stratigraphic distribution. Sample L12, which yielded the highest TOC value, had to be excluded, because it revealed under the microscope a woody structure with intact cell walls, indicating a much younger age than Upper Permian. The samples of the outcrops (11, 14, 15) to the north of the Songliao Basin showed very low organic carbon contents, hence they do not contain a sufficiently large number of vitrinite grains for valid results.

In appendix III all measured Rmin (minimum reflectance) - Rmax (maximum reflectance) pairs for all measured particles in each of the 21 samples are illustrated. The measured vitrinite reflectance of the Upper Palaeozoic source rock samples vary between 2.0 and 5.3 % Ro (ordinary reflectance). In table 2 the Rmin and Rmax values, the number of measured vitrinite particles per sample as well as Ro values and the maximum palaeo-temperature are listed for each sample in ascending order of age.

First, the mentioned parameters and their implications will be explained before the interpretation of results is presented.

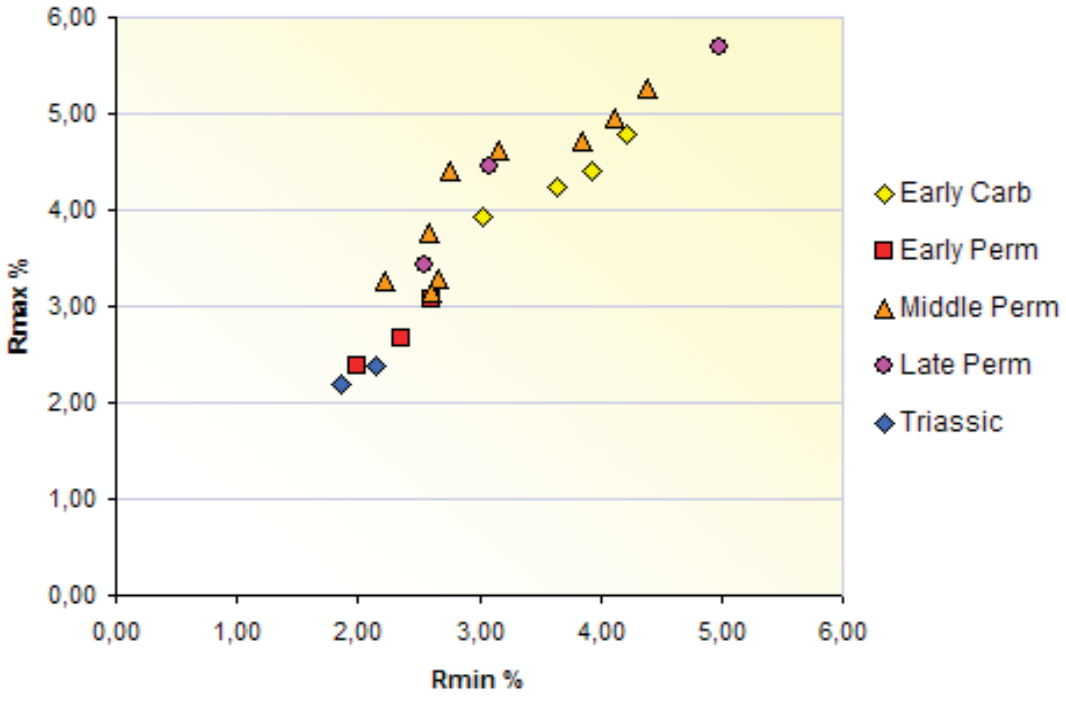

***Figure 43**: Rmin – Rmax plot using the average values of the samples shown in table 2.*

Rmin - Rmax

The bireflectance of vitrinite primarily arises from polymerization of aromatic lamellae in direction of minimum stress and stacking in direction of maximum compression during coalification (Levine and Davis, 1984). Anomalous high anisotropy (i.e. very low Rmin values in combination with high Rmax values) has been recorded for a few data points in the samples T10, T16, T18, T37 and T52 (appendix III) and could be related to local stress (e.g. at the edge of rigid minerals) or due to different precursor material (e.g. liptinite).

In figure 43 the data points of the 21 samples reveal the typical linear relationship between Rmin and Rmax values with increasing maturity. From younger to older an increasing trend of vitrinite reflectance data can be observed, though there are some exceptions. The cause for the deviating values of some Permian samples will be discussed later in the interpretation.

Age	Formation	Sample	Rmax % ∑Rmax/n	Rmin % ∑Rmin/n	n vitrinite grains	Ro % √(Rmax*Rmin)	Ro % (Rmax+Rmin)/2	T °C 104*ln(Ro)+148
Early Carb	Lujuantun	T1	4,41	3,93	36	4,16	4,17	300
Early Carb	Lujuantun	T5	4,78	4,22	29	4,49	4,50	300
Early Carb	Lujuantun	T8	4,23	3,65	25	3,93	3,94	290
Early Carb	Lujuantun	T10	3,93	3,02	27	3,45	3,48	280
Early Perm	Xilin	T31	3,07	2,61	24	2,83	2,84	260
Early Perm	Gegen'aobao	L21	2,66	2,36	34	2,51	2,51	240
Early Perm	Gegen'aobao	L22	2,39	2,00	19	2,19	2,20	230
Mid Perm	Zhesi	T11	3,29	2,66	11	2,96	2,98	260
Mid Perm	Zhesi	T12	3,26	2,22	21	2,69	2,74	250
Mid Perm	Zhesi	T16	4,41	2,76	40	3,49	3,59	280
Mid Perm	Zhesi	T18	4,61	3,17	20	3,82	3,89	290
Mid Perm	Zhesi	T22	3,15	2,61	25	2,87	2,88	260
Mid Perm	Zhesi	T37	3,76	2,58	28	3,11	3,17	270
Mid Perm	Zhesi	T47	4,71	3,85	29	4,26	4,28	300
Mid Perm	Beidashan	L19	5,27	4,39	19	4,81	4,83	310
Mid Perm	Beidashan	L20	4,95	4,12	4	4,52	4,54	310
Late Perm	Linxi	T52	4,46	3,08	25	3,71	3,77	280
Late Perm	Linxi	T56	3,42	2,55	26	2,95	2,99	260
Late Perm	Linxi	L13	5,69	4,98	26	5,32	5,34	320
Triassic	Laolongtou	T23	2,20	1,86	4	2,02	2,03	220
Triassic	Laolongtou	T25	2,39	2,14	3	2,26	2,27	230

Table 2: *Results of vitrinite reflectance measurement of 21 samples in ascending order of age.*

n - number of measured vritinite particles

The larger the number of measured vitrinite particles per sample the higher is the confidentiality of the results. Usually, 50 to 70 Rmin – Rmax measurements per sample should be conducted, however for the investigated samples this number was never attained.

The vitrinite grains were finely dispersed and of very small size, even when using 100x magnification.

The samples T23, T25 and L20 were especially devoid of measurable vitrinite particles, despite of organic carbon contents ranging between 1.08 and 1.35 %. In contrast, sample T16 shows only a TOC of 0.85 %, but 40 vitrinite grains were measured. This contradiction could be related to an initially high content in liptinite in samples T23, T25 and L20. Lipitinite decompose into finest grains due to thermal instability at higher levels of maturity (> 1.3 % Ro). Under the microscope the finest liptinite grains are barely visible anymore, but they get still detected by the Leco instrument while measuring the TOC content. It is likely that the samples T23, T25 and L20 are of the liptinite-rich kerogen type I or II, whereas the organic matter in T16 is probably of kerogen type III, based on the relatively high number of vitrinite grains found in the sample.

Ro – ordinary reflectance

The ordinary reflectance (Ro) was calculated by two different formulas. Hevia and Virgos (1977) suggest to take the mean value of Rmin and Rmax (Ro = (Rmax + Rmin) / 2). Kilby (1988) argues that the previous formula is too general and does not take into account the often significant anisotropy of vitrinite. He states that a better relationship is provided by the equation Ro = √(Rmax*Rmin). Values calculated using Kilby´s formula are generally slightly lower, but the difference is minor (a few hundredth of a percent).

T – peak palaeo-temperature

With ordinary vitrinite reflectance as input parameter, Barker (1988) developed a time-independent equation (T °C = 104*ln (Ro) + 148) to estimate the peak palaeo-temperature the organic matter had been exposed to during its geologic evolution. The resulting values should be rounded to the nearest 10 °C. The error of the estimates is about ± 30 °C. Underwood et al. (1993) comment that the Barker (1988) formula yields lower temperature estimates for a given Ro value than most other time-independent equations.

The temperature estimates vary between 220 °C (Triassic Laolongtou Fm.) to 320 °C (Upper Permian Linxi Fm.).

Interpretation

The organic-rich black shales of the Lower Carboniferous Lujuantun Formation range from 3.5 to 4.5 % (Ro), which in combination with observed foliation and mineralized veins in the outcrops (1, 2) suggest that the thermal regime had reached an anchi-metamorphic stage.

Astonishingly, the Lower Permian samples are characterized by lower Ro values (2.2 – 2.8 % Ro), than those from the Middle Permian Zhesi and Beidashan Formations (2.7 – 4.8 % Ro). The very high vitrinite reflectance of the samples L19 and L20 (outcrop 12) of the Beidashan Formation could be related to thermal heating by granitic intrusions in proximity.

Also the Upper Permian sample L13 from outcrop 10, located close to granitic bodies, reveals an anomalous high value (5.3 % Ro) in comparison to the coeval samples T52 and T56 (3.0 - 3.7 % Ro) (figure 44). So it could be that maturity of samples from outcrops 10 and 12 has

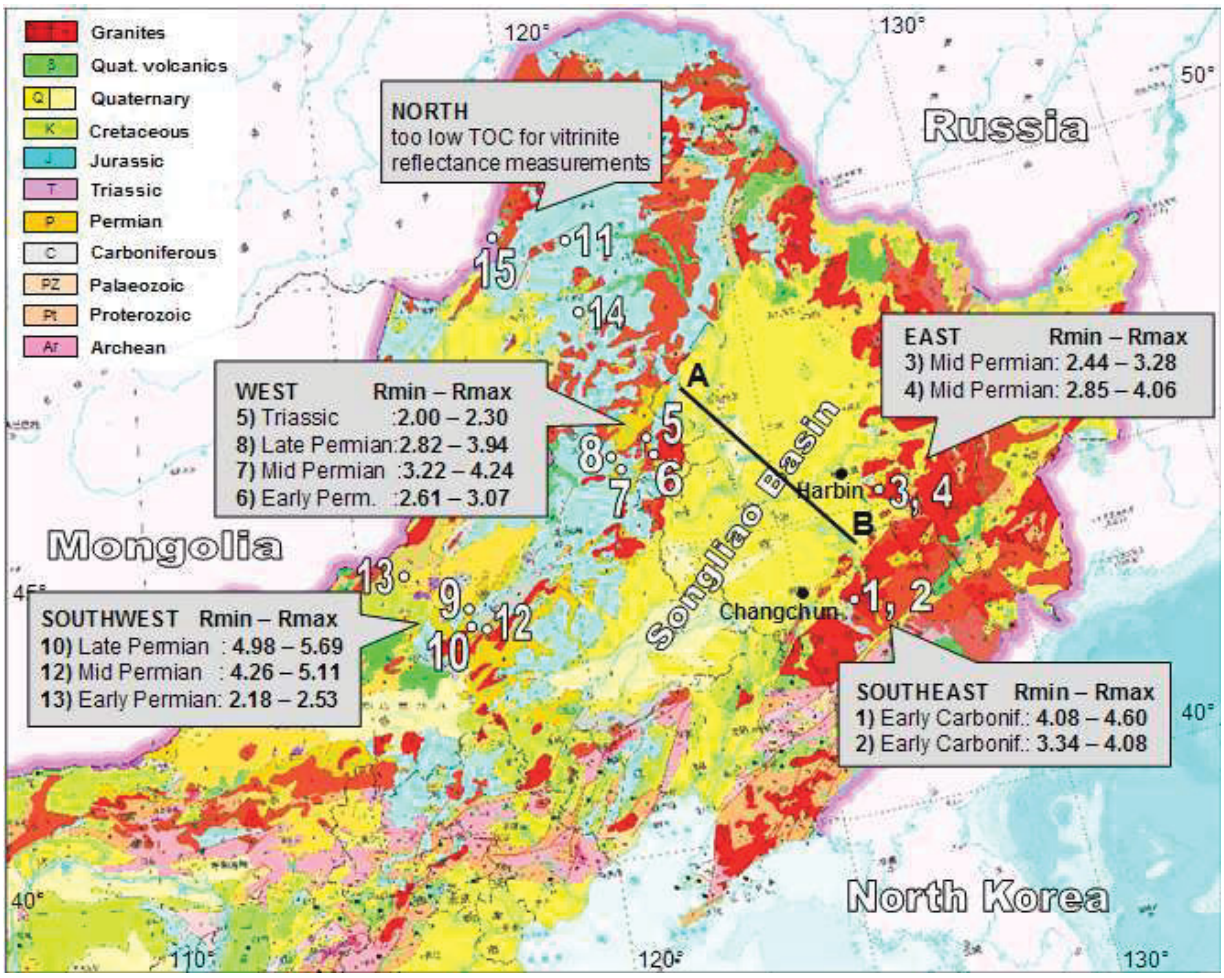

Figure 44: *Map showing Rmin and Rmax values in a spatial and stratigraphic context based on outcrop locations (1-15). Profile A-B refers to figure 45.*

been influenced by magmatic activity. However, this does not explain why Lower Permian samples are less mature than Middle Permian samples, even those which were probably not affected by thermal heating events. Whether the low values of Lower Permian samples are attributable to local phenomena (e.g. tilting of strata, which prevented deep burial) remains unclear.

Apart from the low values from Lower Permian rocks and apart from outcrops 10 and 12, which were probably influenced by magmatic activity, vitrinite reflectance decreases from older to younger formations (Lower Carboniferous: 3.5 - 4.5 % Ro; Middle Permian: 2.7 - 4.3 % Ro; Upper Permian: 3.0 - 3.7 % Ro; Triassic: 2.0 - 2.3 % Ro). This relation suggests that maturation occurred before (Permo-Triassic?) deformation.

In comparison, Ma et al. (2008) report that organic matter in clastic rocks of the Lower Carboniferous Hongshuiquan Formation has a vitrinite reflectance of 2.08 to 2.46 % Ro, whereas organic material in limestones of the same formation yields 3.5 to 4.0 % Ro. The Lujuantun Formation is characterized by vitrinite reflectance values between 2 and 4 % Ro and the Upper Permian Linxi Formation is at an early overmature stage (2.01 -2.71 % Ro). However, sample locations have not been mentioned in the abstract.

Since all samples for this study were taken from surface outcrops, no information on the increase in vitrinite reflectance with depth within Palaeozoic rocks is available. For that reason basin modelling and estimation of palaeo-heat flows, hence determination of the timing of petroleum generation could not be conducted.

In figure 45 a geologic section across the Songliao Basin with isoreflectance lines is displayed. Zhou (1998) used vitrinite reflectance depth trends of five wells along the transect for calibration of a thermal model. The isoreflectance lines are fairly horizontal and parallel to each other, but differential subsidence caused variable thermal maturity of the strata according to the structural position. During time of maximum burial before the late Cretaceous - early Tertiary uplift phase the Qingshankou Formation for example reached a depth of 2300 m in the central depression leading to a higher maturity than in the southeast uplift zone, where the burial depth was only about 1300 m (Zhou, 1998). The boundary between mature and overmature source rocks is at about 2 % Ro. On the basis of vitrinite reflectance - depth plots and the pattern of the isoreflectance lines (figure 45) this boundary is located at a present-day depth of approximately 3500 m.

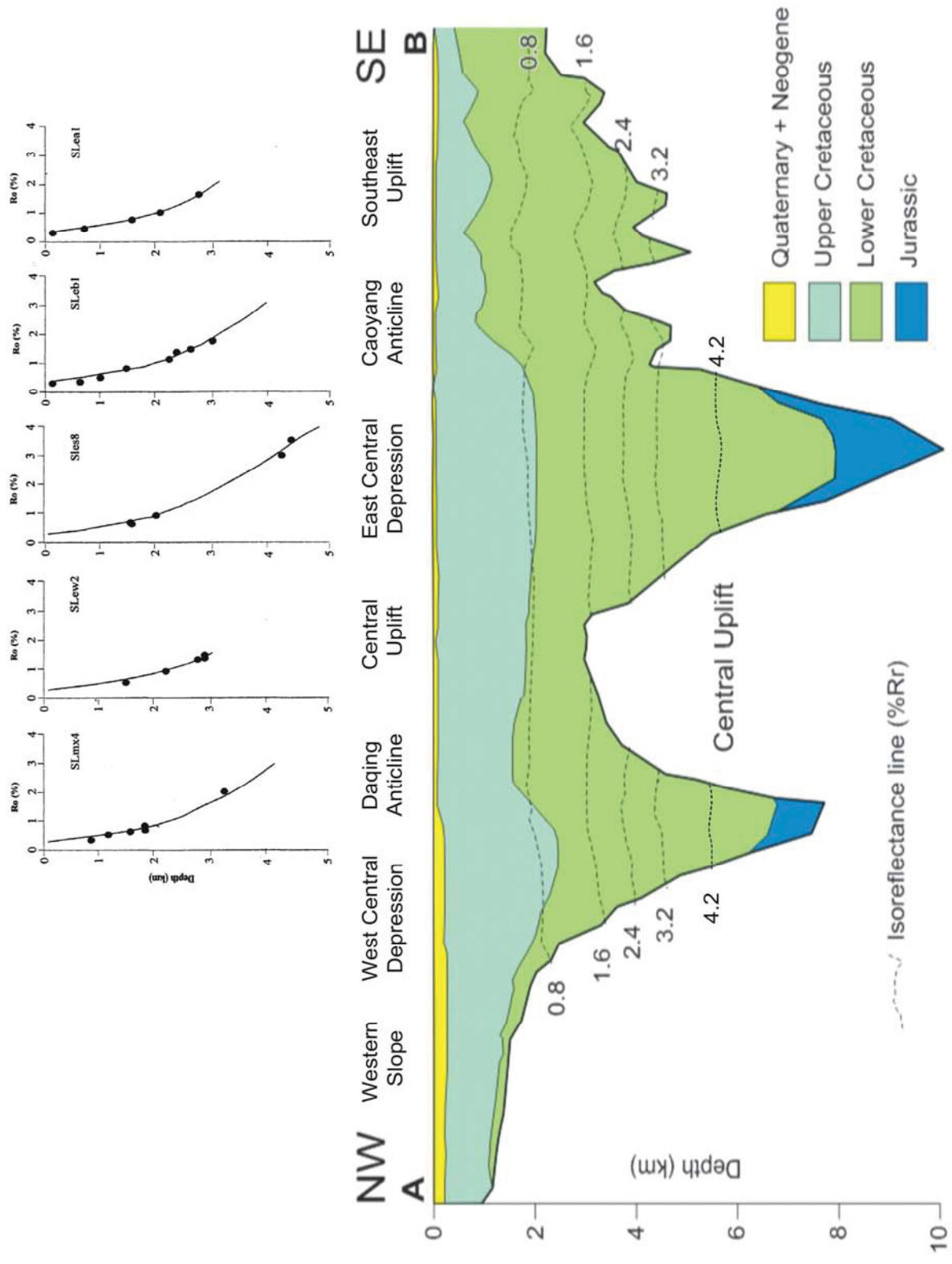

Figure 45: *NW-SE trending cross section of the Songliao Basin showing isoreflectance lines, based on vitrinite reflectance data of five wells (modified after Zhou, 1998). Location indicated in figure 44. The shape and depth of the basin as well as nomenclature is differing from the model in figure 12; west central depression = Qijia-Gulong depression; Caoyang anticline = Chaoyanggou terrace.*

The fact that vitrinite reflectance data of the measured Upper Palaeozoic samples in this study range between 2.0 and 5.3 % Ro suggests that these rocks were buried by sediments at least 3.5 km thick (assuming similar heat flow conditions).

Evaluating the timing of hydrocarbon generation in Palaeozoic rocks, it is important to investigate whether a break in coalification occurs between the Mesozoic-Cenozoic strata in the Songliao Basin and the underlying basement. Vitrinite reflectance of Cretaceous-Cenozoic strata along the margins of the Songliao Basin is low (< 0.8 % Ro according to figure 45). In contrast, vitrinite reflectance of Palaeozoic rocks is consistently > 2.0 % Ro. This suggests a major break in maturity and that most hydrocarbons (including all liquid hydrocarbons) were generated in Palaeozoic rocks before deposition of the Upper Jurassic-Cenozoic fill of the Songliao Basin. However, some additional gas may have been generated in areas where during Cretaceous deep burial vitrinite reflectance was increased (e.g. beneath central depressions).

A simplified conceptual model, subdivided into three stages of the maturation history of the Upper Palaeozoic and Triassic rocks, is shown in figure 46.

A) The first stage illustrates the burial and maturation of undisturbed Palaeozoic and Triassic strata in a ‘Permo-Carboniferous basin’. The required thickness of overburden rocks to cause a maturity level of roughly 2 % Ro in Triassic sediments depends on the palaeo-heat flow regime, which remains unknown. Based on the present vitrinite data, approximately 3 % Ro can be assumed for Permian and 4 % Ro for Carboniferous rocks.

B) The closure of the Palaeo-Asian Ocean in the late Permian and subsequent collision of the North China craton with the Jiameng block induced compression and deformation of the strata. During late Triassic to early Jurassic times, post-collisional uplift led to deep erosion and removal of the post-early Triassic overburden rocks. The formation of the Songliao Basin due to crustal thinning was initiated during the late Juarssic.

C) With ongoing subsidence of the depressions within the Songliao Basin, the underlying basement strata became overprinted by additional coalification. For example, vitrinite reflectance of Triassic rocks may have increased from about 2 to more than 5 % Ro beneath the depocenters of the Songliao Basin (see isoreflectance lines in figure 45). Although the initial maturity of the basements rocks was fairly high, maybe minor amounts of gas were still generated and could have migrated into the overlying fill of the Songliao Basin. In contrast, at the shallow basin margins a significant break in coalification between the Upper Palaeozoic - Triassic and the Meso-Cenozoic strata is probable, because the latter has not reached yet higher levels of maturity.

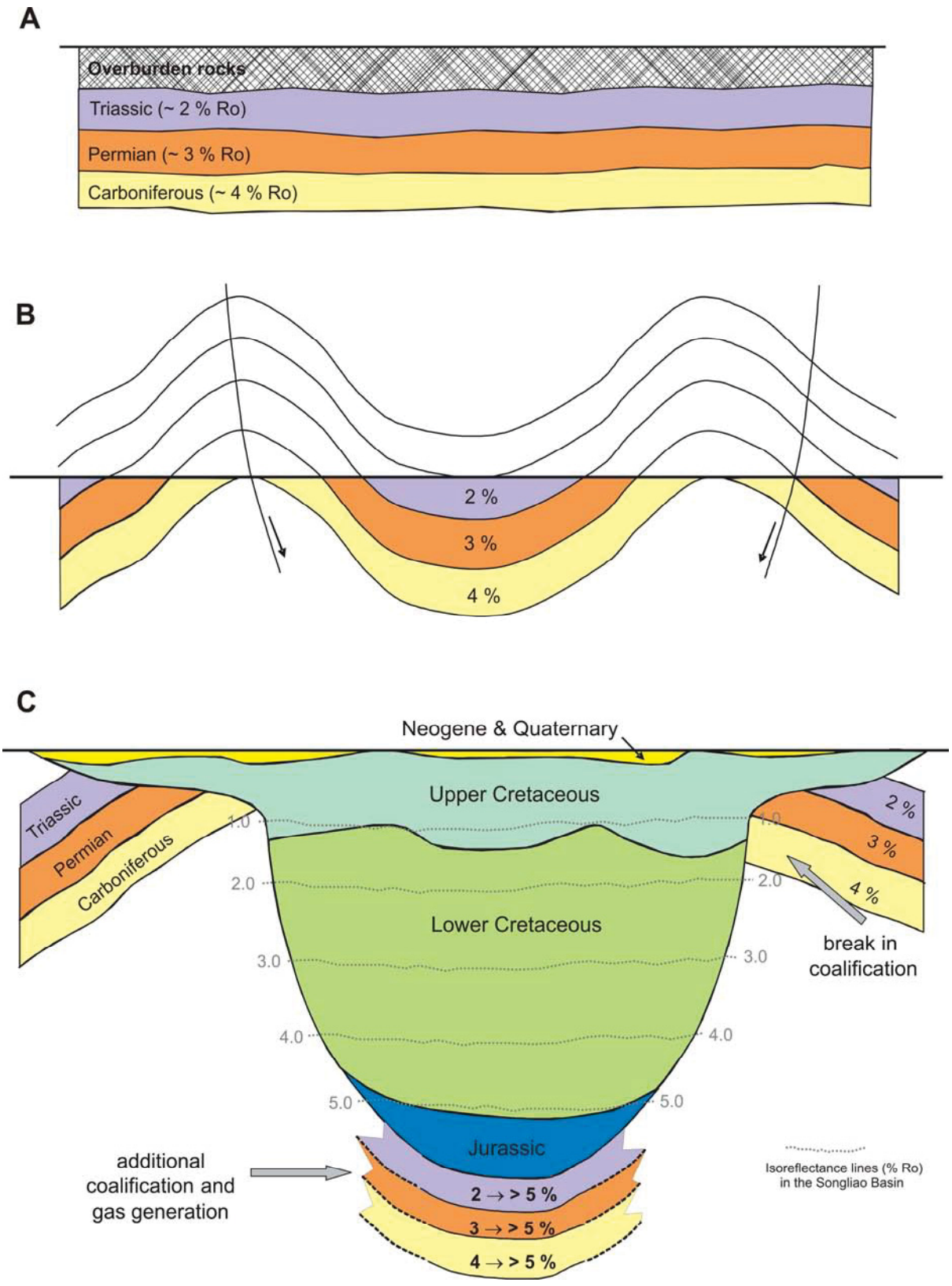

Figure 46: *Simplified conceptual model showing the maturation history of Upper Palaeozoic and Triassic rocks. A: maturation; B: uplift and erosion; C: break in coalification at the shallow margins and additional coalification and minor gas generation beneath the depocenters of the Songliao Basin.*

5.4 X-ray fluorescence analysis

23 samples were selected for the trace element analysis with the Pro-Trace software, based on the continuous stratigraphic successions in outcrops 4 and 8 and relatively high TOC contents in outcrops 1 and 2. Additionally, the principal element contents of the samples of the outcrops 4 and 8 were measured with UniQuant. The data of both methods Pro-Trace and UniQuant are summarized in appendix IV. The inorganic geochemical data yield information on characteristics of the depositional environment such as salinity or oxygen supply during sedimentation. Information about the hinterland is obtained by comparing element concentrations and associations. Typical elements associated with silicates and clay minerals are Ti, Ga, Sc, Zr, whereas Ca, Mg, Sr and Mn are bound to carbonatic rocks. Organic matter often contains elevated concentrations of As, Ge, Mo, V and U (Augustin-Gyurits and Schroll, 1992; Rantitsch et al., 1995; Taylor, 1998)

The results of the UniQant analysis show that the SiO_2 contents are relatively high and range between 64 and 69 weight % for both outcrops. In contrast, the CaO contents do not exceed 1 % except for sample T17, which reveals a slightly elevated content of 2.88 %. Note that T17 is also characterized by the highest TIC content of all studied samples in outcrop 4 (figure 41).
The obviously silica-dominated milieu is reflected by the enrichment factors of trace elements indicated in figure 47. The enrichment factors of 41 elements are referenced to average values of shales by Turekian and Wedepohl (1961) and Taylor (1964). The deviation of element concentrations to the average stays within one order of magnitude, referring to minor variations, at which the graphs of the four outcrops show a good correlation. The highest positive peaks were yielded by the elements Cd, Cs, As, Hf, Ti and Zr followed by Nb, Y, Ce, U, Th and Ga. Cadmium is often associated with sulphides, especially sphalerite (Taylor et al., 1998). However, the samples are rather depleted of typical sulphide forming elements such as Zn, Pb, Cu, Co, Ni; only the Fe concentration is little higher than average. A depletion of Ca and Sr corroborates the results of the UniQuant measurements that the samples derive from a siliciclastic-dominated hinterland and that carbonates are of minor importance. In comparison to other outcrops, the elements Ni, Cr and Co are enriched in samples from outcrop 2, pointing to an influence of (ultra-)basic rocks in the hinterland.

The ratios of several redox-sensitive elements provide information about the oxygenation of the depositional environment. Mn/Ni and V/Cr ratios indicative of the supply of oxygen, as

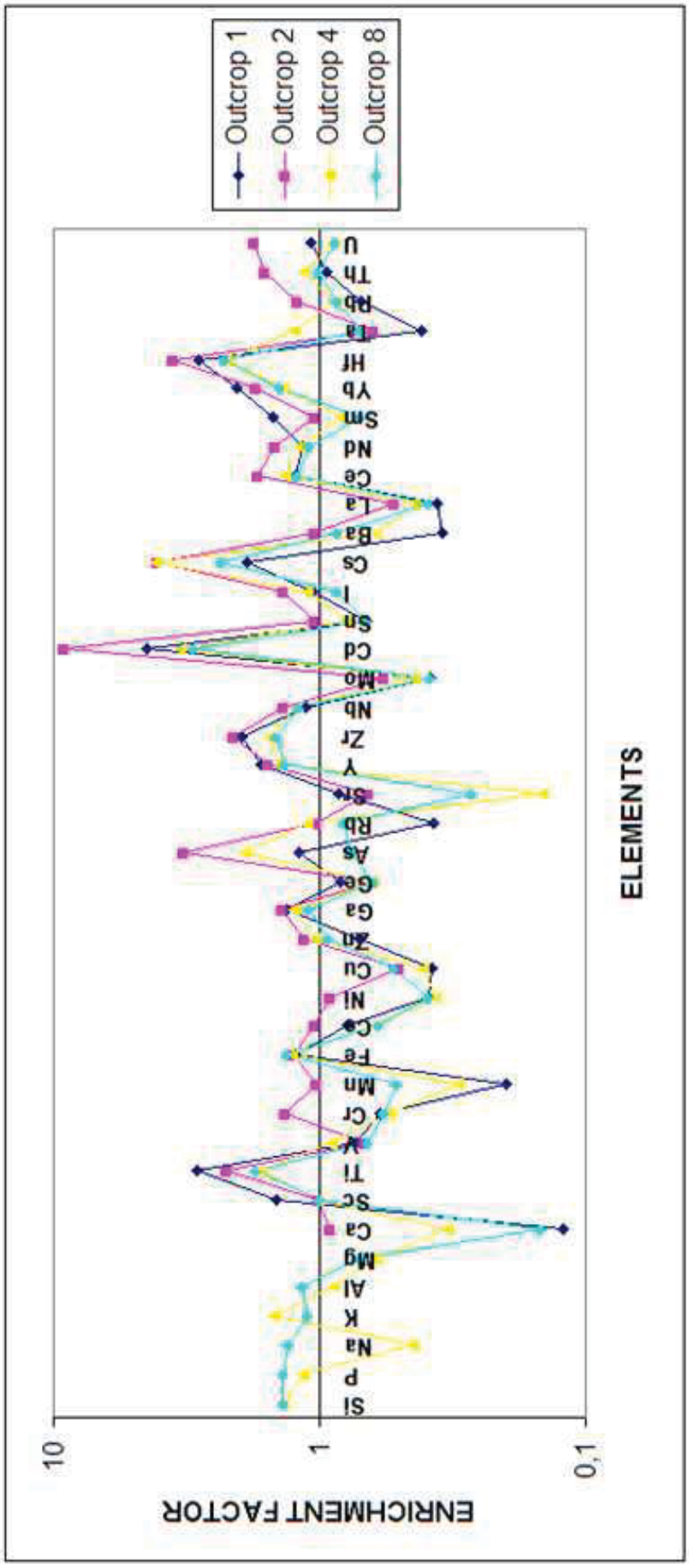

Figure 47: *Relative enrichment or depletion of 41 elements of outcrops 1, 2, 4 and 8 according to average concentrations of shales after Turekian and Wedepohl (1961) and Taylor (1964).*

well as the Ca/Mg ratio to discern between marine and freshwater conditions are listed in table 3. With respect to the Mn/Ni ratio, Wegehaupt (1961) appraised values of 0.5-1.5 for an oxygen-deficient milieu and ratios from 5-10 referring to well oxygenated conditions. Mn/Ni ratios of all samples (with the exception T16) indicate an aerobe depositional setting. The V/Cr ratios do not confirm these results. The values of the samples T3, T16 to T22 and T55 are within the interval from 2 to 10, mirroring anaerobe conditions according to Krejci-Graf (1966) and Ernst (1970). The remainder is characterized by V/Cr ratios of 1 to 2 and <1 in outcrop 2, representing limited oxygen supply and aerobe conditions, respectively.

Outcrop	Sample	Protrace						UniQuant		
		Mn ppm	Ni ppm	Mn/Ni ratio	V ppm	Cr ppm	V/Cr ratio	Ca weight %	Mg weight %	Ca/Mg ratio
1	T1	137	21	6,52	97	55	1,76			
	T3	182	31	5,87	120	50	2,40			
	T5	199	28	7,11	94	51	1,84			
2	T7	2235	79	28,29	79	107	0,74			
	T8	571	74	7,72	94	152	0,62			
	T9	266	50	5,32	94	111	0,85			
	T10	429	45	9,53	84	113	0,74			
4	T16	49	23	2,13	98	48	2,04	0,346	0,800	0,43
	T17	154	24	6,42	98	46	2,13	2,060	1,020	2,02
	T18	302	29	10,41	153	51	3,00	0,344	0,996	0,35
	T19	138	23	6,00	87	43	2,02	0,399	1,120	0,36
	T20	222	24	9,25	128	50	2,56	0,288	1,230	0,23
	T21	404	27	14,96	112	52	2,15	0,616	1,280	0,48
	T22	521	25	20,84	138	57	2,42	0,519	1,030	0,50
8	T48	253	24	10,54	72	46	1,57	0,368	1,050	0,35
	T49	335	22	15,23	81	49	1,65	0,195	1,100	0,18
	T50	637	28	22,75	84	52	1,62	0,222	1,170	0,19
	T51	440	27	16,30	78	53	1,47	0,215	1,090	0,20
	T52	460	25	18,40	85	51	1,67	0,543	1,180	0,46
	T53	265	25	10,60	92	54	1,70	0,275	1,150	0,24
	T54	272	23	11,83	77	52	1,48	0,210	1,000	0,21
	T55	871	38	22,92	122	53	2,30	0,151	1,120	0,13
	T56	347	25	13,88	81	57	1,42	0,492	1,070	0,46

Oxygen supply: aerobic; restricted; anaerobic

Environment: marine; terrestrial

Table 3: *Characterization of the depositional environment by using Mn/Ni, V/Cr and Ca/Mg ratios. The UniQuant measurements were conducted for samples from the outcrops 4 and 8 only.*

Werner (1963) uses Ca/Mg ratios to distinguish between freshwater (Ca/Mg > 5) and marine environments (Ca/Mg < 5). Also here the results are other than expected, because the samples of the terrestrial Linxi Formation (outcrop 8) reveal a clear marine signature. However,

	Ca	Sc	Ti	V	Cr	Mn	Fe	Co	Ni	Cu	Zn	Ga	Ge	As	Rb	Sr	Y	Zr	Nb	Mo	Cd	Sn	I	Cs	Ba	La	Ce	Nd	Sm	Yb	Hf	Ta	Pb	Th	U
Ca	1,00																																		
Sc	0,00	1,00																																	
Ti	0,00	**0,58**	1,00																																
V	-0,03	0,08	0,00	1,00																															
Cr	0,14	-0,01	0,11	-0,03	1,00																														
Mn	**0,67**	-0,01	-0,01	-0,02	0,17	1,00																													
Fe	0,22	0,01	-0,05	0,02	0,02	**0,43**	1,00																												
Co	0,36	0,10	0,10	0,03	0,38	**0,42**	0,04	1,00																											
Ni	**0,44**	0,00	0,06	-0,01	**0,80**	**0,52**	0,04	**0,69**	1,00																										
Cu	0,00	0,00	-0,03	0,00	0,02	0,07	0,04	0,05	0,06	1,00																									
Zn	0,42	-0,12	-0,16	0,01	0,15	0,30	0,03	0,30	0,31	0,07	1,00																								
Ga	-0,01	0,12	0,35	0,08	0,22	-0,06	-0,21	0,11	0,09	-0,01	0,00	1,00																							
Ge	0,00	**0,44**	0,24	0,05	-0,01	0,01	0,01	0,09	0,00	0,00	-0,04	0,13	1,00																						
As	0,17	0,00	0,01	0,09	**0,40**	0,11	0,03	**0,58**	**0,49**	0,01	0,33	0,21	0,00	1,00																					
Rb	0,00	-0,37	-0,28	0,06	0,05	-0,01	-0,07	0,00	0,01	0,04	0,21	0,08	-0,14	0,17	1,00																				
Sr	0,19	0,35	**0,59**	-0,04	0,23	0,15	0,01	0,35	0,32	0,03	0,00	0,07	0,12	0,05	**-0,42**	1,00																			
Y	0,03	0,39	**0,55**	0,06	0,11	0,00	0,00	0,19	0,12	0,00	-0,01	**0,54**	0,21	0,08	-0,02	0,23	1,00																		
Zr	0,05	0,16	**0,66**	0,00	**0,52**	0,00	-0,13	0,25	0,36	0,01	0,00	**0,65**	0,07	0,25	0,00	**0,43**	**0,56**	1,00																	
Nb	0,00	-0,07	0,01	-0,02	0,26	-0,01	0,15	0,00	0,10	0,03	0,03	0,36	-0,01	0,07	0,36	-0,01	0,12	0,26	1,00																
Mo	0,16	0,01	0,00	0,01	0,18	0,21	0,00	**0,44**	0,34	0,03	0,21	0,01	0,00	**0,43**	0,02	0,06	0,02	0,07	0,00	1,00															
Cd	0,11	-0,03	0,03	-0,19	0,08	0,05	-0,01	0,04	0,09	-0,02	0,01	0,08	-0,04	0,02	0,01	0,06	0,09	0,14	0,09	0,02	1,00														
Sn	0,04	-0,02	0,01	0,00	0,24	0,00	0,00	0,07	0,17	0,01	0,12	0,25	-0,01	0,18	0,15	0,00	0,20	0,16	0,19	0,00	0,13	1,00													
I	0,07	0,04	0,01	0,02	0,02	0,05	0,08	0,03	0,05	0,01	0,02	0,02	0,01	0,06	0,01	0,00	0,08	0,03	0,00	0,01	0,02	0,18	1,00												
Cs	0,00	-0,11	-0,05	0,11	0,13	-0,02	-0,15	0,01	0,05	0,00	0,13	0,27	-0,04	0,32	**0,69**	-0,11	0,00	0,05	0,20	0,06	0,03	0,19	0,02	1,00											
Ba	0,05	-0,33	-0,10	-0,18	0,34	0,20	0,00	0,06	0,30	0,26	0,16	-0,01	-0,15	0,04	0,15	0,00	-0,04	0,00	0,24	0,07	0,06	0,05	0,00	0,03	1,00										
La	0,11	-0,01	0,00	0,08	0,38	0,14	0,00	0,21	0,37	0,08	0,21	0,27	0,02	0,36	0,39	0,00	0,16	0,24	**0,46**	0,11	0,05	0,18	0,02	0,30	0,20	1,00									
Ce	0,04	-0,01	0,08	0,01	**0,45**	0,01	-0,06	0,12	0,31	0,07	0,06	**0,52**	0,00	0,28	0,29	0,00	**0,40**	**0,48**	**0,63**	0,06	0,16	0,39	0,05	0,27	0,15	**0,59**	1,00								
Nd	0,09	0,00	0,12	0,02	0,36	0,07	-0,01	0,16	0,31	0,08	0,10	**0,43**	0,00	0,19	0,15	0,03	**0,46**	**0,45**	**0,49**	0,06	0,14	0,22	0,02	0,13	0,11	**0,71**	**0,78**	1,00							
Sm	0,00	0,23	0,31	0,03	0,01	-0,01	-0,02	0,04	0,01	0,00	-0,01	0,29	0,03	0,01	0,00	0,07	**0,52**	0,26	0,12	0,00	0,02	0,06	0,05	0,01	0,02	0,10	0,21	-0,15	1,00						
Yb	-0,01	0,06	0,26	0,00	0,03	0,06	-0,12	0,00	0,00	-0,01	0,03	0,15	0,03	0,00	-0,04	0,07	0,23	0,17	0,02	0,14	0,04	0,17	0,01	0,00	0,02	0,00	0,07	-0,21	0,12	1,00					
Hf	0,01	0,05	0,39	0,00	**0,68**	0,01	-0,05	0,19	**0,43**	0,01	0,00	**0,40**	0,01	0,18	0,00	0,27	0,35	**0,69**	0,29	0,06	0,04	0,14	0,00	0,03	0,07	0,30	**0,47**	-0,34	0,12	0,07	1,00				
Ta	-0,14	0,00	0,00	0,09	-0,01	-0,09	-0,03	0,04	0,04	0,04	-0,01	0,08	0,01	0,01	0,20	0,16	0,00	0,00	0,09	0,05	0,04	0,00	0,01	0,16	0,00	0,11	0,05	0,00	0,02	-0,02	0,00	1,00			
Pb	0,16	0,00	0,00	0,01	0,16	0,23	0,03	0,38	0,35	0,29	0,30	0,02	0,03	0,31	0,06	0,01	0,09	0,05	0,08	0,28	0,03	0,13	0,09	0,01	0,20	0,25	0,21	0,07	0,11	-0,02	0,06	0,01	1,00		
Th	0,08	-0,04	0,03	0,00	**0,65**	0,06	-0,05	0,21	**0,50**	0,05	0,15	**0,42**	0,02	0,39	0,32	0,01	0,22	**0,43**	**0,57**	0,11	0,22	**0,46**	0,05	0,37	0,34	**0,62**	**0,84**	0,34	0,07	0,04	**0,43**	0,04	0,29	1,00	
U	0,39	0,01	0,15	-0,01	**0,52**	0,36	0,04	**0,45**	**0,67**	0,02	0,12	0,19	0,00	0,31	0,00	0,33	0,28	**0,45**	0,13	0,09	0,27	0,28	0,10	0,03	0,18	0,37	0,38	**0,43**	0,08	0,03	0,32	0,00	0,31	**0,52**	1,00

Correlation coefficient: ± 0.40 to 0.60 ± 0.60 to 0.99

Table 4: *Correlation coefficients of 35 elements.*

because both Ca and Mg concentrations are very low and probably present not only in carbonate minerals, but also in silicates, the calculated ratios are not useful as indicators of the depositional environment.

The correlation coefficients (r) of the elements are illustrated in table 4. The fact that Ca does not correlate with the Sr ($r = 0.19$) supports that Ca is incorporated in minerals other than carbonates (e.g., plagioclase). Though Mn and Ca are correlated ($r = 0.67$), it is more likely that Mn is associated with sulphide-forming elements such as Fe, Co and Ni. High correlation coefficients ($r > 0.60$) reveal the element pairs (Ti/Zr), (Cr/Ni), (Cr/Hf), (Cr/Th), (Co/Ni), (Ni/U), (Ga/Zr), (Rb/Cs), (Zr/Hf), (Nb/Ce), (La/Nd), (Ce/Nd), (La/Th) and (Ce/Th). The good Cr/Ni covariance ($r = 0.80$) corroborates the existence of mafic to ultramafic rocks in the hinterland.

6. CONCLUSIONS

For evaluation of the source rock potential of the Upper Palaeozoic and Triassic basement strata of the Songliao Basin 83 samples were collected from outcrops surrounding the basin. To determine the quality and maturity of the potential source rocks of both marine and terrestrial origin the following analysis were carried out:

- Leco: Two third of the black shale samples showed a TOC value between 0.5 to 1.5 %, which refer to fair to good quality. Five samples with an early Carboniferous and late Permian age (outcrops 1 and 10) revealed excellent organic carbon contents ranging from 2 to 5 %.

  Nearly all samples are characterized by very low sulphur contents and high TOC/S ratios. Only samples from the Middle Permian Zhesi Formation in the lower part of outcrop 4 reveal TOC/S ratios characteristic for marine deposits.

- Rock Eval pyrolysis: During heating the samples to 550 °C hydrocarbons were neither liberated nor generated, portending that the measured samples are overmature. Because of too low HI and OI values at this stage of maturity no conclusions can be drawn upon the original type of organic matter and the depositional environment.

- Vitrinite reflectance: The vitrinite data of the samples vary from 2.2 to 5.7 Rmax (2.0 to 5.3 % Ro), corroborating the results of the Rock Eyal pyrolysis that the samples are overmature. Thermal heating of nearby granitic intrusions seem to have affected the maturity of some Middle and Upper Permian samples. The relatively low vitrinite reflectance values of Lower Permian samples (2.4 to 3.1 % Rmax) could be related to local tilting of the strata before or during coalification, though that remains speculative.

- X-ray fluorescence analysis: The results of the UniQuant principal element analysis shows that the SiO_2 content makes up for 64 to 69 weight %, whereas the CaO content of the samples is very low, suggesting a siliciclastic-dominated environment. The relative enrichment of the elements Ti and Zr support this statement. In outcrop 2 the samples are characterized by elevated Ni, Cr and Co contents, pointing to some basic

rocks in the hinterland. Mn/Ni and V/Cr ratios refer partly to restricted oxygen circulation or even aerobe conditions during deposition.

Based on these data it stands to reason to consider the source rocks of the Upper Palaeozoic and Triassic basement of the Songliao Basin as overmature and without any hydrocarbon generation potential.

However, some gas in the Songliao Basin may have derived from basement rocks beneath the depocenters of the Mesozoic/Cenozoic basin despite of the high maturity. The general increase in vitrinite reflectance from younger to older strata indicates that maturation of the basement rocks occurred before (Permo-Triassic?) deformation, which was probably related to the collision of the North China micro-continent with the Jiameng block. Based on the measured vitrinite data (> 2 % Ro) the basement strata must have been buried deep enough to reach temperatures above 200 °C, though the thickness of overburden rocks remains unknown. Deep erosion and removal of the overburden rocks might have taken place during the Triassic - Juarssic uplift phase. With the formation of the Songliao Basin in the late Jurassic, an additional thermal overprint of Palaeozoic and Triassic rocks might have occurred at the base of the depressions. However, it is unlikely that larger amounts of gas were generated and trapped in the overlying fill of the Songliao Basin, because of the initially high maturity of the basements rocks.

Between the sediments at the shallow margins of the Songliao Basin and basement rocks a significant break in coalification is to expect, since the maturity of the first does not exceed 0.8 % Ro. This implies, even if the basement rocks had a remaining hydrocarbon generation potential (which has not been confirmed by the present Rock Eval data), the present-day thermal regime would not be sufficient to release hydrocarbons from the Upper Palaeozoic and Triassic rocks.

Concluding, apart from at most little contribution of gas during the subsidence of the depressions of the Songliao Basin, the generated hydrocarbons of basement rocks were probably lost during the post-collisional uplift phase in late Triassic to early Jurassic times.

7. REFERENCES

Arakawa, Y., Saito, Y. & Amakawa, H. (2000): Crustal development of the Hida belt, Japan: Evidence from Nd-Sr isotopic and chemical characteristics of igneous and metamorphic rocks. – Tectonophysics, 328, 183-204.

Augustin-Gyurits K. & Schroll, E. (1992): Beitrag zur geochemischen Charakterisierung österreichischer Kohlen (Contribution to the Geochemical Characterization of Coal from Austria). – Mitt. Ges. Geol. Bergbaustud. Österr., 38, 195-211, Wien.

Badrach, G., Cunningham, W. D. & Windley, B. F. (2002): A new terrane subdivision for Mongolia: implications for the Phanerozoic crustal growth of Central Asia. – Journal of Asian Earth Sciences, 21, 87-110.

Barker, C. E. (1988): Geothermics of petroleum systems: Implications for stabilization of kerogen maturation after a geologically brief heating duration at peak temperature. In: Magoon L. (ed.), Petroleum Systems of the United States. – United States Geological Survey Bulletin, 1870, 26-29.

Berner, R. A. (1984): Sedimentary pyrite formation: An update. – Geochimica et Cosmochimica Acta, 48, 605-615.

Brouwer, P. (2003): Theory of XRF PANalytical BV, The Netherlands.

Buslov, M. M., Saphonova, I. Yu, Wanatabe, T., Obut, O. T., Fujiwara, Y., Iwata, K., Semakov, N. N., Sugai, Y., Smirnova, L. V. & Kazansky, A. Yu. (2001): Evolution of the Paleo-Asian Ocean (Altai-Sayan region, Central Asia) and collision of possible Gondwana-derived terranes with the southern marginal part of the Siberian continent. – The Geoscience Journal, 5, 203-224.

Cai, X. (1995): An application of basin simulation technique in Songliao Basin. – Acta Petrol. Sin., 16, 22-29.

Cao, C. (1989): The ophiolite belts of northeastern China. – Journal of Southeast Asian Earth Sciences, 3, 233-236.

Cao, X., Dang, Z. X., Jiang, J. S. & Wang, H. D. (1992): The composite Jiamusi terrane (in Chinese with English and Russian abstracts). – Jilin Publishing House of Science and Technology, 224 pp.

Cawood, P. A. (2005): Terra Australia Orogen: Rodinia breakup and development of the Pacific and Iapetus margins of Gondawana during the Neoproterozoic and Paleozoic. – Earth Science Reviews, 69, 249-279.

Cheng, R., Liu, Z. & Wang, P. (1997): Geological significance of volcanic events in the eastern part of the Songliao Basin (in Chinese). – Earth Science, Journal of China University of Geoscience, 22 (1), 57-61.

Choi, D. K., Kim, D. H., Sohn, J. W. & Lee, S. B. (2003): Trilobite faunal successions across the Cambrian-Ordovician boundary intervals in Korea and their correlation with China and Australia. – Journal of South East Asian Earth Sciences, 21, 781-793.

Cope, T., Ritts, B. D., Darby, B. J., Fildani, A. & Graham, S. A. (2005): Late Paleozoic sedimentation on the Norh China Block: implications for regional tectonics and climate change. – International Geology Review, 47, 270-296.

De Jong, K., Xiao, W., Windley, B. F., Masago, H. & Lo, C. (2006): Ordovician $^{40}Ar/^{39}Ar$ phengite ages from the blueschist-facies Ondor Sum subductio-accretion complex (Inner Mongolia) and implications for the early Paleozoic history of continental blocks in China and adjacent areas. – Amer. J. Sci., 306, 799-845.

Dobretsov, N. L. (2003): Evolution of structures of the Urals, Kazakhstan, Tien Shan, and Altai-Sayan region within the Ural-Mongolian Fold Belt (Paleoasian Ocean). – Russian Geology and Geophysics, 44, 5-27.

Dobretsov, N. L., Buslov, M. M. & Vernikovsky, V. A. (2003): Neoproterozoic to Early Ordovician evolution of the Paleo-Asian Ocean: Implications to the break-up of Rodinia. – Gondwana Research, 6, 143-159.

Ehiro, M. (2000): Relationships in tectonic framework among the South Kitakami and Hayachine tectonic belts, Kurosegawa Belt, and 'Paleo-Ryoke Belt'. – Memoir of the Geological Society of Japan, 56, 53-64.

Energy Information Administration (2006) – http://www.eia.doe.gov/emeu/cabs/China/Oil.html.

Ernst, W. (1970): Geochemical facies analysis. – Methods in Geochemistry and Geophysics, Elsevier, Amsterdam.

Espitalié, J. & Joubert, L. (1987): Use of T_{max} as maturation index in petroleum exploration. In: Kumar et al., (eds.), Petroleum Geochemistry and Exploration in the Afro-Asian Region, 67-73, Balkerma, Rotterdam.

Espitalié, J., Laporte, J. L., Madec, M., Marquis F., Leplat, P., Paulet, J. & Boutefeu, A. (1977): Méthode rapide de caractérisation des roches mères, de leur potentier de leur degré d'évolution. – Rev. Inst. Franc. du Petr., 32, 23-42.

Fortey, R. A. & Cocks, L. R. M. (2003): Palaeonological evidence bearing on global Ordovician-Silurian continental reconstructions. – Earth Science Reviews, 61, 245-307.

Gao, Q. & Liu, Y. (1984): Distribution and evaluation of isoprenoids in the source rocks and crude oils in the Songliao Basin. In: Yang, W. (ed.), Songliao Basin – History of Daqing oil field (in Chinese). – Chinese Petroleum Geology, Petroleum Industry Press, 2, 238-244, Beijing.

Geological Survey of China (2004): Geological map of NE China, scale 1: 4,000,000. – Geological Publishing House, Beijing.

Gordienko, I. V. (2006): Geodynamic evolution of late Balkaids and Paleozoids in the folded periphery of the Siberian Craton. – Russian Geology and Geophysics, 47 (1), 53-70.

Gradstein, F. M., Agterberg, F. P., Ogg, J. G., Hardenbol, J., Van Veen, P., Thierry, J. & Huangzehui (1994): A Mesozoic time scale. – J. Geophys. Res., 99, 24051-24074.

Guo, F., Fan, W. M., Wang, Y. J. & Li, C. W. (2004): Upper Paleozoic basalts in the southern Yangtze Block: Geochemical and Sr-Nd isotopic evidence for asthenosphere-lithosphere interaction and opening of the Palaeo-Tethyan Ocean. – International Geology Review, 46, 332-346.

HBGMR (Heilongjiang Bureau of Geology and Mineral Resources) (1993): Regional Geology of Heilongjiang Province (in Chinese with English abstract). – Geological Publishing House, 347-438, Beijing.

Hevia, V. & Virgos, J. M. (1977): The rank and anisotropy of anthracites: The indicatine surface in uniaxial and biaxial substances. – J. Microsc., 109, 23-28.

Hou, D., Huang, Q., Kong, Q., Feng, Z. & Huang, F. (1999): Transgression and generation of low-maturity hydrocarbon in Songliao Basin (in Chinese with English abstract). – Journal of Jianghan Petroleum Institute, 21 (1), 26-28.

Hu, J. & Krylov, H. A., chairmen (1996): Songliao Basin. In: Petroleum potential maps of northeast Asia. – China Petroleum Industry Press, Beijing, China, 1 sheet, scale 1: 1,610,000.

Hu, W., Cai, C., Wu, Z. & Li, J. (1998): Structural style and its relation to hydrocarbon exploration in the Songliao Basin, northeast China. – Marine and Petroleum Geology, 15, 41-55.

Hu, X., Xu, C. & Niu, S. (1990): Evolution of the Early Paleozoic Continental Margin in Northern Margin of the North China Platform (in Chinese with English abstract). – Peking University Press, 216 pp, Beijing.

IMBGMR (Inner Mongolian Bureau of Geology and Mineral Resources) (1990): Regional Geology of Inner Mongolian Autonomous Region (in Chinese with English abstract). – Geological Publishing House, 725 pp, Beijing.

IMBGMR (Inner Mongolian Bureau of Geology and Mineral Resources) (1991): Regional Geology of Inner Mongolian Autonomous Region (in Chinese with English abstract). – Geological Publishing House, Geological Memoirs, Series 2, n. 25, 725 pp, Beijing.

Ishiwatari, A. & Tsujimori, T. (2003): Paleozoic ophiolites and blueschists in Japan and Russian Primorye in the tectonic framework of East Asia: A systhesis. – The Island Arc, 12, 190-206.

Jahn, B., Wu, F. Y. & Chen, B. (2000): Granitoids of the Central Asian Orogenic Belt and continental growth in the Phanerozoic. – Transactions of the Royal Society of Edinburgh, Earth Sciences, 91, 181-193.

Jahn, B., Wu, F., Capdevila, R., Fourcade, S., Wang, Y. & Zhao, Z. (2001): Highly evolved juvenile granites with tetrad REE patterns: the Woduhe and Baerzhe granites from the Great Xing'an (Khingan) Mountains in NE China. – Lithos, 59, 171-198.

JBGMR (Jilin Bureau of Geology and Mineral Resources) (1988): Regional Geology of Jilin Province (in Chinese with English abstract). – Geological Publishing House, 301-385, Beijing.

Jia, D. C., Hu, R., Lu, Y. & Qiu, X. (2004): Collision belt between the Khanka block and the North China block in the Yanbian Region, Northeast China, Journal of Asian Earth Sciences, 23, 211-219.

Jiang, H., Liu, Z. & Xu, L. (2008): The Hydrocarbon Exploration Prospects of Permo-carboniferous in northeast China (abs.). In: Ren, S., Liu, Y., Qiao, D. & Zhang, X. (eds.), Workshop on petroleum geology and mineral resources in Northeastern Asia, Abstract Volume, 43.

Khain, E. V., Bibikova, E. V., Salnikova, E. B., Kröner, A., Gibsher, A. S., Didenko, A. N., Degtyarev, K. E. & Fedotova, A. A. (2003): The Palaeo-Asian Ocean in the Neoproterozoic and early Palaeozoic: new geochronologic data and palaeotectonic reconstructions. – Precambrain Research, 122, 329-358.

Khanchuk, A. I., Ratkin, V. V., Ryazantseva, M. D. Golozubov, V. V. & Gonokhova, N. B. (1996): Geology and mineral deposits of Primorskiy Krai. – Russian Academy of Science, Geological Institute, Far East Branch, Dalnauka, 61 pp, Vladivostok.

Kheraskova, T. N., Didenko, A. N., Bush, V. A. & Volozh, Yu A. (2003): The Vendian-Early Paleozoic history of the continental margin of Eastern Paleogondwana, Paleoasian Ocean, and Central Asian Foldbelt. – Russian Journal of Earth Sciences, 5, 165-184.

Kilby, W. E. (1988): Recognition of vitrinite with non-uniaxial negative reflectance characteristics. – Int. J. Coal Geol., 9, 267-285.

Killops, S. D. & Killops, V. J. (1997): Einführung in die organische Geochemie. – Ferdinand Enke Verlag, 230 pp, Stuttgart.

Kojima, S., Kemkin, I. V., Kametaka, M. & Ando, A. (2000): A correlation of accretionary complexes of southern Sikhote Alin of Russia and the Inner Zone of Southwest Japan. – The Geoscience Journal, 4, 175-185.

Kong, Q. (1984): Carbon isotopes of the organic matter in oils and sedimentary rocks, Songliao Basin and their geological application. In: Yang, W. (ed.), Songliao Basin – History of Daqing oil field (in Chinese). – Chinese Petroleum Geology, Petroleum Industry Press, 2, 245-251, Beijing.

Krejci-Graf, K. (1966): Geochemische Faziesdiagnostik. – Freiberger Forsch.-H. RC, 224, Freiberg.

Kusznir, N. J., Roberts, A. M. & Morley C. K. (1995): Forward and reverse modelling of rift formation. In: Lambiase, J. J. (ed.), Hydrocarbon Habitat in Rift Basins). – Geol. Soc. Spec. Pub., 88, 33-56.

Laurent-Charvet, S., Charvet, J., Monié, P. & Shu, L. S. (2003): Late Palaeozoic strike-slip shear zones in eastern central Asia (NW China): New structural and geochronological data. – Tectonics, 22 (2), 1009.

Levine, J. R. & Davis, A. (1984): Optical anisotropy of coals as an indicator of tectonic deformation, Broad Top coal field, Pennsylvania. – Geol. Soc. Amer. Bull., 95, 100-108.

Levine, J. R. & Davis, A. (1989 b): Reflectance anisotropy of Upper Carboniferous coals in the Appalachian foreland basin, Pennsylvania, U.S.A. – Int. J. Coal Geol., 13, 341-373.

Li, D. (1995) Hydrocarbon habitat in the Songliao rift basin, China. In: Lambiase, J. J. (ed.), Hydrocarbon habitat in rift basins. – Geol. Soc. Special Publication, 80, 317-329.

Li, D., Jiang, R. & Katz, B. J. (1995): Petroleum generation in the nonmarine Qingshankou Formation (Lower Cretaceous), Songliao Basin, China. In: Katz, B. (ed.), Petroleum Source Rocks. – Springer Verlag, 131-147, Berlin.

Li, J. Y. (2006): Permian geodynamic setting of Northeast China and adjacent regions: closure of the Paleo-Asian Ocean and subduction of the Paleo-Pacific Plate. – Journal of Asian Earth Sciences, 26, 207-224.

Li, T., Rullkötter, J., Radke, M., Schaefer, R. G. & Welte, D. H. (1987): Crude oil geochemistry of the southern Songliao Basin. – Erdöl und Kohle – Erdgas - Petrochemie vereinigt mit Brennstoff Chemie, 40 (8), 337-346.

Li, Z. X. & Powell, C. McA. (2001): An outline of the palaeogeographic evolution of the Australasian region since the beginning of the Neoproterozoic. – Earth Science Reviews, 53, 231-235.

Lin, W., Faure, M., Nomade, S., Shang, Q. & Renne, P. R. (2008): Permian-Triassic amalgamation of Asia: Insights from Northeast China sutures and their place in the final collision of North China and Siberia. – C. R. Geoscience, 340, 190-201.

Liu, Y., Jin, W., Ma, Z., Zhang, X., Wang, C., Chi, X., Xu, W., Wen, Q., Han, G. & Wu, L. (2008): Late Paleozoic – Mesozoic tectonic evolution in the NE China (abs.). In: Ren, S., Liu, Y., Qiao, D. & Zhang, X. (eds.), Workshop on petroleum geology and mineral resources in Northeastern Asia, Abstract Volume, 167 pp.

Lu, F., Zhu, Q., Li, S., Xie, Y. & Zheng, J. (1997): Mesozoic volcanism surrounding Songliao Basin, China – Implication for the relationship with evolution of basin. – Journal of China University of Geoscience, 8 (1), 72-77.

Ma, L., Yang, J. & Ding, Z. (1989): Songliao Basin - an intracratonic continental sedimentary basin of combination type. In: Zhu X. (ed.), Chinese Sedimentary Basins, Elsevier, 77-87, Amsterdam.

Ma, Z., Peng, X., Liu, L., Wang, C., Sun, Y., Hu, D., Zheng, C. & Yu, J. (2008): Late Palaeozoic Strata in NE China - New Prospect for Hydrocarbon Oil and Gas Exploration in NE China (abs.). In: Ren, S., Liu, Y., Qiao, D. & Zhang, X. (eds.),

Workshop on petroleum geology and mineral resources in Northeastern Asia, Abstract Volume, 167 pp.

McKenzie, D. P. (1978): Some remarks on the development of sedimentary basino. – Earth Planet. Sci. Lett., 40, 25-32.

Meert, J. G., Nédélec, A., Hall, C., Wingatee, M. T. D. & Rakotondrazafy, M. (2001): Paleomagnetism, geochronology and tectonic implications of the Cambrain-age Carion granite, Central Madagascar. – Tectonophysics, 340, 1-21.

Metcalfe, I. (1996): Gondwanaland dispersion, Asian accretion and evolution of Eastern Tethys. – Australian Journal of Earth Sciences, 43, 605-623.

Metcalfe, I. (1998): Palaeozoic and Mesozoic geological evolution of the SE Asian region: multidisciplinary constraints and implications for biogeography. In: Hall, R. & Holloway, J. D. (eds.), Biogeography and Geological Evolution of SE Asia. – Backhuys Publishers, 25-41, Leiden.

Metcalfe, I. (2002): Permian tectonic framework and palaeogeography of SE Asia. – Journal of Asian Earth Sciences, 20, 551-566.

Mossakovsky, A. A., Ruzhentsev, S. V., Samygin, S. G. & Kheraskova, T. N. (1993): The Central-Asian folded belt: a geodynamic evolution and history of origin. – Geotektonika, 6, 3-33.

Mossakovsky, A. A., Ruzhentsov, S. V., Samygin, S. G. & Kheraskova, T. N. (1994): Central Asian fold belt: geodynamic evolution and formation history. – Geotectonics, 27, 445-473.

Mukhopadhyay, P. K. & Dow, W. G. (1994): Vitrinite reflectance as a maturity parameter - applications and limitations. – ACS Symposium Series, 570, 1-24.

Nie, F. & Bjørlykke, A. (1999): Nd and Sr isotope constraints on the age and origin of Proterozoic meta-mafic volcanic rocks in the Bainaimiao-Wenduermiao district, south-central Inner Mongolia, China. – Continental Dynamics, 4, 1-14.

Nokleberg, W. J., Parfenov, L. M., Monger, J. W. H., Norton, I. O., Khanchuk, A. I., Stone, D. B., Scotese, C. R., Scholl, D. W. & Fujita, K. (2001): Phanerozoic tectonic evolution of the Circum-North Pacific. – United States Geological Survey Professional Paper, 1626, 122 pp.

Nokleberg, W. J., Badarch, G., Berzin, N. A., Diggles, M. F., Hwang, D. H., Khanchuk, A. I., Miller, R. J., Naumova, V. V., Obolenskiy, A. A., Ogasawara, M., Parfenov, L. M., Prokopiev, A. V., Rodionov, S. M. & Yan, H. (eds.) (2004): Digital Files for Northeast Asia Geodynamics, Mineral Deposit Location, and Metallogenic Belt Maps, Stratigraphic Columns, Description of Map Units, and Description of Metallogenic Belts. – United States Geological Survey Open-File Report 2004-1252, http://pubs.usgs.gov/of/2004/1252/of2004-1252.pdf.

Nøttvedt, A., Gabrielsen, R. H. & Steel, R. J. (1995): Tectonostratigraphy and sedimentary architecture of rift basins, with reference to the northern North Sea. – Mar. Petrol. Geol., 12, 881-901.

Pang, X. & Lerche, I. (1997): Constraints on hydrocarbon migration from the Qingshankou source rock in the west of the Songliao Basin, China. – Petrol. Geosci., 3, 73-94.

Pavićević, M. K. & Amthauer, G (2000): Physikalisch-chemische Untersuchungsmethoden in den Geowissenschaften. – Schweizerbart'sche Verlagsbuchhaltung, Band 1, 252 pp, Stuttgart.

Peters, K. E. (1986): Guidelines for evaluating petroleum source rock using programmed pyrolysis. – AAPG Bulletin, 70, 318-329.

Petroconsultants (1996): Petroleum Exploration and Production Database: Petroconsultants, Inc., P.O. Box 740619, 6600 Sands Point Drive, Houston, TX 77274-0619, USA, or Petroconsultants, Inc., P.O. Box 152, Chemin de la Mairie, 1258 Perly, Geneva, Switzerland.

Pickering, K. T. & Smith, A. G. (1995): Arcs and backarc basins in the Early Paleozoic Iapetus Ocean. – The Island Arc, 4, 1-67.

Rantitsch, G., Sachsenhofer, R. F. & Schroll, E. (1995): Anorganische Geochemie mesozoischer Kohlen der Ostalpen (Österreich). – Archiv für Lagerstättenforschung der Geologischen Bundesanstalt, 18, 121-133, Wien.

Ryder, R. T., Jin, Q., McCabe, P. J., Nuccio, V. F. & Persiti, F. (2003): Qingshankou-Putaohua/Shaertu and Jurassic Coal-Denglouku/Nongan Total Petroleum Systems in the Songliao Basin, China. – U.S. Geological Survey Bulletin, 2203-A, 41 pp; available at http://pubs.usgs.gov/bul/b2203-a.

Schenk, H. J., Witte, E. G., Littke, R. & Schwochau, K. (1989): Structural modifications of vitrinite and alginite concentrates during pyrolytic maturation at different heating rates. In: Durand, B. & Behar, F. (eds.), Advances in Organic Geochemistry. – Org. Geochem., 16, 943-950.

Schwans, P., Bohacs, K. M., Hohensee, V. K., Lin, F. C. Gao, R.Q., Qiu, J. Y., Sun, S. H. & Li, F. J. (1997): Nonmarine sequence stratigraphy. – Impact on source, reservoir and seal distribution in a rift setting, Cretaceous Songliao Basin, China (abs.).- AAPG Bull., 81 (8), 1411.

Şengör, A. M. C., Natal'in, B. A. & Burtman, V. S. (1993): Evolution of the Altaid tectonic collage and Palaeozoic crustal graowth in Eurasia. – Nature, 364, 299-307.

Şengör, A. M. C. & Natal'in, B. A. (1996): Paleotectonics of Asia. In: Yin, A. & Harrison, T. M. (eds.), The tectonic evolution of Asia. – Cambridge University Press, 486-640, Cambridge.

Shang, Q. (2004): Occurrence of Permian Radiolarians in central and eastern Neimongol (Inner Mongolia) and their geological significance for the North China Orogen. – Chin. Sci. Bull., 49, 2613-2619.

Shao, J. (1989): Continental crust accretion and tectono-magmatic activity at the northern margin of the Sino-Korean plate. – Journal of South East Asian Earth Sciences, 3, 57-62.

Song, T. (1997): Inversion styles in the Songliao Basin (northeast China) and estimation of the degree of inversion. – Tectonophysics, 283 (3-4), 173-188.

Stach, E., Mackowsky, M. T., Teichmüller, M., Taylor, G. H., Chandra, D. & Teichmüller, R. (1982): Stach's Textbook of Coal Petrology, 3rd edition. – Gebrüder Borntrager, 535 pp, Berlin.

Suess, E. (1901a): Das Antlitz der Erde, vol. 3, pt.1, F. Tempsky, Wien.

Tang, K. (1990): Tectonic development of Paleozoic fold belts at the northern margin of the Sino-Korean craton. – Tectonics, 9, 249-260.

Taylor, G. H., Teichmüller, M., Davis, A., Diessel, C. F. K., Littke, R. & Robert, P. (1998): Organic petrology. – Gebrüder Borntraeger, 704 pp, Berlin, Stuttgart.

Taylor, S. R. (1964): Abundance of chemical elements in the continental crust: a new table. – Geochim. Cosmochim. Acta, 8, 1273-1285, 1 Tab., Oxford, New York (Pergamon)

Tazawa, J. I. (2002): Late Paleozoic brachiopod faunas of the South Kitakami Belt, northeast Japan, and their paleobiogeographic and tectonic implications. – The Island Arc, 11, 287-301.

Tissot, B. & Welte, D. H. (1978): Petroleum Formation and Occurrence. – Springer, 538 pp, New York.

Tissot, B. & Welte, D. H. (1984): Petroleum Formation and Occurrence, 2nd edition. – Springer, 699 pp, Berlin.

Torsvik, T. H. & Cocks, L. R. M. (2004): Earth geography from 400 to 250 Ma: a palaeomagnetic, faunal and facies review. – J. Geol. Soc., 161, 555-572.

Turekian, K. K. & Wedepohl, K. H. (1961): Distribution of elements in same mayor unites of the Earth's crust. - Geol. Soc. Amer. Bull., 72, 172-202, Washington.

Ulmishek, G. (1993): Geology and hydrocarbon resources of onshore basins in eastern China. – U.S. Geological Survey Open-File-Report, 93 (4), 150 pp.

Underwood, M. B., Laughland, M. M. & Kang, S. M. (1993): A comparison among organic and inorganic indicators of diagenesis and low-temperature metamorphism, Tertiary Shimano Belt, Shikoku, Japan. – Special Paper - Geol. Soc. Amer., 273, 45-61.

USGS (United States Geological Survey) (2000): World Petroleum Assessment. – http://certmapper.cr.usgs.gov/rooms/we/index.jsp.

Veevers, J. J. (2004): Gondwanaland from 650-500 Ma assembly through 320 Ma merger in Pangea to 185-100 Ma breakup: supercontinental tectonics via stratigraphy and radiometric dating. – Earth Science Reviews, 68, 1-132.

Wang, C., Jin, W., Zhang, X., Ma, Z., Chi, X., Liu, Y. & Li, N. (2008): New understanding of the late paleozoic tectonics in Northeastern china and adjacent areas. – Journal of Stratigraphy, 32 (2), 119-136.

Wang, C. & Xing, S. (1991): Measurement and geologic application of homogenization temperature and salinity of inclusions in authigenic quartz of sandstone (in Chinese with English abstract). – Acta Sedimentologica Sinica, 9 (3), 106-115.

Wang, D., Liu, Z. & Liu, L. (1994): Evolution of the Songliao Basin and Eustatic Change of Sea Level (in Chinese with English abstract). – China Geological Press, 157 pp, Beijing.

Wang, L. & Hu, S. (1993): The sedimentary environments in Liufangzi basin and their control of coal and bentonite (in Chinese with English abstract). – Journal of Changchun College of Geology, 23 (3), 306-311.

Wang, P., Zhou, Y. & Wang, D. (1994): Direct dating for non-marine sedimentary sequence and isotope chronology of basin analysis (in Chinese with English abstract). – World Geology, 13 (3), 124-131.

Wang, Q. & Liu, X. Y. (1986): Paleoplate tectonics between Cathaysia and Angaraland in Inner Mongolia, China. – Tectonics, 5, 1073-1088.

Wegehaupt, H. (1961): Zur Petrographie und Geochemie des höheren Westfal A von Westerholt. – Fortschr. Geol. Rheinld. Westf., 3, Krefeld.

Werner, H. (1963): Über das Ca/Mg-Verhältnis in Torf und Kohle. – Fortschr. Geol. Rheinld. Westf., 10, 279-282, Krefeld.

Wilde, S. A., Zhang, X. & Wu, F. (2000): Extension of a newly identified 500 Ma metamorphic terrane in NE China: further U-Pb SHRIMP dating of the Mashan complex, Heilongjiang province, China. – Tectonophysics, 328, 115-130.

Windley, B. F., Kröner, A., Guo, J., Qu, G., Li, Y. & Zhang, C. (2002): Neoproterozoic to Palaeozoic geology of the Altai orogen, Chinese central Asia: New zircon age data and tectonic evolution. – The Journal of Geology, 110, 719-737.

Windley, B. F., Alexeiev, D., Xiao, W., Kröner, A. & Badarch, G. (2007): Tectonic models for accretion of the Central Asian Orogenic Belt. – J. Geol. Soc., 164, 31-47.

Wu, C., Li, S. & Chen, S. (1991): The statistical prediction of the vitrinite reflectance and study of the anciant geothermal field in the Songliao Basin, China. – Journal of China University of Geosciences, 2 (1), 91-101.

Wu, F. Y., Ye, M. & Zhang, S. H. (1995): The geodynamic model of the Manzhouli-Sifenghe geoscience transect (in Chinese with English abstract). – J. Earth Sci., 20, 535-539.

Wu, F. Y., Jahn, B., Wilde, S. & Sun, D. (2000): Phanerozoic crustal growth: U-Pb and Sr-Nd isotopic evidence from granites in northeastern China. – Tectonophysics, 328, 89-113.

Wu, F. Y., Sun, D., Li, H., Jahn, B. & Wilde, S. (2002): A-type granites in northeastern China: age and geochemical constraints on their petrogenesis. – Chemical Geology, 187, 143-173.

Wu, F. Y., Jahn, B., Wilde, S., Lo, C., Yui, T., Lin, Q., Ge, W. & Sun, D. (2003): Highly fractionated I-type granites in NE China (I): geochronology and petrogenesis. – Lithos, 66, 241-273.

Wu, Q. & Xie, Y. (1985): Geothermal heat flow in the Songliao Basin. – Seismol. Geol., 7, 59-64.

Xiao, W., Windley, B. F., Hao, J. & Zhai, M. (2003): Accretion leading to collision and the Permian Solonker Suture, Inner Mongolia, China: Termination of the Central Asian Orogenic Belt. – Tectonics, 22 (6), 1069.

Xiao, W., Windley, B. F., Badarch, G., Sun, S., Li, J., Qin, K. & Wang, Z. (2004 a): Palaeozoic accretionary and convergent tectonics of the southern Altaids: implications for the growth of Central Asia. – J. Geol. Soc., 161, 339-342, London.

Xiao, W., Zhang, L., Qin, K., Sun, S. & Li, J. (2004 b): Paleozoic accretionary and collisional tectonics of the eastern Tienshan (China): implications for the continental growth of Central Asia. – Amer. J. Sci., 304, 370-395.

Xu, S. & Wang, H. (1981): Deltaic deposits a large lake basin. In: Mason, J. F. (ed.), Geology in China, 202-213, New York.

Xu, B. & Chen, B. (1997): Framework and evolution of the Middle Paleozoic orogenic belt between Siberia and North China Plates in northern Inner Mongolia. – Sci. China, 40, 463-469.

Yang, C. & Shen, D. (1986): Stratigraphical division and correlation of the Mesozoic coal-bearing series in the eastern edge of the Songliao Basin in Jilin Province (in Chinese with English abstract). – Jilin Geology, 3, 50-59.

Yang, J. (1981): Development characteristics of structure and petroleum accumulation in the Songliao Basin, China. – Report of the Scientific Research and Design Institute of Daqing Oil Field, China, 20pp.

Yang, J. (1985): New development in exploration of Songliao Basin. – China Oil, 2 (4), 39-42.

Yang, W. (1984): Oil and gas distribution and prediction of exploration prospects in the Songliao Basin. In: Yang, W. (ed.), Songliao Basin - History of Daqing oil field (in Chinese). – Chinese Petroleum Geology, Petroleum Industry Press, 2, 1-14, Beijing.

Yang, W. (1985): Daqing oil field, People's Republic of China – A giant Field with oil of nonmarine origin. – AAPG Bull., 69 (7), 1101-1111.

Yang, W., Gao, R., Li, Y. & Zhang, M. (1984): Generation and evolution of hydrocarbon in the Songliao lacustrine basin. In: Yang, W. (ed.), Songliao Basin - History of Daqing oil

field (in Chinese). – Chinese Petroleum Geology, Petroleum Industry Press, 2, 208-218, Beijing.

Yang, W., Li, Y. & Gao, R. (1985): Formation and evolution of nonmarine petroleum in Songliao Basin, China. – AAPG Bull., 69 (7), 1112-1122.

Ye, M., Zhang, S. H. & Wu, F. Y. (1994): The classification of the Paleozoic tectonic units in the area crossed by Manzhouli-Sifenghe geoscience transect (in Chinese with English abstract). – J. Changchun Uni. Earth Sci., 24, 241-245.

Ye, S. & Wei, K. (1996): Condensed section and new evidence of marine inundation in Cretaceous, Songliao Basin (in Chinese with English abstract). – Earth Science, Journal of China University of Geosciences, 21 (3), 267-271.

Yoshida, K. & Machiyama, H. (2004): Provenanace of Permian sandstones, South Kitakami Terrane, Northeast Japan: implications for Permian arc evolution. – Sedimentary Geology, 166, 185-207.

Yu, H., Cai, X., Han, S., Yi, W. & Zhu, D. (2003): Distribution of the Carboniferous-Permian and its tectonic characteristics in Songliao basin. – Geotectonia et Metallogenia, 27 (3), 277-281.

Yu, J. J., Xu, Z. G. & Xu, F. S. (1996): Tectonic setting of Ordovician volcanic rocks in northwestern Xiaoxing'anling, Heilongjiang Province (in Chinese with English abstract). – Acta Geoscientia Sunica, 17, 54-64.

Yu, Z., Pang, X. & Pepper, A. S. (1997): Petroleum generation and migration modelling in Daqing oil field, Songliao basin, China (abs.). In: AAPG 1997 Annual Meeting Abstracts (Dallas, Texas, April 6-9, 1997), 6, A129.

Zhai G., Gao, W., An, Z., Li, J., Wu, S., Ying, F., Song, J., Cheng, K., Qui, Y., Xu, D., Dai, J., Tang, X., Xu, Z., Zhou, K., Guan, D., Tong, Z., Xue, C., Liu, F., Wang, X. & Xue, S. (eds.) (2000): Petroleum Geology of China. – Petroleum Industry Press, 650 pp, Beijing.

Zhang, J. (1984): Distribution and analysis of exploration effect for subtle oil and gas pools in Songliao Basin. In: Yang, W. (ed.), Songliao Basin - History of Daqing oil field (in Chinese). – Chinese Petroleum Geology, Petroleum Industry Press, 2, 35-46, Beijing.

Zhang, Y. & Tang, K. (1989): Pre-Jurassic tectonic evolution of the intercontinental region and the suture zone between the North China and Siberia platforms. – Journal of South East Asian Earth Sciences, 3, 47-55.

Zhao, X. X., Coe, R. S., Zhou, Y. X., Wu, H. R. & Wang, J. (1990): New palaeomagnetic results from northern China: Collision and suturing with Siberia and Kazakhstan. – Tectonophysics, 181, 43-81.

Zhou, Y. (1998): Reconstruction of Burial and Thermal History, Oil Generation and Migration in the Songliao Basin, Northeastern China. – Jül 3592, Forschungszentrum Jülich.

Zhou, Y. & Littke, R. (1999): Numerical simulation of the thermal maturation, oil generation and migration in the Songliao Basin, northeastern China. – Marine and Petroleum Geology, 16, 771-792.

Zonenshain, L. P. (1973): The evolution of Central Asian geosynclines through sea-floor spreading. – Tectonophysics, 19, 213-232.

Zonenshain, L. P., Kuzmin, M. I. & Kononov, M. V. (1985): Absolute recontructions of the Paleozoic oceans. – Earth Planet. Sci. Lett., 74, 103-116.

Zonenshain, L. P., Kuz'min, M. I. & Natapov, L. M. (1990): Geology of the USSR: a Plate Tectonic Synthesis. – American Geophysical Union, Geodynamic Series, 21, 242 pp, Washington, DC.

8. APPENDICES

Appendix I: Outcrop data

Appendix II: Leco data (TOC, TIC, S, TOC/S)

Appendix III: Vitrinite reflectance data (Rmin-Rmax plots)

Appendix IV: X-ray fluorescence analysis (Pro-Trace and UniQuant)

Appendix I: Outcrop data

Outcrops are sorted in ascending order of stratigraphic age from the early Devonian to Triassic. GPS coordinates of sample locations are indicated.

outcrops	samples	N	E	Height	Age	Formation	comments	strike / dip
14	L23	48° 54' 52"	121° 17' 55"	807	early Devon	Wunuer	≈ Niqiuhe Fm	
	L24	48° 54' 51"	121° 17' 59"	818	early Devon	Wunuer		
1	T1	43° 10' 10.6"	126° 01' 05.6"	287	Early Carbon	Lujuantun	foliation &	
S of	T2				Early Carbon	Lujuantun	mineralized	
Mingcheng	T3	43° 10' 09.1"	126° 01' 04.2"	289	Early Carbon	Lujuantun	veins	
	T4				Early Carbon	Lujuantun		145/65 dark
	T5	43° 10' 07.0"	126° 01' 00.5"	293	Early Carbon	Lujuantun		limestone
2	T7	43° 16' 33.9"	126° 00' 13.6"	277	Early Carbon	Lujuantun		
S of	T8	43° 16' 33.8"	126° 00' 14.2"	274	Early Carbon	Lujuantun		
Yangtong	T9	43° 16' 32.9"	126° 00' 17.8"	270	Early Carbon	Lujuantun		148/63
Shan	T10	43° 16' 33.9"	126° 00' 19.4"	270	Early Carbon	Lujuantun		
15	L25	50° 37' 44"	119° 22' 09"	680	Early Carbon	Hongshuiquan		
	L26				Early Carbon	Hongshuiquan		
	L27				Early Carbon	Hongshuiquan		
	L28	50° 37' 11"	119° 21' 25"	601	Early Carbon	Hongshuiquan		
13	L21	45° 16' 47.2"	116° 38' 09.0"	949	Early Perm	Gegen`aobao		
	L22				Early Perm	Gegen`aobao		
11	L14	50° 19' 53.6"	121° 46' 18.9"	1011	Early Perm	Gegen`aobao		
	L15				Early Perm	Gegen`aobao		
	L16	50° 19' 53.8"	121° 46' 18.0"	1020	Early Perm	Gegen`aobao		
6	T31	47° 11' 11.9"	122° 29' 56.6"	270	Early Perm	Xilin		
S of	T32	47° 11' 10.5"	122° 29' 57.3"	272	Early Perm	Xilin		200/70 basalt
Xilin	T33	47° 11' 08.2"	122° 29' 57.7"	274	Early Perm	Xilin		156/74 bedding
3	T11	45° 23' 12.0"	127° 11' 35.5"	219	Middle Perm	Zhesi		
S of	T12				Middle Perm	Zhesi		260/66
Yuquan	T13				Middle Perm	Zhesi		
(Harbin)	T14				Middle Perm	Zhesi		
	T15				Middle Perm	Zhesi		
4	T16	45° 23' 30.9"	127° 09' 46.1"	200	Middle Perm	Zhesi		090/70 limestone
Quarry	T17				Middle Perm	Zhesi		
Yuquan	T18				Middle Perm	Zhesi		090/47 limestone
	T19				Middle Perm	Zhesi		
	T20				Middle Perm	Zhesi		
	T21				Middle Perm	Zhesi		075/62 limestone
	T22	45° 23' 31.0"	127° 09' 43.9"	192	Middle Perm	Zhesi		
7	T34	46° 31' 08.0"	121° 24' 11.6"	445	Middle Perm	Zhesi		
	T35	46° 31' 08.6"	121° 24' 09.9"	446	Middle Perm	Zhesi		140/80
	T36	46° 31' 09.6"	121° 24' 09.6"	447	Middle Perm	Zhesi		
SE of	T37	46° 31' 10.6"	121° 24' 07.3"	448	Middle Perm	Zhesi	(270/12) //	285/30
Suolun	T38	46° 31' 11.8"	121° 24' 04.9"	452	Middle Perm	Zhesi		090/68
	T39	46° 31' 22.0"	121° 23' 50.9"	451	Middle Perm	Zhesi	181/65 foliat.	170/45
	T40	46° 31' 26.2"	121° 23' 50.2"	452	Middle Perm	Zhesi		160/75
	T41	46° 31' 29.7"	121° 23' 49.7"	452	Middle Perm	Zhesi	pencil struct.	
	T42	46° 31' 34.1"	121° 23' 49.5"	454	Middle Perm	Zhesi	Qz vein	195/75
	T43	46° 31' 37.9"	121° 23' 46.8"	425	Middle Perm	Zhesi	(110/35)	180/55
	T44	46° 31' 42.8"	121° 23' 38.3"	442	Middle Perm	Zhesi		
	T45	46° 32' 09.1"	121° 23' 08.3"	449	Middle Perm	Zhesi		330/60
	T46	46° 32' 18.3"	121° 23' 00.6"	455	Middle Perm	Zhesi		320/55
	T47	46° 32' 52.9"	121° 22' 32.9"	455	Middle Perm	Zhesi	020/32 foliat.	060/80 bedding

outcrops	samples	N	E	Height	Age	Formation	comments	strike / dip
9	L1	44° 31' 48.3"	117° 32' 26.7"	1234	Middle Perm	Zhesi		
	L2	44° 31' 39.2"	117° 32' 22.6"	1251	Middle Perm	Zhesi		
12	L17	44° 00' 25.8"	117° 46' 49.1"	1177	Middle Perm	Beidashan	≈ Zhesi Fm	
	L18				Middle Perm	Beidashan		
	L19				Middle Perm	Beidashan		
	L20				Middle Perm	Beidashan		
10	L3	44° 06' 19.2"	117° 39' 19.0"	1323	Late Permian	Linxi		
	L4				Late Permian	Linxi		
	L5				Late Permian	Linxi		
	L6				Late Permian	Linxi		
	L7				Late Permian	Linxi		
	L8				Late Permian	Linxi		
	L9				Late Permian	Linxi		
	L10				Late Permian	Linxi		
	L11				Late Permian	Linxi		
	L12				Late Permian	Linxi		
	L13	44° 06' 14.4"	117° 39' 23.8"	1281	Late Permian	Linxi		
8	T48	46° 37' 51.9"	121° 14' 50.7"	500	Late Permian	Linxi		240/50
	T49	46° 37' 55.7"	121° 14' 44.4"	506	Late Permian	Linxi	ripple struct	290/51
N of	T50	46° 37' 55.4"	121° 14' 38.9"	505	Late Permian	Linxi		
Suolun	T51	46° 37' 55.8"	121° 14' 33.3"	520	Late Permian	Linxi		
	T52	46° 37' 55.7"	121° 14' 26.2"	511	Late Permian	Linxi		
	T53	46° 38' 00.0"	121° 14' 17.1"	509	Late Permian	Linxi	bioturbation	
	T54	46° 38' 14.3"	121° 13' 56.6"	510	Late Permian	Linxi	plant remains	
	T55	46° 38' 16.0"	121° 13' 50.0"	511	Late Permian	Linxi		152/78
	T56	46° 38' 23.9"	121° 13' 41.3"	509	Late Permian	Linxi		190/45
5	T23	47° 32' 50.7"	122° 28' 48.7"	340	Triassic	Laolongtou		
SW of	T24	47° 32' 51.1"	122° 28' 49.3"	340	Triassic	Laolongtou	flysh like	
Zhalantun	T25	47° 32' 51.2"	122° 28' 49.6"	340	Triassic	Laolongtou	sediments	
(Inner Mong.)	T26	47° 32' 51.5"	122° 28' 50.2"	340	Triassic	Laolongtou	thin bedded	
	T27	47° 32' 50.9"	122° 28' 50.4"	340	Triassic	Laolongtou		
	T28	47° 32' 50.8"	122° 28' 49.2"	340	Triassic	Laolongtou		
	T29	47° 32' 50.8"	122° 28' 48.8"	340	Triassic	Laolongtou	slump	
	T30	47° 32' 49.7"	122° 28' 47.0"	340	Triassic	Laolongtou		
2	T6	43° 16' 33.9"	126° 00' 13.6"	277	Triassic	Laolongtou		

Palaeoenvironment

Appendix II: Leco data (TOC, TIC, S, TOC/S)

Outcrop	Sample	Age	C total %	C inorganic %	C organic %	S %	TOC / S	Facies
1	T1	Early Carbon	4,594	0,000	4,638	0,050	92,5	marine
S of	T2	Early Carbon	3,656	2,178	1,479	0,745	2,0	marine
Mingcheng	T3	Early Carbon	2,637	0,084	2,554	0,530	4,8	marine
	T4	Early Carbon	11,410	10,989	0,421	0,048	8,9	marine
	T5	Early Carbon	3,589	0,563	3,026	0,429	7,1	marine
2	T6	Triassic	0,332	0,000	0,352	0,012	29,1	terrestrial
S of	T7	Early Carbon	3,859	2,636	1,223	0,016	76,2	marine
Yangtong	T8	Early Carbon	2,748	0,780	1,968	0,022	89,9	marine
Shan	T9	Early Carbon	2,521	0,759	1,762	0,029	61,6	marine
	T10	Early Carbon	2,454	0,644	1,811	0,101	17,9	marine
3	T11	Middle Perm	1,517	0,474	1,043	0,201	5,2	marine
S of	T12	Middle Perm	2,173	1,127	1,046	0,281	3,7	marine
Yuquan	T13	Middle Perm	0,849	0,232	0,617	0,020	31,6	marine
(Harbin)	T14	Middle Perm	0,980	0,019	0,961	0,019	50,7	marine
	T15	Middle Perm	0,899	0,011	0,887	0,018	48,3	marine
4	T16	Middle Perm	0,877	0,026	0,851	0,300	2,8	marine
Quarry	T17	Middle Perm	1,606	0,801	0,805	0,316	2,5	marine
Yuquan	T18	Middle Perm	1,456	0,283	1,173	0,455	2,6	marine
	T19	Middle Perm	0,906	0,051	0,855	0,293	2,9	marine
	T20	Middle Perm	0,827	0,022	0,804	0,270	3,0	marine
	T21	Middle Perm	1,041	0,081	0,960	0,121	7,9	marine
	T22	Middle Perm	1,134	0,025	1,109	0,017	63,5	marine
5	T23	Triassic	1,103	0,015	1,088	0,013	81,4	terrestrial
SW of	T24	Triassic	0,912	0,000	0,914	0,012	75,7	terrestrial
Zhalantun	T25	Triassic	1,088	0,006	1,081	0,015	74,0	terrestrial
(Inner Mong.)	T26	Triassic	1,023	0,010	1,013	0,017	58,9	terrestrial
	T27	Triassic	0,991	0,029	0,962	0,016	61,3	terrestrial
	T28	Triassic	0,533	0,000	0,577	0,013	46,0	terrestrial
	T30	Triassic	0,785	0,014	0,772	0,012	64,6	terrestrial
6	T31	Early Perm	0,621	0,000	0,649	0,011	61,4	terrestrial
S of	T32	Early Perm	0,451	0,000	0,456	0,009	51,3	terrestrial
Xilin	T33	Early Perm	0,529	0,011	0,517	0,008	65,6	terrestrial
7	T34	Middle Perm	0,254	0,000	0,265	0,006	41,6	marine
SE of	T35	Middle Perm	0,618	0,000	0,772	0,011	68,8	marine
Suolun	T36	Middle Perm	0,967	0,202	0,765	0,011	67,3	marine
	T37	Middle Perm	1,456	0,018	1,438	0,011	132,2	marine
	T38	Middle Perm	0,764	0,034	0,730	0,010	74,0	marine
	T39	Middle Perm	0,912	0,082	0,830	0,016	52,1	marine
	T40	Middle Perm	0,789	0,058	0,731	0,012	62,5	marine
	T41	Middle Perm	0,854	0,038	0,816	0,010	78,3	marine
	T42	Middle Perm	0,691	0,000	0,746	0,009	86,5	marine
	T43	Middle Perm	0,947	0,000	0,984	0,008	129,5	marine
	T44	Middle Perm	0,933	0,000	0,938	0,008	117,3	marine
	T45	Middle Perm	0,928	0,000	0,932	0,008	110,7	marine
	T46	Middle Perm	0,738	0,000	0,742	0,010	71,7	marine
	T47	Middle Perm	2,003	0,031	1,972	0,100	19,8	marine

Outcrop	Sample	Age	C total %	C inorganic %	C organic %	S %	TOC / S	Facies
8	T48	Late Permian	0,881	0,000	0,902	0,009	104,2	terrestrial
N of	T49	Late Permian	1,143	0,000	1,183	0,015	80,6	terrestrial
Suolun	T50	Late Permian	0,986	0,000	1,029	0,011	89,8	terrestrial
	T51	Late Permian	0,990	0,000	1,012	0,011	88,4	terrestrial
	T52	Late Permian	1,251	0,000	1,303	0,011	114,3	terrestrial
	T53	Late Permian	1,270	0,015	1,255	0,014	90,3	terrestrial
	T54	Late Permian	1,237	0,000	1,250	0,016	77,6	terrestrial
	T55	Late Permian	0,840	0,000	0,928	0,017	56,0	terrestrial
	T56	Late Permian	1,502	0,000	1,518	0,025	60,5	terrestrial
9	L1	Middle Perm	5,987	5,757	0,230	0,035	6,6	marine
	L2	Middle Perm	6,938	6,750	0,189	0,015	12,8	marine
10	L3	Late Permian	0,544	0,000	0,567	0,005	122,1	terrestrial
	L4	Late Permian	1,101	0,016	1,085	0,007	165,2	terrestrial
	L5	Late Permian	0,708	0,006	0,702	0,007	93,8	terrestrial
	L6	Late Permian	0,503	0,000	0,510	0,005	94,7	terrestrial
	L7	Late Permian	0,616	0,000	0,632	0,006	111,0	terrestrial
	L8	Late Permian	0,615	0,000	0,623	0,004	147,6	terrestrial
	L9	Late Permian	0,706	0,059	0,647	0,020	32,8	terrestrial
	L10	Late Permian	0,704	0,002	0,702	0,005	140,3	terrestrial
	L11	Late Permian	0,660	0,000	0,678	0,008	80,6	terrestrial
	L12	Late Permian	5,756	0,771	4,985	0,016	314,6	terrestrial
	L13	Late Permian	5,142	2,648	2,494	0,012	209,1	terrestrial
11	L14	Early Permian	0,223	0,000	0,230	0,010	22,7	terrestrial
	L15	Early Permian	0,732	0,522	0,210	0,014	14,8	terrestrial
	L16	Early Permian	0,280	0,000	0,305	0,016	19,2	terrestrial
12	L17	Middle Perm	1,768	0,756	1,012	0,016	62,1	marine
	L18	Middle Perm	1,100	0,012	1,088	0,019	56,5	marine
	L19	Middle Perm	1,114	0,000	1,132	0,139	8,1	marine
	L20	Middle Perm	1,334	0,000	1,352	0,011	122,6	marine
13	L21	Early Permian	1,729	0,854	0,874	0,017	52,3	terrestrial
	L22	Early Permian	1,347	0,422	0,925	0,020	45,9	terrestrial
14	L23	Early Devon	10,773	10,685	0,088	0,009	9,8	marine
15	L25	Early Carbon	11,148	10,567	0,580	0,008	77,1	marine
	L26	Early Carbon	12,330	11,994	0,336	0,003	132,5	marine
	L27	Early Carbon	8,095	7,957	0,138	0,007	19,3	marine
	L28	Early Carbon	9,093	8,956	0,136	0,006	22,2	marine

TOC

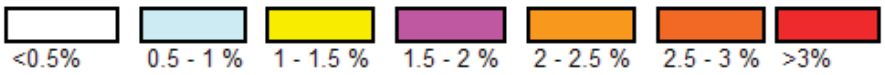

TOC / S

Appendix III: Vitrinite reflectance data (Rmin-Rmax plots)

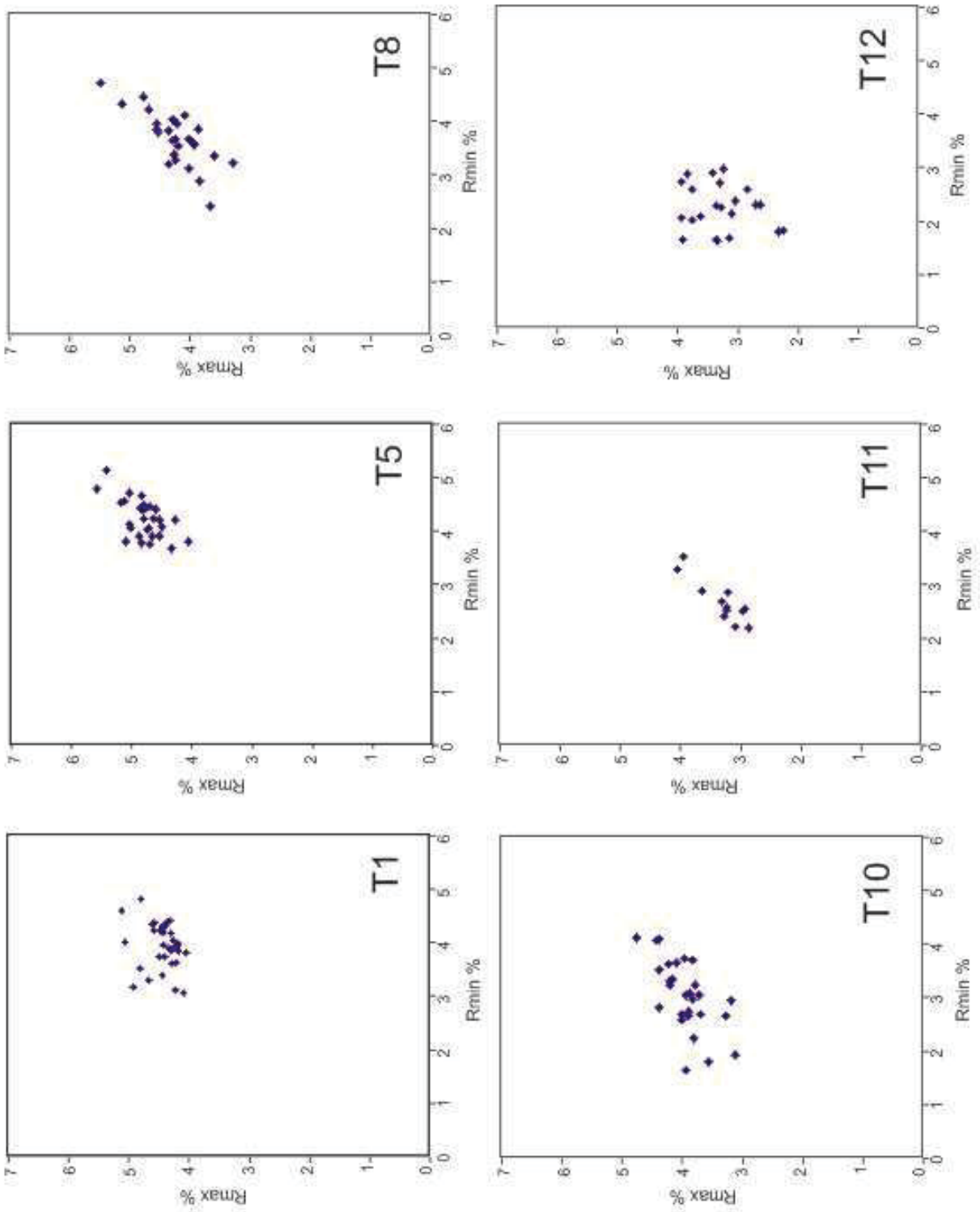

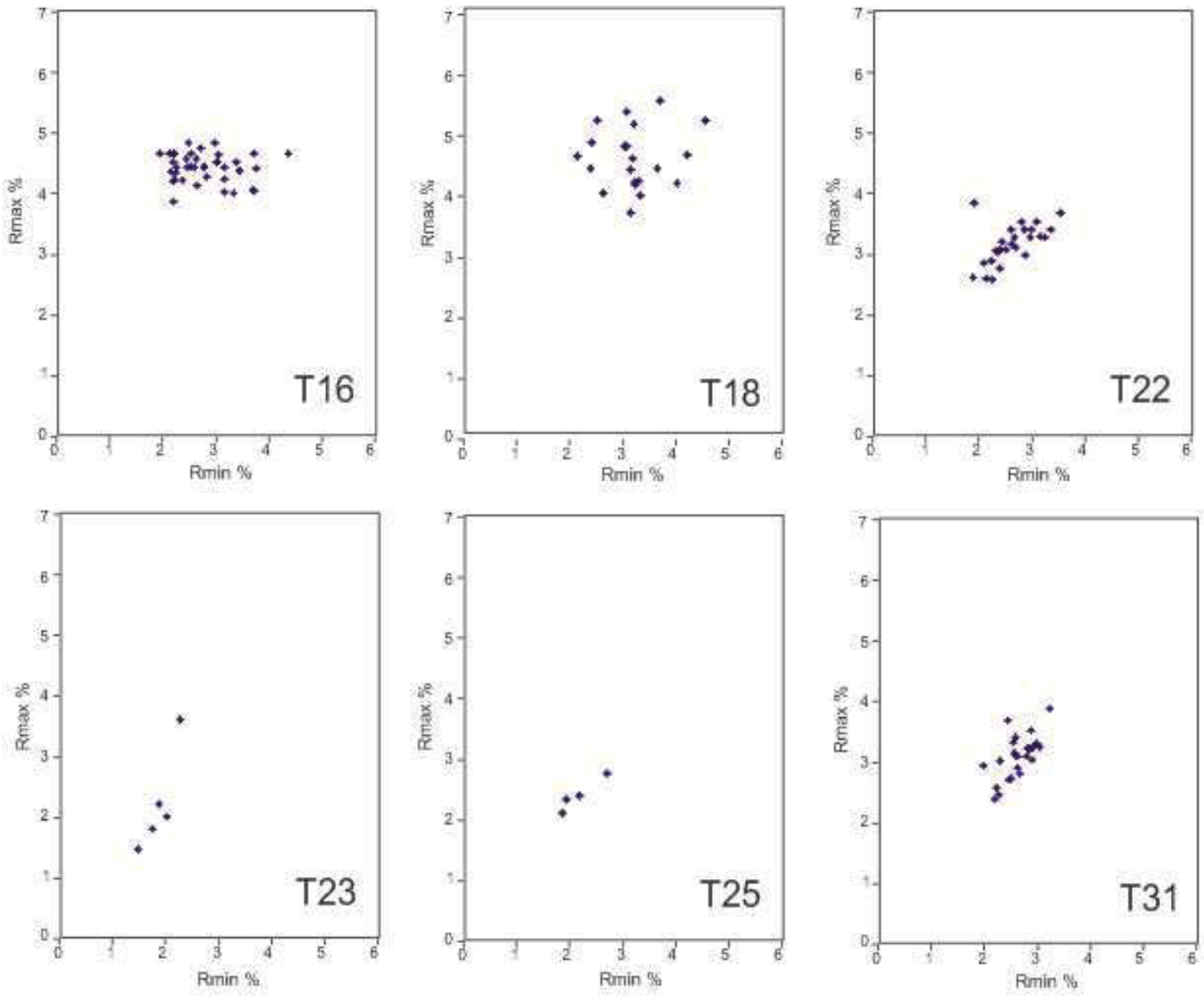
T16
T18
T22
T23
T25
T31
Rmax %
Rmin %

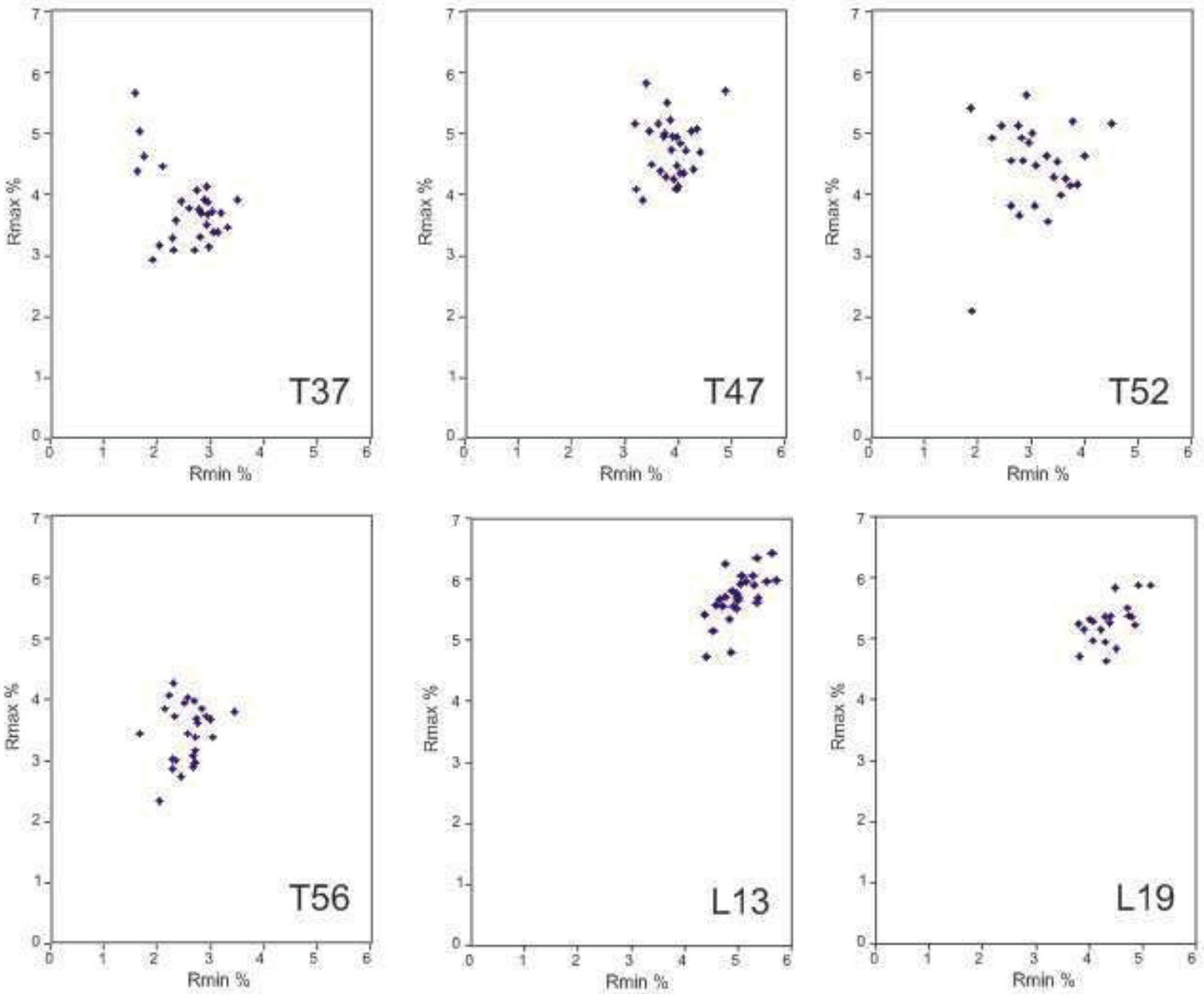
T37
T47
T52
T56
L13
L19
Rmax %
Rmin %

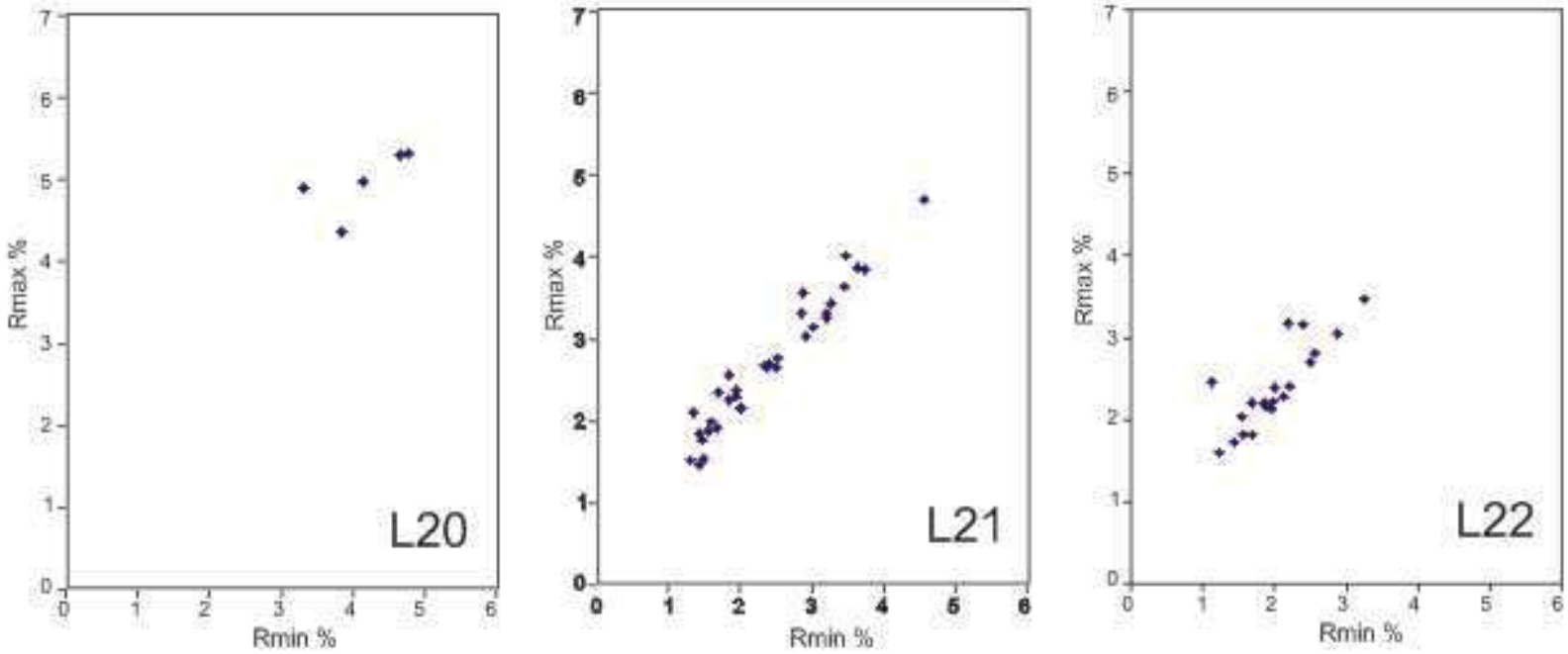
Rmax %
Rmin %
L20
L21
L22

Appendix IV: X-ray fluorescence analysis data

Pro-Trace: contents of trace elements (ppm)

PANalytical Montanuniversität Leoben
Results quantitative - ProTrace

Seq.	Sample	Sum of conc. (%)	CaO Ca (ppm)	Sc Sc (ppm)	TiO2 Ti (ppm)	V V (ppm)	Cr Cr (ppm)	Mn Mn (ppm)	Fe2O3 Fe (ppm)	Co Co (ppm)	Ni Ni (ppm)	Cu Cu (ppm)	Zn Zn (ppm)	Ga Ga (ppm)	Ge Ge (ppm)	As As (ppm)	Se Se (ppm)	
1	T1	6,294	971	19	13748	97	55	137	46793	10	21	16	62	23	1	9	1	
2	T3	7,79	5043	23	13592	120	50	182	57591	20	31	21	76	28	2	21	0	
3	T5	6,934	4348	19	12761	94	51	199	50496	15	28	14	63	25	1	17	1	
	Average - outcrop 1		**2660**	**19**	**13255**	**96**	**53**	**168**	**51627**	**15,0**	**26,7**	**17,0**	**67**	**25,3**	**1,3**	**15,7**	**0,7**	
4	T7	15,288	59860	14	9171	79	107	2235	79470	26	79	22	134	21	1	42	0	
5	T8	7,004	12631	14	10679	94	152	571	43898	23	74	22	120	26	1	58	0	
6	T9	6,286	3084	14	11781	94	111	266	45503	15	50	29	83	31	1	33	0	
7	T10	5,799	4665	11	9885	84	113	429	41047	15	45	17	96	27	1	37	0	
	Average - outcrop 2		**20060**	**13,3**	**10379**	**88**	**121**	**875**	**52480**	**19,8**	**62,0**	**22,5**	**108**	**26,3**	**1,0**	**42,5**	**0,0**	
8	T16	4,793	3775	14	7613	98	48	49	34999	13	23	20	101	25	1	33	0	
9	T17	7,657	23495	12	7881	98	46	154	43463	14	24	14	126	24	1	38	1	
10	T18	7,203	3801	14	7751	153	51	302	58656	13	29	20	94	23	1	40	1	
11	T19	6,872	4428	11	7217	87	43	138	55586	9	23	18	88	23	1	21	0	
12	T20	7,291	3199	12	7388	128	50	222	60681	11	24	18	99	24	1	15	1	
13	T21	7,866	6848	16	7953	112	52	404	61978	11	27	21	99	23	1	16	1	
14	T22	7,199	5724	13	7894	138	57	521	56265	12	25	17	93	24	1	13	0	
	Average - outcrop 4		**7324**	**13,1**	**7671**	**116**	**50**	**256**	**53090**	**11,9**	**25,0**	**18,3**	**100**	**23,7**	**1,0**	**25,1**	**0,6**	
15	T48	6,986	4204	13	7638	72	46	253	56238	9	24	24	93	21	1	0	0	
16	T49	6,97	2165	13	7962	81	49	335	57832	10	22	12	59	20	1	7	0	
17	T50	7,014	2497	14	8248	84	52	637	57227	10	28	26	91	21	1	7	0	
18	T51	6,299	2307	11	7789	78	53	440	50871	13	27	24	101	21	1	5	0	
19	T52	7,724	6025	12	7603	85	51	460	61759	11	25	25	97	20	1	7	0	
20	T53	7,307	3023	14	7924	92	54	265	60397	10	25	25	89	21	1	5	0	
21	T54	6,138	2259	11	8255	77	52	272	49114	8	23	22	69	19	1	12	0	
22	T55	7,129	1649	15	7248	122	53	871	59832	22	38	33	106	21	1	44	1	
23	T56	6,791	5291	14	8889	81	57	347	51774	10	25	23	86	22	1	3	0	
	Average - outcrop 8		**3269**	**13,0**	**7951**	**86**	**52**	**431**	**56116**	**11,4**	**26,3**	**23,8**	**88**	**20,7**	**1,0**	**10,0**	**0,1**	

Br	Rb	Sr	Y	Zr	Nb	Mo	Ag	Cd	Sn	Sb	Te	I	Cs	Ba	La	Ce	Nd
Br	Rb	Sr	Y	Zr	Nb	Mo	Ag	Cd	Sn	Sb	Te	I	Cs	Ba	La	Ce	Nd
(ppm)	(ppm)	(ppm)	(ppm)	(ppm)	(ppm)	(ppm)	(ppm)	(ppm)	(ppm)	(ppm)	(ppm)	(ppm)	(ppm)	(ppm)	(ppm)	(ppm)	(ppm)
1	48	190	43	318	12	1	1	1	4	0	2	3	7	141	34	76	36
0	59	249	46	319	13	1	0	0	4	0	0	3	10	196	35	77	33
0	50	325	40	305	12	1	0	3	4	0	1	1	11	267	31	65	29
0,3	**52**	**255**	**43**	**314**	**12,3**	**1,0**	**0,3**	**1,3**	**4,0**	**0,0**	**1,0**	**2,3**	**9,3**	**201**	**33,3**	**72,7**	**32,7**
0	100	295	41	302	13	2	4	4	5	0	0	4	12	580	48	90	41
0	133	246	38	344	15	2	0	0	6	0	0	2	21	615	45	94	37
0	190	100	49	375	18	1	0	4	8	2	4	4	23	639	56	134	52
0	155	144	36	326	14	1	1	3	6	0	0	2	26	578	44	89	36
0,0	**145**	**196**	**41**	**337**	**15,0**	**1,5**	**1,3**	**2,8**	**6,3**	**0,5**	**1,0**	**3,0**	**20,5**	**603**	**48,3**	**101,8**	**41,5**
0	173	31	37	262	14	2	1	3	4	0	0	0	26	341	40	85	34
0	158	47	37	263	14	1	0	1	6	1	0	4	17	361	38	81	34
0	170	34	37	239	13	1	0	0	5	0	1	3	23	326	48	79	35
0	154	25	35	247	14	1	0	2	5	0	0	4	21	331	35	75	28
0	141	36	38	235	13	1	0	1	4	2	0	0	17	342	38	85	35
0	142	62	36	243	13	1	0	0	5	1	1	4	22	356	41	76	33
0	146	70	38	246	14	1	0	0	4	0	0	2	19	433	43	78	37
0,0	**155**	**44**	**37**	**248**	**13,6**	**1,1**	**0,1**	**1,0**	**4,7**	**0,6**	**0,3**	**2,4**	**20,7**	**356**	**40,4**	**79,9**	**33,7**
0	98	96	37	226	14	1	1	2	5	0	0	1	8	548	34	72	34
0	99	83	35	225	13	1	0	2	4	0	0	2	10	466	33	67	25
0	122	69	33	228	13	1	0	0	3	0	0	4	15	520	37	72	33
0	120	63	34	229	13	1	3	3	4	0	2	0	14	553	36	69	32
0	110	83	35	217	13	0	1	1	6	0	0	0	11	404	35	70	29
0	115	66	37	226	12	1	1	0	6	1	3	6	13	448	31	73	27
0	108	90	32	240	13	1	0	0	2	0	0	1	12	503	30	74	28
0	127	60	37	224	12	2	0	0	4	5	0	3	13	525	41	74	32
0	126	118	35	266	15	1	1	0	2	0	0	0	9	512	45	73	34
0,0	**114**	**81**	**35**	**231**	**13,1**	**1,0**	**0,8**	**0,9**	**4,0**	**0,7**	**0,6**	**1,9**	**11,7**	**498**	**35,8**	**71,6**	**30,4**

Sm Sm (ppm)	Yb Yb (ppm)	Hf Hf (ppm)	Ta Ta (ppm)	W W (ppm)	Hg Hg (ppm)	Tl Tl (ppm)	Pb Pb (ppm)	Bi Bi (ppm)	Th Th (ppm)	U U (ppm)
9	6	9	0	13	0	0	13	0	11	3
8	5	8	1	6	0	0	12	0	12	4
10	5	7	0	10	0	0	17	0	11	5
9,0	**5,3**	**8,0**	**0,3**	**9,7**	**0,0**	**0,0**	**14,0**	**0,0**	**11,3**	**4,0**
5	3	8	0	12	0	1	29	0	17	8
5	4	12	0	9	0	1	27	0	19	5
15	6	11	2	7	1	1	31	0	24	7
0	5	9	1	14	0	1	10	0	18	6
6,3	**4,5**	**10,0**	**0,8**	**10,5**	**0,3**	**1,0**	**24,3**	**0,0**	**19,5**	**6,5**
4	4	6	0	24	1	1	12	0	14	2
10	5	5	1	55	1	0	23	0	14	4
4	4	7	2	15	0	1	16	0	14	4
1	1	6	1	13	0	0	18	0	13	3
6	3	8	1	10	0	0	15	0	13	3
4	3	6	2	14	0	0	22	0	14	4
6	5	6	0	13	0	0	16	0	14	3
5,0	**3,6**	**6,3**	**1,0**	**20,6**	**0,3**	**0,3**	**17,4**	**0,0**	**13,7**	**3,3**
3	5	7	0	4	0	0	20	0	13	4
3	3	6	0	36	0	0	9	0	12	3
6	3	6	2	11	0	0	14	0	12	3
5	4	6	1	24	2	0	21	0	14	3
2	6	6	0	8	0	0	12	0	11	3
6	4	6	0	12	1	1	14	0	12	3
0	4	6	1	18	0	0	14	0	12	3
5	2	6	1	8	0	1	36	0	13	4
8	2	8	1	19	0	0	14	0	11	3
4,2	**3,7**	**6,3**	**0,7**	**15,6**	**0,3**	**0,2**	**17,1**	**0,0**	**12,2**	**3,2**

UniQuant: contents of principal elements (weight %)

ProbenIdent = T16

Compound	Wt%	StdErr	El	Weight%	StdErr
SiO2	68.50	0.52	Si	32.02	0.24
Al2O3	19.29	0.44	Al	10.21	0.23
K2O	5.22	0.12	K	4.34	0.10
Fe2O3	3.82	0.19	Fe	2.67	0.13
MgO	1.33	0.13	Mg	0.800	0.077
TiO2	0.757	0.020	Ti	0.454	0.012

CaO	0.484	0.052	Ca	0.346	0.037
S	0.189	0.009	S	0.189	0.009
P2O5	0.134	0.005	Px	0.0586	0.0020
Na2O	0.105	0.011	Na	0.0781	0.0085
BaO	0.0374	0.0050	Ba	0.0335	0.0044
ZrO2	0.0369	0.0011	Zr	0.0273	0.0008
V2O5	0.0211	0.0016	V	0.0118	0.0009
Rb2O	0.0201	0.0007	Rb	0.0184	0.0007
ZnO	0.0134	0.0009	Zn	0.0108	0.0007
Cr2O3	0.0071	0.0015	Cr	0.0049	0.0010
As2O3	0.0062	0.0031	As	0.0047	0.0023
Y2O3	0.0057	0.0010	Y	0.0045	0.0008
NiO	0.0052	0.0010	Ni	0.0041	0.0008

ProbenIdent = T17

Compound	Wt%	StdErr	El	Weight%	StdErr
SiO2	64.07	0.53	Si	29.95	0.25
Al2O3	19.77	0.44	Al	10.46	0.23
K2O	5.29	0.12	K	4.39	0.10
Fe2O3	4.81	0.21	Fe	3.36	0.15
CaO	2.88	0.18	Ca	2.06	0.13
MgO	1.70	0.14	Mg	1.02	0.09
TiO2	0.787	0.021	Ti	0.472	0.013
S	0.265	0.013	S	0.265	0.013
Na2O	0.106	0.012	Na	0.0785	0.0085
P2O5	0.100	0.004	Px	0.0438	0.0015
BaO	0.0427	0.0049	Ba	0.0382	0.0044
ZrO2	0.0383	0.0011	Zr	0.0284	0.0009
V2O5	0.0230	0.0017	V	0.0129	0.0010
MnO	0.0230	0.0016	Mn	0.0178	0.0012
Rb2O	0.0193	0.0007	Rb	0.0176	0.0007
ZnO	0.0167	0.0010	Zn	0.0134	0.0008
Cr2O3	0.0097	0.0015	Cr	0.0066	0.0011
WO3	0.0095	0.0018	W	0.0075	0.0014
As2O3	0.0089	0.0031	As	0.0067	0.0024
Tb4O7	0.0066	0.0028	Tb	0.0056	0.0023
NiO	0.0065	0.0010	Ni	0.0051	0.0008
Y2O3	0.0065	0.0009	Y	0.0051	0.0007
SrO	0.0059	0.0007	Sr	0.0050	0.0006
Co3O4	0.0051	0.0011	Co	0.0037	0.0008

ProbenIdent = T18

Compound	Wt%	StdErr	El	Weight%	StdErr
SiO2	67.08	0.52	Si	31.36	0.24
Al2O3	18.13	0.43	Al	9.60	0.23
Fe2O3	6.29	0.24	Fe	4.40	0.17
K2O	4.83	0.11	K	4.01	0.09
MgO	1.65	0.14	Mg	0.996	0.085
TiO2	0.744	0.020	Ti	0.446	0.012
CaO	0.480	0.051	Ca	0.343	0.037
S	0.300	0.015	S	0.300	0.015
P2O5	0.154	0.005	Px	0.0670	0.0023
Na2O	0.108	0.012	Na	0.0799	0.0087
BaO	0.0405	0.0046	Ba	0.0363	0.0041
MnO	0.0371	0.0018	Mn	0.0287	0.0014
ZrO2	0.0338	0.0011	Zr	0.0250	0.0008

V2O5	0.0316	0.0017	V	0.0177	0.0010
Rb2O	0.0202	0.0007	Rb	0.0185	0.0007
ZnO	0.0119	0.0009	Zn	0.0096	0.0007
Cr2O3	0.0099	0.0015	Cr	0.0068	0.0010
Co3O4	0.0085	0.0011	Co	0.0062	0.0008
As2O3	0.0061	0.0030	As	0.0046	0.0023
Y2O3	0.0059	0.0010	Y	0.0046	0.0008
NiO	0.0055	0.0010	Ni	0.0043	0.0008
Nd2O3	0.0054	0.0019	Nd	0.0046	0.0017

ProbenIdent = T19

Compound	Wt%	StdErr	El	Weight%	StdErr
SiO2	68.12	0.52	Si	31.85	0.24
Al2O3	17.85	0.43	Al	9.45	0.22
Fe2O3	5.98	0.23	Fe	4.19	0.16
K2O	4.37	0.11	K	3.63	0.09
MgO	1.86	0.15	Mg	1.12	0.09
TiO2	0.693	0.019	Ti	0.415	0.011
CaO	0.558	0.060	Ca	0.399	0.043
S	0.184	0.009	S	0.184	0.009
Na2O	0.104	0.011	Na	0.0771	0.0084
P2O5	0.0960	0.0034	Px	0.0419	0.0015
BaO	0.0347	0.0049	Ba	0.0311	0.0044
ZrO2	0.0343	0.0011	Zr	0.0254	0.0008
Rb2O	0.0186	0.0007	Rb	0.0170	0.0007
V2O5	0.0180	0.0016	V	0.0101	0.0009
MnO	0.0162	0.0015	Mn	0.0125	0.0012
ZnO	0.0112	0.0009	Zn	0.0090	0.0007
Co3O4	0.0063	0.0011	Co	0.0046	0.0008
Cr2O3	0.0060	0.0014	Cr	0.0041	0.0010
Y2O3	0.0057	0.0009	Y	0.0045	0.0007

ProbenIdent = T20

Compound	Wt%	StdErr	El	Weight%	StdErr
SiO2	68.09	0.52	Si	31.83	0.24
Al2O3	17.16	0.42	Al	9.08	0.22
Fe2O3	6.69	0.24	Fe	4.68	0.17
K2O	3.73	0.10	K	3.09	0.08
MgO	2.04	0.16	Mg	1.23	0.09
TiO2	0.726	0.020	Ti	0.435	0.012
Na2O	0.651	0.071	Na	0.483	0.052
CaO	0.403	0.043	Ca	0.288	0.031
S	0.169	0.008	S	0.169	0.008
P2O5	0.149	0.005	Px	0.0651	0.0023
BaO	0.0379	0.0050	Ba	0.0339	0.0045
ZrO2	0.0326	0.0011	Zr	0.0241	0.0008
MnO	0.0318	0.0017	Mn	0.0246	0.0013
V2O5	0.0275	0.0017	V	0.0154	0.0009
Rb2O	0.0190	0.0007	Rb	0.0174	0.0006
ZnO	0.0128	0.0009	Zn	0.0103	0.0008
Cr2O3	0.0084	0.0015	Cr	0.0057	0.0010
Co3O4	0.0075	0.0011	Co	0.0055	0.0008
Y2O3	0.0063	0.0009	Y	0.0050	0.0007
Nd2O3	0.0058	0.0020	Nd	0.0050	0.0017

ProbenIdent = T21

Compound	Wt%	StdErr	El	Weight%	StdErr
SiO2	65.85	0.53	Si	30.79	0.25
Al2O3	18.29	0.43	Al	9.68	0.23
Fe2O3	6.90	0.25	Fe	4.83	0.17
K2O	3.90	0.10	K	3.23	0.09
MgO	2.12	0.16	Mg	1.28	0.10
CaO	0.862	0.092	Ca	0.616	0.066
TiO2	0.787	0.021	Ti	0.472	0.013
Na2O	0.762	0.083	Na	0.565	0.061
P2O5	0.187	0.007	Px	0.0815	0.0028
S	0.104	0.005	S	0.104	0.005
MnO	0.0563	0.0020	Mn	0.0436	0.0015
BaO	0.0431	0.0050	Ba	0.0386	0.0045
ZrO2	0.0334	0.0011	Zr	0.0247	0.0008
V2O5	0.0259	0.0017	V	0.0145	0.0009
Rb2O	0.0157	0.0007	Rb	0.0144	0.0007
ZnO	0.0115	0.0009	Zn	0.0092	0.0007
Cr2O3	0.0097	0.0015	Cr	0.0066	0.0010
SrO	0.0075	0.0007	Sr	0.0063	0.0006
Co3O4	0.0073	0.0011	Co	0.0054	0.0008
NiO	0.0056	0.0011	Ni	0.0044	0.0008
Ga2O3	0.0052	0.0007	Ga	0.0039	0.0005
Y2O3	0.0051	0.0009	Y	0.0040	0.0007

ProbenIdent = T22

Compound	Wt%	StdErr	El	Weight%	StdErr
SiO2	66.54	0.52	Si	31.11	0.24
Al2O3	18.45	0.43	Al	9.76	0.23
Fe2O3	6.23	0.24	Fe	4.35	0.17
K2O	4.00	0.10	K	3.32	0.09
MgO	1.70	0.14	Mg	1.03	0.09
Na2O	1.09	0.11	Na	0.808	0.084
TiO2	0.762	0.020	Ti	0.457	0.012
CaO	0.726	0.077	Ca	0.519	0.055
P2O5	0.236	0.008	Px	0.103	0.004
MnO	0.0718	0.0021	Mn	0.0556	0.0016
BaO	0.0553	0.0049	Ba	0.0495	0.0043
ZrO2	0.0351	0.0011	Zr	0.0260	0.0008
V2O5	0.0287	0.0017	V	0.0161	0.0010
Rb2O	0.0180	0.0007	Rb	0.0165	0.0006
ZnO	0.0120	0.0009	Zn	0.0096	0.0007
SrO	0.0099	0.0007	Sr	0.0084	0.0006
Cr2O3	0.0086	0.0015	Cr	0.0059	0.0010
S	0.0077	0.0006	S	0.0077	0.0006
Co3O4	0.0074	0.0011	Co	0.0054	0.0008
Y2O3	0.0053	0.0009	Y	0.0042	0.0007

ProbenIdent = T48

Compound	Wt%	StdErr	El	Weight%	StdErr
SiO2	68.69	0.51	Si	32.11	0.24
Al2O3	16.93	0.42	Al	8.96	0.22
Fe2O3	6.06	0.23	Fe	4.24	0.16
K2O	3.01	0.09	K	2.50	0.08
Na2O	1.95	0.15	Na	1.44	0.11

MgO	1.74	0.15	Mg	1.05	0.09
TiO2	0.729	0.020	Ti	0.437	0.012
CaO	0.514	0.055	Ca	0.368	0.039
P2O5	0.155	0.005	Px	0.0678	0.0024
BaO	0.0611	0.0047	Ba	0.0547	0.0042
MnO	0.0333	0.0017	Mn	0.0258	0.0013
ZrO2	0.0304	0.0010	Zr	0.0225	0.0008
V2O5	0.0167	0.0014	V	0.0094	0.0008
SrO	0.0118	0.0007	Sr	0.0100	0.0006
ZnO	0.0115	0.0009	Zn	0.0092	0.0007
Rb2O	0.0104	0.0006	Rb	0.0095	0.0006
Cr2O3	0.0062	0.0014	Cr	0.0042	0.0009
S	0.0061	0.0006	S	0.0061	0.0006
Co3O4	0.0061	0.0011	Co	0.0045	0.0008
Y2O3	0.0053	0.0008	Y	0.0042	0.0006
NiO	0.0051	0.0010	Ni	0.0040	0.0008

ProbenIdent = T49

Compound	Wt%	StdErr	El	Weight%	StdErr
SiO2	68.18	0.52	Si	31.87	0.24
Al2O3	16.83	0.42	Al	8.91	0.22
Fe2O3	6.35	0.24	Fe	4.44	0.17
K2O	3.06	0.09	K	2.54	0.08
Na2O	2.25	0.16	Na	1.67	0.12
MgO	1.83	0.15	Mg	1.10	0.09
TiO2	0.777	0.021	Ti	0.466	0.013
CaO	0.272	0.029	Ca	0.195	0.021
P2O5	0.203	0.007	Px	0.0886	0.0031
BaO	0.0574	0.0048	Ba	0.0514	0.0043
MnO	0.0476	0.0018	Mn	0.0369	0.0014
ZrO2	0.0333	0.0011	Zr	0.0247	0.0008
S	0.0177	0.0009	S	0.0177	0.0009
V2O5	0.0157	0.0015	V	0.0088	0.0008
Rb2O	0.0116	0.0006	Rb	0.0106	0.0006
SrO	0.0113	0.0007	Sr	0.0096	0.0006
Cr2O3	0.0078	0.0014	Cr	0.0053	0.0010
WO3	0.0075	0.0017	W	0.0059	0.0013
ZnO	0.0071	0.0008	Zn	0.0057	0.0006
Co3O4	0.0064	0.0011	Co	0.0047	0.0008
Y2O3	0.0057	0.0008	Y	0.0045	0.0006

ProbenIdent = T50

Compound	Wt%	StdErr	El	Weight%	StdErr
SiO2	67.56	0.52	Si	31.58	0.24
Al2O3	17.20	0.42	Al	9.10	0.22
Fe2O3	6.31	0.24	Fe	4.41	0.17
K2O	3.72	0.10	K	3.09	0.08
MgO	1.94	0.15	Mg	1.17	0.09
Na2O	1.68	0.14	Na	1.25	0.10
TiO2	0.803	0.022	Ti	0.482	0.013
CaO	0.310	0.033	Ca	0.222	0.024
P2O5	0.187	0.007	Px	0.0815	0.0029
MnO	0.0858	0.0022	Mn	0.0665	0.0017
BaO	0.0654	0.0048	Ba	0.0586	0.0043

ZrO2	0.0306	0.0011	Zr	0.0227	0.0008
V2O5	0.0194	0.0015	V	0.0109	0.0009
Rb2O	0.0149	0.0007	Rb	0.0136	0.0006
S	0.0144	0.0007	S	0.0144	0.0007
ZnO	0.0102	0.0009	Zn	0.0082	0.0007
SrO	0.0088	0.0007	Sr	0.0074	0.0006
Co3O4	0.0084	0.0011	Co	0.0062	0.0008
Cr2O3	0.0074	0.0015	Cr	0.0051	0.0010
NiO	0.0067	0.0010	Ni	0.0053	0.0008

ProbenIdent = T51

Compound	Wt%	StdErr	El	Weight%	StdErr
SiO2	68.90	0.51	Si	32.21	0.24
Al2O3	16.74	0.41	Al	8.86	0.22
Fe2O3	5.67	0.23	Fe	3.97	0.16
K2O	3.80	0.10	K	3.16	0.08
MgO	1.80	0.15	Mg	1.09	0.09
Na2O	1.57	0.14	Na	1.16	0.10
TiO2	0.776	0.021	Ti	0.465	0.013
CaO	0.300	0.032	Ca	0.215	0.023
P2O5	0.170	0.006	Px	0.0743	0.0026
BaO	0.0667	0.0050	Ba	0.0597	0.0045
MnO	0.0615	0.0020	Mn	0.0476	0.0016
ZrO2	0.0341	0.0011	Zr	0.0252	0.0008
V2O5	0.0217	0.0016	V	0.0122	0.0009
Rb2O	0.0153	0.0007	Rb	0.0140	0.0006
S	0.0128	0.0007	S	0.0128	0.0007
ZnO	0.0126	0.0009	Zn	0.0101	0.0007
SrO	0.0091	0.0007	Sr	0.0077	0.0006
Cr2O3	0.0074	0.0015	Cr	0.0051	0.0010
Co3O4	0.0068	0.0011	Co	0.0050	0.0008
Y2O3	0.0063	0.0009	Y	0.0050	0.0007

ProbenIdent = T52

Compound	Wt%	StdErr	El	Weight%	StdErr
SiO2	67.75	0.52	Si	31.67	0.24
Al2O3	16.44	0.41	Al	8.70	0.22
Fe2O3	6.91	0.25	Fe	4.84	0.17
K2O	3.37	0.10	K	2.80	0.08
MgO	1.96	0.15	Mg	1.18	0.09
Na2O	1.54	0.13	Na	1.14	0.10
CaO	0.759	0.081	Ca	0.543	0.058
TiO2	0.746	0.020	Ti	0.447	0.012
P2O5	0.259	0.009	Px	0.113	0.004
MnO	0.0645	0.0021	Mn	0.0500	0.0016
BaO	0.0487	0.0049	Ba	0.0436	0.0044
ZrO2	0.0324	0.0011	Zr	0.0240	0.0008
V2O5	0.0202	0.0016	V	0.0113	0.0009
S	0.0187	0.0009	S	0.0187	0.0009
Rb2O	0.0134	0.0007	Rb	0.0123	0.0006
ZnO	0.0126	0.0009	Zn	0.0101	0.0008
SrO	0.0106	0.0007	Sr	0.0090	0.0006
Cr2O3	0.0098	0.0015	Cr	0.0067	0.0010
Co3O4	0.0085	0.0011	Co	0.0062	0.0008
Y2O3	0.0061	0.0009	Y	0.0048	0.0007
NiO	0.0060	0.0011	Ni	0.0047	0.0008

ProbenIdent = T53

Compound	Wt%	StdErr	El	Weight%	StdErr
SiO2	67.73	0.52	Si	31.66	0.24
Al2O3	17.01	0.42	Al	9.00	0.22
Fe2O3	6.71	0.25	Fe	4.70	0.17
K2O	3.54	0.10	K	2.94	0.08
MgO	1.90	0.15	Mg	1.15	0.09
Na2O	1.44	0.13	Na	1.06	0.10
TiO2	0.780	0.021	Ti	0.468	0.013
CaO	0.384	0.041	Ca	0.275	0.029
P2O5	0.271	0.009	Px	0.118	0.004
BaO	0.0562	0.0047	Ba	0.0503	0.0042
MnO	0.0358	0.0017	Mn	0.0277	0.0014
ZrO2	0.0334	0.0011	Zr	0.0247	0.0008
V2O5	0.0192	0.0016	V	0.0108	0.0009
S	0.0145	0.0007	S	0.0145	0.0007
Rb2O	0.0135	0.0007	Rb	0.0123	0.0006
ZnO	0.0114	0.0009	Zn	0.0092	0.0007
Cr2O3	0.0112	0.0015	Cr	0.0077	0.0010
SrO	0.0078	0.0007	Sr	0.0066	0.0006
Y2O3	0.0060	0.0009	Y	0.0047	0.0007
Co3O4	0.0056	0.0011	Co	0.0041	0.0008

ProbenIdent = T54

Compound	Wt%	StdErr	El	Weight%	StdErr
SiO2	69.53	0.51	Si	32.51	0.24
Al2O3	16.46	0.41	Al	8.71	0.22
Fe2O3	5.54	0.22	Fe	3.87	0.16
K2O	3.40	0.10	K	2.83	0.08
Na2O	1.84	0.15	Na	1.36	0.11
MgO	1.66	0.14	Mg	1.00	0.09
TiO2	0.831	0.022	Ti	0.498	0.013
CaO	0.294	0.031	Ca	0.210	0.022
P2O5	0.191	0.007	Px	0.0833	0.0029
BaO	0.0624	0.0050	Ba	0.0559	0.0045
MnO	0.0361	0.0018	Mn	0.0280	0.0014
ZrO2	0.0358	0.0011	Zr	0.0265	0.0008
S	0.0224	0.0011	S	0.0224	0.0011
V2O5	0.0173	0.0015	V	0.0097	0.0009
Rb2O	0.0139	0.0007	Rb	0.0127	0.0006
SrO	0.0111	0.0007	Sr	0.0094	0.0006
ZnO	0.0104	0.0009	Zn	0.0084	0.0007
Cr2O3	0.0096	0.0015	Cr	0.0066	0.0010
Co3O4	0.0072	0.0011	Co	0.0053	0.0008
Y2O3	0.0063	0.0009	Y	0.0050	0.0007
CuO	0.0052	0.0008	Cu	0.0042	0.0006

ProbenIdent = Theloy T55

Compound	Wt%	StdErr	El	Weight%	StdErr
SiO2	68.32	0.52	Si	31.94	0.24
Al2O3	16.32	0.41	Al	8.64	0.22
Fe2O3	6.75	0.25	Fe	4.72	0.17
K2O	3.80	0.10	K	3.15	0.08

MgO	1.86	0.15	Mg	1.12	0.09
Na2O	1.47	0.13	Na	1.09	0.10
TiO2	0.727	0.020	Ti	0.436	0.012
CaO	0.211	0.023	Ca	0.151	0.016
P2O5	0.162	0.006	Px	0.0707	0.0025
MnO	0.124	0.003	Mn	0.0959	0.0020
BaO	0.0614	0.0051	Ba	0.0550	0.0045
SO3	0.0381	0.0042	Sx	0.0153	0.0017
ZrO2	0.0338	0.0011	Zr	0.0250	0.0008
V2O5	0.0297	0.0017	V	0.0166	0.0010
Rb2O	0.0162	0.0007	Rb	0.0148	0.0007
ZnO	0.0136	0.0010	Zn	0.0109	0.0008
Cr2O3	0.0114	0.0015	Cr	0.0078	0.0010
Co3O4	0.0089	0.0011	Co	0.0065	0.0008
As2O3	0.0076	0.0033	As	0.0058	0.0025
SrO	0.0075	0.0007	Sr	0.0063	0.0006
Nd2O3	0.0068	0.0019	Nd	0.0058	0.0017
Y2O3	0.0061	0.0009	Y	0.0048	0.0007
NiO	0.0059	0.0011	Ni	0.0046	0.0009

ProbenIdent = T56

Compound	Wt%	StdErr	El	Weight%	StdErr
SiO2	66.23	0.52	Si	30.96	0.25
Al2O3	18.43	0.43	Al	9.75	0.23
Fe2O3	5.87	0.23	Fe	4.11	0.16
K2O	3.92	0.10	K	3.26	0.09
MgO	1.78	0.15	Mg	1.07	0.09
Na2O	1.59	0.14	Na	1.18	0.10
TiO2	0.891	0.024	Ti	0.534	0.014
CaO	0.688	0.073	Ca	0.492	0.052
P2O5	0.284	0.010	Px	0.124	0.004
BaO	0.0651	0.0049	Ba	0.0583	0.0044
S	0.0501	0.0025	S	0.0501	0.0025
MnO	0.0477	0.0019	Mn	0.0369	0.0015
ZrO2	0.0404	0.0012	Zr	0.0299	0.0009
V2O5	0.0222	0.0016	V	0.0124	0.0009
SrO	0.0166	0.0008	Sr	0.0140	0.0007
Rb2O	0.0153	0.0007	Rb	0.0140	0.0006
ZnO	0.0119	0.0009	Zn	0.0096	0.0007
Cr2O3	0.0085	0.0015	Cr	0.0058	0.0010
Co3O4	0.0079	0.0011	Co	0.0058	0.0008
Y2O3	0.0054	0.0009	Y	0.0043	0.0007
Nd2O3	0.0052	0.0019	Nd	0.0045	0.0017
NiO	0.0051	0.0010	Ni	0.0040	0.0008